

NON-LINEAR MATHEMATICAL MODELING
OF GEAR ROTOR BEARING SYSTEMS
INCLUDING BEARING CLEARANCE

A THESIS SUBMITTED TO THE
GRADUATE SCHOOL OF NATURAL AND APPLIED SCIENCES
OF
THE MIDDLE EAST TECHNICAL UNIVERSITY

BY

NİYAZİ ERSAN GÜRKAN

IN PARTIAL FULLFILLMENT OF THE REQUIREMENTS
FOR
THE DEGREE OF MASTER OF SCIENCE
IN
THE DEPARTMENT OF MECHANICAL ENGINEERING

November 2005

Approval of the Graduate School of Natural and Applied Sciences

Prof. Dr. Canan ÖZGEN
Director

I certify that this thesis satisfies all the requirements as a thesis for the degree of Master of Science.

Prof. Dr. Kemal İDER
Head of Department

This is to certify that we have read this thesis and that in our opinion it is fully adequate, in scope and quality, as a thesis for the degree of Master of Science.

Prof. Dr. H. Nevzat ÖZGÜVEN
Supervisor

Examining Committee Members:

Prof. Dr. Samim ÜNLÜSOY (METU, ME) _____

Prof. Dr. H. Nevzat ÖZGÜVEN (METU, ME) _____

Prof. Dr. Mehmet ÇALIŞKAN (METU, ME) _____

Prof. Dr. Sahir ARIKAN (METU, ME) _____

Assoc. Prof. Dr. Ozan TEKİNALP (METU, AEE) _____

I hereby declare that all information in this document has been obtained and presented in accordance with academic rules and ethical conduct. I also declare that, as required by these rules and conduct, I have fully cited and referenced all material and results that are not original to this work.

Niyazi Ersan GÜRKAN

Signature:

ABSTRACT

NON-LINEAR MATHEMATICAL MODELING OF GEAR-ROTOR-BEARING SYSTEMS INCLUDING BEARING CLEARANCE

GÜRKAN, Niyazi Ersan

M.S. Department of Mechanical Engineering

Supervisor: Prof. Dr. H. Nevzat ÖZGÜVEN

November 2005, 130 pages

In this study, a non-linear mathematical model of gear-rotor systems which consists of elastic shafts on elastic bearings with clearance and coupled by a non-linear gear mesh interface is developed. The mathematical model and the software (NLGRD 2.0) developed in a previous study is extended to include the non-linear effects due to bearing clearances by using non-linear bearing models. The model developed combines the versatility of using finite element method and the rigorous treatment of non-linear effect of backlash and bearing clearances on the dynamics of the system.

The software uses the output of Load Distribution Program (LDP), which computes loaded static transmission error and mesh compliance for the contact points of a typical mesh cycle, as input. Although non-varying mesh compliance is assumed in the model, the excitation effect of time varying mesh stiffness is indirectly included through the loaded static transmission error, which is taken as a displacement input into the system.

Previous computer program which was written in Fortran 77 is rewritten by using MatLAB 7.0 and named as NLGRD (Non-Linear Geared Rotor Dynamics) Version 3.0. The program is highly flexible and open to further developments. The

program calculates dynamic to static load ratio, dynamic transmission error, forces and displacements at bearings.

The mathematical model suggested and the code (NLGRD version 3.0) are validated by comparing the numerical results obtained from the model suggested with experimental data available in literature. The results are also compared with those of previously developed non-linear models. The effects of different system parameters such as bearing stiffness, bearing clearance and backlash on the gears are investigated. The emphasis is placed on the interaction of clearances in bearings with other system parameters.

Key words: Gear dynamics, Gear mesh modeling, Non-linear gear dynamics, Non-linear bearings, Dynamic to static load ratio

ÖZ

YATAK BOŞLUKLARI İÇEREN DİŞLİ-ŞAFT-YATAK SİSTEMLERİNİN DOĞRUSAL OLMAYAN ELEMANLARLA MATEMATİK MODELLENMESİ

GÜRKAN, Niyazi Ersan

Yüksek Lisans, Makine Mühendisliği Bölümü

Tez Yöneticisi: Prof. Dr. H. Nevzat ÖZGÜVEN

Kasım 2005, 130 Sayfa

Bu çalışmada, dişlilerle birleştirilmiş ve boşluk içeren elastik yataklar üzerindeki millerden oluşmuş dişli-rotor sistemlerinin dişli boşluğunu da dikkate alan, doğrusal olmayan matematik modeli geliştirilmiştir. Bir önceki çalışmada geliştirilmiş olan matematiksel model ve yazılım (NLGRD V2.0), doğrusal olmayan yatak modelleri kullanılarak, yatak boşluklarından kaynaklanan doğrusal olmayan etkileri içerecek şekilde genişletilmiştir. Geliştirilen model, sonlu elemanlar yönteminin esnekliğiyle, doğrusal olmayan sistemlerin analiz imkanını birleştirerek yatak boşluklarının sistemin dinamiğine etkisinin ayrıntılı bir inceleyebilmektedir.

Yazılım, statik iletim hatasını ve dişliler arasındaki direngenliği tipik bir dişli döngüsündeki temas noktaları için hesaplayan Yük Dağılım Programı'nın (LDP) çıktısını girdi olarak kullanır. Modelde sabit bir kavrama direngenliği olduğu varsayılmasına rağmen, zamanın fonksiyonu olan kavrama direngenliğinin tahrik etkisi, sisteme yerdeğiştirme girdisi olarak alınan bu statik iletim hatası aracılığıyla dolaylı yoldan dikkate alınmıştır.

Önceki çalışmada Fortran 77 kullanılarak yazılmış olan program, MatLAB 7.0 kullanılarak yeniden yazılmış ve NLGRD (Doğrusal Olmayan Dişli Rotor

Dinamiđi) Versiyon 3.0 olarak adlandırılmıřtır. Program olduka esnek ve geliřmelere aıktır. Yazılım; dinamik faktörü, dinamik iletim hatasını, yataklardaki tepki kuvvetleri ve yataklardaki deplasmanı hesaplamaktadır.

Önerilen matematik model ve geliřtirilen yazılım (NLGRD versiyon 3.0), elde edilen sayısal sonuçların literatürde bulunan deneysel sonuçlarla karşılaştırılmasıyla doğrulanmıřtır. Sonuçlar, aynı zamanda önceki doğrusal olmayan modellerle bulunan sonuçlarla da karşılaştırılmıřtır. Yatak direngenliđi, yataklardaki boşluklar ve dişlilerdeki boşluklar gibi çeřitli sistem parametrelerinin etkileri incelenmiřtir. Yataklardaki boşlukların doğrusal olmayan özelliklerinin diđer sistem özellikleriyle etkileřimleri üzerinde özellikle durulmuřtur.

Anahtar Kelimeler: Diřli dinamiđi, Diřli kavrama modeli, Doğrusal olmayan diřli dinamiđi, Doğrusal olmayan yataklar, Dinamik faktör.

To the one who did not leave me alone...

ACKNOWLEDGEMENTS

The author wishes to express his Deepest gratitude and appreciation to his sUpervisor Prof. Dr. H. Nevzat ÖZGÜVEN for his continuous help and guidance and encouragement throughout this studY.

The author would also like to thank his parents Şevkiye and Mustafa GÜRKAN and his brother Hilmi GÜRKAN for their endless help since the beGinning of primary school till the end of master stUdy.

TABLE OF CONTENTS

PLAGIARISM.....	iii
ABSTRACT	iv
ÖZ	vi
DEDICATION	viii
ACKNOWLEDGEMENTS	ix
TABLE OF CONTENTS	x
LIST OF TABLES	xiii
LIST OF FIGURES	xiv
NOMENCLATURE	xvi
ABBREVIATIONS	xix

CHAPTERS

1	INTRODUCTION.....	1
1.1	General.....	1
1.2	Literature Survey	2
1.2.1	Dynamic Factor	2
1.2.2	Mathematical Models	4
1.3	Scope of the Thesis.....	15
2	PROBLEM FORMULATION AND DYNAMIC MODELING OF SYSTEM ELEMENTS	17
2.1	Introduction	17
2.2	Theory.....	18
2.3	Formulation of System Elements	19
2.3.1	Finite Element Modeling of Flexible Shafts.....	19
2.3.2	Formulation of Rigid Disks	21
2.3.3	Formulation of Nonlinear Bearings.....	21
2.3.4	Formulation of Gear Mesh	24

3	MODELING OF NONLINEARITIES BY DESCRIBING FUNCTIONS.....	34
3.1	Introduction	34
3.2	Theory.....	34
3.3	Sinusoidal Input Describing Functions	35
3.4	Describing Function of Dead-Zone Element.....	36
3.5	Periodic Input Describing Functions	37
3.6	Forced Periodic Response	38
3.6.1	Modeling Gear Mesh Interface using Describing Functions.....	39
3.6.2	Modeling Bearing Clearances using Describing Functions	42
4	SOLUTION TECHNIQUE AND COMPUTER PROGRAM NLGRD V3.0	46
4.1	Solution Technique.....	46
4.2	Computer Program	50
4.2.1	Pre-Processor VGR 3.0	52
4.2.2	Processor NLGRD V3.0.....	53
4.2.3	Post Processor.....	56
5	VERIFICATION AND COMPARISON	58
5.1	Introduction	58
5.2	Experimental Validation.....	58
5.2.1	Verification by Kubo’s Experimental Setup	58
5.2.2	Verification by Munro’s Experimental Setup	62
5.3	Comparison with Other Mathematical Models	66
5.3.1	Comparison with DYTE and DYTEM.....	66
5.3.2	Comparison with Kahraman’s Models.....	68
6	PARAMETRIC STUDY AND DISCUSSION.....	72
6.1	Introduction	72
6.2	Effect of Bearing Properties	72
6.2.1	Effect of Bearing Stiffness	72
6.2.2	Effect of Bearing Clearance	76
6.2.3	Interaction Between Bearing Stiffness and Clearance	79
6.3	Effect of Gear Backlash.....	83

6.4	Interaction Between Gear Backlash and Bearing Clearance	86
7	CONCLUSIONS AND RECOMMENDATIONS	88
7.1	Conclusions	88
7.2	Recommendation for Future Work.....	92
	REFERENCES	93
	APPENDICES	93
A	FINITE ELEMENT MATRICES FOR ROTORS AND RIGID DISKS	106
A.1	Rotor Element Matrices	106
A.1.1	Translational Mass Matrix	106
A.1.2	Rotational Mass Matrix.....	106
A.1.3	Torsional Mass Matrix.....	107
A.1.4	Axial Incremental Stiffness Matrix.....	107
A.1.5	Transverse Stiffness Matrix	108
A.1.6	Damping Incremental Stiffness Matrix.....	108
A.1.7	Torsional Stiffness Matrix	109
A.2	Rigid Disk Matrices	109
A.2.1	Translational Mass Matrix	109
A.2.2	Rotational Mass Matrix.....	109
B	INSTALLATION	110
B.1	Installation.....	110
B.2	Visual Geared Rotors 3.0 (VGR 3.0).....	111
C	USER MANUAL.....	113
C.1	Introduction.....	113
C.2	Pre-processor.....	114
C.2.1	Bearing Element.....	115
C.2.2	Weight Element	115
C.2.3	Rotor Element.....	116
C.2.4	Gear Element	118
C.3	Post Processor	129

LIST OF TABLES

Table 5.1 Parameters of Kubo's Setup	60
Table 5.2 Parameters of Munro's Setup	63
Table 6.1 Bearing Properties of Systems I, II, III, IV and V.....	73

LIST OF FIGURES

Figure 2.1 A typical geared rotor system	19
Figure 2.2 Finite Element Rotor	20
Figure 2.3 Schematic Representation of Nonlinear Bearings.....	22
Figure 2.4 Exact and approximate bearing deflection functions	23
Figure 2.5 Dynamic model of a spur gear mesh interface.....	24
Figure 2.6 A typical static transmission error function	28
Figure 2.7 Typical input screen of LDP	30
Figure 2.8 Typical output screen of LDP	30
Figure 2.9 STE Approximations.....	31
Figure 2.10 Backlash Nonlinearity in Gear Pairs.....	33
Figure 3.1 Symmetrical Dead-Zone Nonlinearity	36
Figure 4.1 Iteration scheme used for calculating $\{X\}$ at a particular frequency	51
Figure 4.2 Main Window of user interface	54
Figure 4.3 Assembly order of a geared rotor system.....	55
Figure 4.4 Post processor window.....	57
Figure 5.1 Configuration of Kubo's Setup	59
Figure 5.2 Comparison of NLGRD results with Kubo's Experiment	61
Figure 5.3 Configuration of Munro's System	62
Figure 5.4 Comparison with Munro's experiment at design load (DL)	65
Figure 5.5 Comparison with Munro's experiment at $\frac{3}{4}$ DL	65
Figure 5.6 Comparison between NLGRD V3.0 and DYTE.....	67
Figure 5.7 Comparison between NGRD V3.0 and DYTEM.....	68
Figure 5.8 Comparison between NGRD V3.0 and Kahraman's 1-DOF model	69
Figure 5.9 Comparison between NGRD V3.0 and Kahraman's 3-DOF model.....	70
Figure 6.1 Effect of Bearing Stiffness on DSLR (System I, II and III).....	74
Figure 6.2 Effect of Bearing Stiffness on DSLR (System I and IV)	74
Figure 6.3 Effect of Bearing Stiffness on DSLR for Different k_b/k_h Ratios.	75
Figure 6.4 Effect of Bearing Clearance on DSLR for Kubo's Setup (backlash=0) 77	
Figure 6.5 Effect of Bearing Clearance on DSLR for $k_b/k_h=13$ (backlash=0)	77

Figure 6.6 Effect of Bearing Clearance on Maximum Bearing Force ($k_b/k_h=13$, backlash=0).....	78
Figure 6.7 Effect of k_b/k_h on Max. Bearing Force (with no bearing clearance).....	80
Figure 6.8 Effect of k_b/k_h on Max. Bearing Force (with clearance of 0.003 mm) ..	80
Figure 6.9 Effect of Bearing Clearance on Max. Bearing Force (for $k_b/k_h=50$).....	81
Figure 6.10 Effect of Gear Backlash on DSLR for $k_b/k_h>1000$ (b is in mm).....	84
Figure 6.11 Effect of Gear Backlash on Maximum Bearing Force (for $k_b/k_h>1000$)	85
Figure 6.12 Effect of Gear Backlash on Maximum Bearing Force (for $k_b/k_h=13$) .	86
Figure 6.13 Effect of Gear Backlash for Different Bearing Clearances on Maximum Bearing Force for $k_b/k_h=13$	87
Figure B.1 Main Window of VGR 3.0	114
Figure B.2 Bearing Data Window	115
Figure B.3 Weight Data Window	115
Figure B.4 Rotor Data Window	116
Figure B.5 Shaft Material Data Window	117
Figure B.6 Shaft Misalignment Data Window	117
Figure B.7 Shaft Dimensions Data Window.....	118
Figure B.8 Gear Data Window	119
Figure B.9 Gear Mesh Data Window	120
Figure B.10 Static Transmission Error Data Window	120
Figure B.11 Data Window	121
Figure B.12 Gear Geometry Data Window	122
Figure B.13 Tooth Data Window.....	123
Figure B.14 Tooth Model Data Window	124
Figure B.15 Gear Material Data Window.....	125
Figure B.16 Gear Lead Modification Window	125
Figure B.17 Gear Involute Modification Window.....	126
Figure B.18 Program Control Window.....	127
Figure B.19 Title and Filenames Window.....	128
Figure B.20 Post processor window	130

NOMENCLATURE

•	Differentiation with respect to time
$\{ \}^T, []^T$	Transpose of $\{ \}, []$
a_m, b_m	Coefficients of Fourier Series
$()_b$	Subscript b denotes the bearing
b	Gear backlash
b_b	Radial clearance in bearing
[C]	Damping Matrix
C_m	Average viscous damping coefficient of gear mesh
EI	Bending stiffness per unit curvature
E_t	Complex amplitude of STE
$e_t(t)$	Internal displacement excitation at the gear mesh point
$\{f\}$	Vector of forces
$\{F\}$	Complex amplitude vector of forces
$f_h(p)$	Nonlinear displacement function for relative displacement between gear pair
$f_b(p)$	Nonlinear displacement function for bearing coordinates
G	Shear modulus
$\{G\}$	Complex amplitude vector of internal quasi-linear forces
$()_h$	Subscript h denotes the gear mesh
[H]	Structural damping matrix
i	Iteration number
I_g, I_p	Mass moment of inertia of gear and pinion respectively
I_L, I_M	Mass moment of inertia of load and motor respectively
I_D, I_P	Diametral and polar mass moment of inertia
j	Unit imaginary number
k	Total number of bearings in the system

k_b	Bearing stiffness
k_h	Average mesh stiffness
$[K]$	Stiffness matrix
m	Harmonic component index
m^d	Mass of disk
m^e	Mass per unit length of rotor element
m_p, m_g	Mass of pinion and gear respectively
$[M]$	Mass matrix
n	Total number of harmonic components considered
$\{N\}$	Vector of internal nonlinear forces
p	Relative displacement along the pressure line between meshing gear
P	Complex amplitude of relative displacement P
$\{q\}$	Displacement vector
r_g, r_p	Base circle radii of gear and pinion respectively
R	Relaxation factor
t	time variable
T	Period
T_g, T_p	Gear and pinion torques respectively
W	Static transmitted load
W_1	Mesh forces on gear and pinion respectively
$\{x\}$	Vector of displacements
$\{X\}$	Vector of complex amplitudes of displacements
$\{X_1\}$	Coordinates associated to nonlinear elements
$\{X_2\}$	Coordinates associated to linear elements
y_g, y_p	Displacements in y direction of gear and pinion respectively
Y_g, Y_p	Complex amplitudes of displacements in y direction of gear and pinion respectively
V	pitch line velocity
$[\alpha]$	Quasi-linear receptance matrix

$[\beta]$	Linear dynamic stiffness matrix
$[\Delta]$	Describing functions matrix
$[\gamma]$	Linear receptance matrix
η_h	Hysteric loss factor
η_v	Viscous damping factor
ν	Describing function term
ν_m	Describing function term for m^{th} harmonic component
θ_g, θ_p	Angular rotations of gear and pinion respectively
ω	Excitation frequency
ω_n	Gear mesh torsional resonance frequency

ABBREVIATIONS

AGMA	American Gear Manufacturing Association
DOF	Degree(s) of freedom
DF	Describing function
DSLRL	Dynamic to static load ratio (also named as dynamic factor)
DYTE	Dynamic Transmission Error Program
DYTEM	Dynamic Transmission Error Program- Multi DOF
FFT	Fast Fourier Transformation
LDP	Load Distribution Program
NLGRD	Nonlinear Geared Rotor Dynamics Program
SDOF	Single degree of freedom
OSU	Ohio State University
VB x.0	Visual Basic, version x.0

CHAPTER I

1 INTRODUCTION

1.1 General

With the increased demand for high speed machinery, the mathematical modeling of dynamic analysis of gears has gained importance. Numerous mathematical models have been developed for different purposes in the past three decades.

Moreover, in order to minimize noise and failures by dynamic loads, it is now essential to accurately predict the dynamic behavior of geared systems. As the transmitted power and rotational speed increases, dynamic loads become more significant for the design of gears. Especially when the wear behavior and noise radiation are considered, dynamic loads are much more effective compared with static loads.

Reducing the effective transmission error by stringent quality control measures in gear manufacture and profile modifications are the convenient approaches followed in reducing the gear noise. While these steps are beneficial, they seldom provide dramatic reductions in gear noise and they fail to recognize the contribution of the system dynamics.

Therefore consideration of the effects of gear train dynamics should be included to have a more through design study. In many cases, the system dynamics cause the design to be enormously sensitive to manufacturing induced transmission error. Thus, it is advantageous to minimize the design sensitivity through the use of dynamic analysis for the applications that are sensitive to gear noise.

However, the problem of geared rotor dynamics is difficult to handle due to the change of the number of meshing gear teeth pair in one tooth contact cycle, which leads to variable mesh stiffness. Presence of backlash and other type of nonlinearities will complicate the problem further. Therefore several assumptions must be made before modeling the system. It is obvious that the type of the model, which should be used for a reliable dynamic analysis, depends upon the object of the study as well as the relative dynamic properties of different elements in the system and its configuration. (Özgüven and Houser, 1988b):

Some of the important parameters in gear dynamics are:

- Backlash
- System elements:
 - Gear-mesh interface
 - Prime mover and load inertia
 - Shaft inertia and stiffness
 - Bearing stiffness and clearance
- Gyroscopic effects
- Friction at gear mesh
- Excitations:
 - External excitations
 - Internal excitations

1.2 Literature Survey

1.2.1 Dynamic Factor

The actual tooth load of gears in mesh consists of two main components: a static component corresponding to the transmitted power (which is almost equal to the total load at low speeds of rotation) and a dynamic component which provides a fluctuating increment due to dynamic action. Therefore the history of the dynamic modeling of gears starts with the studies determining dynamic factors.

The dynamic factor (which was then called as *speed factor*) is first introduced by Walter in 1868 (Fisher, 1968) as the ratio of the static load to the dynamic load.

$$\text{Dynamic Factor} = \text{SL}/\text{DL} \quad (1.1)$$

where SL is the static load and DL is the dynamic load.

This factor is then estimated by Barth (1968) as:

$$\text{Dynamic factor} = \frac{600}{600 + V} \quad (1.2)$$

where V is the pitch line velocity in feet per minute.

When it is found that this formula was too conservative at high speeds, Ross (1927) recommended the modified form as:

$$\text{Dynamic factor} = \frac{78}{78 + \sqrt{V}} \quad (1.3)$$

which received acceptance as one of the standard factors used by the American Gear Manufacturing Association (AGMA). This formula and several modified forms of it are still being used in some fields.

Seireg and Houser (1970) used the experimental tests results and developed a new semi-empirical formula for dynamic tooth load that takes into account gear geometries, manufacturing error and operating loads and speeds. It is given as:

$$\text{Dynamic factor} = \sqrt{\frac{78}{78 + \sqrt{V}}} \quad (1.4)$$

Buckingham (1963) attempted to include the effect of flywheels, pulleys, etc. mounted on the gear shaft on the dynamic factor by using empirical equations. He came up with two equations for calculating the dynamic load. It can be regarded that the second equation is just an approximation to the first one. The fundamental Buckingham equation is (Shigley, 1963):

$$W_d = W^t + \sqrt{W_a(2W_2 - W_a)} \quad (1.5)$$

where W_d is dynamic load, W^t is transmitted load, W_a is acceleration load and W_2 is the force required to deform the teeth.

The approximate Buckingham equation is given as (Faires, 1965)

$$W_d = W^t + \frac{0.05V(FC + W^t)}{0.05V + \sqrt{FC + W^t}} \quad (1.6)$$

where F is face width, C is deformation factor and V is pitch line velocity.

Tucker (1971) modified Tuplin equation (Tuplin, 1958) to combine the different dynamic factors being used at that time by AGMA. This research continued in the 1970 and 1980's to find a simple dynamic factor formula. The dynamic factor equations in current AGMA standards (AGMA 218.01) are functions of gear pitch line velocity and the quality of the gears.

In a recently proposed ISO method (ISO TC/60), however, three different approaches are suggested for the calculation of the dynamic factor. While the most complex of them requires a comprehensive dynamic analysis to consider the resonance effects, simplified method predicts the dynamic factor in the sub-critical zone.

1.2.2 Mathematical Models

There are many models for gear dynamics in literature. The objects of these models vary from noise control to stability analysis. Mathematical models developed for the dynamic analysis of gears range from simple single degree-of-freedom (SDOF) models to non-linear rotor dynamic models. An extensive review of the literature on dynamic modeling of gears has been given by Özgüven and Houser (1988a).

In 1931, several works carried by the ASME Researches Committee were published. After the development of the dynamic load equation in this report, little

was done until 1950's. A detailed discussion of these pre-1950 studies was given by Fisher (1961) and Buckingham (1949).

In 1950 a new period in gear dynamics was initiated which incorporated the use of vibratory models in the dynamic analysis of gears. Such mathematical models made it possible to study other dynamic properties of geared system in addition to the dynamic loads.

The first vibratory model of a geared system was introduced by Tuplin (1950). The system is represented by an equivalent constant mesh stiffness and an equivalent mass. By the addition and subtraction of wedges with different shapes at the base of the spring, which represent the mesh stiffness, the gear errors were modeled.

It was the Strauch (1953) who seemed to have the first study considering a periodic excitation. He considered the step changes in mesh stiffness due to changing from single pair to double pair tooth contact.

The effect of various forms of assumed tooth error was discussed by Reswick (1955). He used a simple dynamic model consisting of two masses constrained to move in a horizontal direction and excited by a parabolic or constant acceleration cam which was suddenly moved downward at the pitch line velocity.

Harris (1958) seems to have been the first to emphasize the importance of transmission error by showing that the behavior of spur gears at low speeds can be summarized in a set of static transmission error curves. In his SDOF model, the variation of tooth stiffness, non-linearity in tooth stiffness due to contact loss and manufacturing errors were taken into account. The computational results in general confirmed Harris's contention that non-linear effects are insignificant when damping is more than about 0.07 times of critical.

Utagawa and Harada (1960) suggested an undamped SDOF model which consists of an effective mass and a time varying mesh stiffness. Indeed, the

dynamic loads predicted by the model illustrated good correspondence with experimental work.

Gregory, et al. (1963) extended the theoretical analysis of Harris and made comparisons with experimental observations. The torsional vibratory model of Gregory et al. included sinusoidal-type stiffness variation as an approximation.

Retting, Bosch and Aida et al. (1965-1970) presented the examples of other studies in this area. Each author modeled the vibration characteristics of gears by considering the excitation terms due to tooth profile errors and pitch errors, and by including the variation of teeth mesh stiffness.

Nakamura (1967) investigated the separation of tooth meshing with a SDOF model. He accounted for single and double tooth pair contact with a square wave tooth mesh stiffness variation and used a sinusoidal representation of tooth errors. He adopted a numerical piece-wise solution and concluded that the largest dynamic load occurs immediately after the separation at a specific speed.

Kohler, Pratt and Thomson (1970) developed a six DOF dynamic model with four torsional DOF in the direction of the tooth force on each shaft. They concluded that dynamic loads and noise result primarily from the steady state vibration of a gear system when forced by static transmission error.

Wang and Morse (1972) used the transfer matrix method to obtain the torsional response of a general gear train system excited by external torque. Their model includes shaft and gear web stiffness as well as constant mesh stiffness. Later, Wang extended the model to include gear tooth backlash, linear and nonlinear damping elements.

Wallace and Seireg (1973) used a finite element model to study the stress, deformation and fracture in gear teeth when subjected to dynamic loading. In their model, the gear is treated as a continuum and the mass of the investigated tooth is included.

Rettig (1975) modeled a single stage gear system with six DOF (four lateral and two translation) with all lateral freedoms being in the same direction. The model includes variable tooth mesh stiffness and a simplified formula for the dynamic factor calculations.

Salzer et al. (1977) proposed a six DOF model for a car gearbox which includes time dependent gear tooth stiffness, non-linear bearing stiffness, loss of contact and spacing errors. A real time modeling of the gearbox and analogue computer solutions are used.

Zorzi and Nelson (1977) developed a finite element model for determining the dynamic behavior of a rotor. He used a Rayleigh beam finite element including the effects of the translational and rotary inertia, gyroscopic moments, internal damping and the axial load.

Remmers (1978) expressed the static transmission error of a spur gear as Fourier series in his damped vibratory model. The coupling of the gear pair is represented by a viscous damping and a constant mesh stiffness. The effect of spacing errors, load, design contact ratio and profile modifications are included in the model.

Kubo (1978) used a torsional vibratory model to predict tooth fillet stress and to study the vibration of helical gears with manufacturing and alignment errors. Periodic change of total tooth stiffness was included in the model.

Nelson (1979) utilized Timoshenko beam theory for establishing the shape functions. He derived the system matrices including the effects of rotary inertia, gyroscopic moments, axial load, and shear deformations.

The non-linear vibrations due to gear errors were studied by Kishor (1979) with a constant tooth mesh stiffness model. The model consisted of two gears, two

disks and two shafts. An approximate solution method was employed to solve the system equations.

Kubo and Kiyono (1980) constructed a model for a helical gear pair. The model included torsional and translational degrees of freedom, shaft stiffness, as well as variable mesh stiffness. The model was used to estimate the dynamic exciting force due to both profile and lead errors and due to periodic change of tooth stiffness. Several tooth error forms were investigated and it was concluded that the convex tooth form error is the most harmless among the different kinds studied.

Lees and Pandey (1980) used a finite element model of a gear box to establish a direct link between vibration and gear forces. Additional components were used in this finite element model to represent a gear mesh. The bearing vibration measured at the bearing was used to estimate the gear errors and resulting tooth forces.

In the work published by Iida et al. (1980), the coupled torsional-transverse vibration of geared system is considered. In their work a two shaft-two gear system was analyzed by assuming that one of the shafts was rigid, and the response to gear eccentricity and mass unbalance was determined. They showed that transverse vibrations couples with torsional vibrations even though gyroscopic effects are neglected.

Mark (1982) modeled a gear fatigue test apparatus by assuming rigid shafts, rigid gear bodies, and rigid bearing supports. However, the model included the inertia of the shafts and the damping between the slave gear and its shafting. He used a Fourier series representation of the excitation and the computations were carried out, for the most part, in the frequency domain by using the fast Fourier transform computational algorithm.

Troeder et al. (1983) constructed a model which included torsional, lateral and axial vibration of a helical gear pair-shaft-bearing-system. Fourier expansion of

tooth mesh stiffness in the form of a square wave was used in the model. Tooth profile errors, as well as pitch errors were considered in the model developed for a parametric study. The effect of torque change was studied.

An eight DOF model for single stage spur and helical gears is constructed by Küçükay (1984). The model includes the axial vibration of rigid disks which represent gear blanks, as well as torsional, transverse and tipping motions. Periodic tooth mesh stiffness, tooth errors and external torque were considered. The load dependent contact ratio and nonlinearities due to separation of teeth are also considered in the model. Steady state solution for the determination of dynamic tooth displacements and loads were found by using perturbation methods, by using a linearized model in the computation of the loads.

Spots (1984) used the famous spring-wedge analogy of Tuplin to estimate simply the dynamic load to be used in gear design. A SDOF model is used with a constant stiffness. The dynamic load is expressed as the multiplication of the same powers of velocity, stiffness and mass. The equation for dynamic load was then obtained by using the condition that the expression was to be dimensionally homogeneous.

Iwatsubo et al. (1984) studied the rotor dynamics problem of geared shafts by including a constant mesh stiffness and the forcing due to unbalanced mass. The effect of tooth profile error and backlash was neglected. The transfer matrix method was employed in the solution and free and forced vibration analyses were made and the natural frequencies of the resulting linear system were obtained.

Neriya et al. (1985) used the finite element method for dynamic analysis of geared trained rotors. They modeled a single gear as a two mass-two spring-two damper system, one of the set representing a tooth and the other one representing the gear itself. The shafts were also included, and the coupling between torsional and flexural motion was considered in the model. A constant mesh stiffness was assumed. The response of the system to mass unbalance and geometric eccentricity

in the gear was calculated, and the resulting dynamic tooth load was determined by using undamped modes of the system and the equivalent modal damping values.

Lin and Huston (1986) constructed a torsional model for the design of spur gear systems. A variable mesh stiffness was calculated by taking a tooth as a cantilever beam and by considering also the flexibility of the fillet and foundation and the local compliance due to contact forces. Constant damping coefficients are assumed and the friction between gear teeth was included in the model with a frictional torque. A linearized iterative procedure was used for the numerical solution and a computer program is developed.

Özgüven and Houser (1988) developed a SDOF non-linear model for the dynamic analysis of a gear pair. The model includes the effects of variable mesh stiffness and mesh damping, gear errors, profile modifications, and backlash. Two methods are suggested and a computer program is developed for calculating the dynamics mesh and tooth force, dynamic factors and dynamic transmission error by using measured or calculated static transmission error data. They showed that using a constant mesh stiffness with a displacement excitation at the mesh point representing the loaded static transmission error is a very good approach for including the time variation effect of the mesh stiffness.

Kahraman and Singh (1990) developed a SDOF non-linear model. The frequency response characteristics of a spur gear pair with backlash are studied for both external and internal excitations. The mesh stiffness is assumed to be constant. Two solution methods were used, namely the digital simulation technique and the method of harmonic balance. Later, Kahraman and Singh (1991a) extended the SDOF model to include the bearings dynamics. The three DOF model includes the nonlinearities associated with radial clearances in rolling bearings and gear backlash. The mesh stiffness is assumed to be constant. The interactions and differences between internal static transmission error excitation and external torque excitation are discussed.

Kahraman and Singh (1991b) extended further the single and three DOF models to include a sinusoidal or a periodic mesh stiffness. The interactions between the mesh stiffness variation, gear backlash, and bearing clearance were investigated. They found a strong interaction between time-varying mesh stiffness and gear backlash, whereas the coupling between the time varying mesh stiffness and bearing nonlinearities is observed to be weak.

Özgüven (1991a) extended the model of the previous study (Özgüven and Houser, 1988b) to include the effects of shaft and bearings dynamics. The six DOF nonlinear model includes a spur gear pair, two shafts, two inertia representing the load and prime mover, and bearings. The effect of lateral-torsional vibration coupling on the dynamics of gears is studied.

Özgüven and Özkan (1984) extended the rotor dynamics model of Zorzi and Nelson (1977) to include the combined effects of shear deformation and the internal damping. In their model, they considered the effects of rotary inertia, gyroscopic moments, axial load, internal viscous and hysteric damping and transverse shear deformations.

Kahraman et. al. (1992) used the rotor dynamics model of Özgüven and Özkan (1984) and included a gear pair to the system. The model includes the rotary inertia of shaft elements, the axial load of shaft, flexibility and damping of bearings, material damping of shafts, and the stiffness and the damping of gear mesh. The mesh stiffness is assumed to be constant and the coupling between the torsional and the transverse vibration of gears were considered. The excitation effect of mesh stiffness variation is included in the analysis as a harmonic excitation.

Kesan and Özgüven (1992) extended the model of Kahraman et al. for helical gears. The effect of the higher harmonic terms of the Fourier series representation of the periodic loaded static transmission error function is also included in the analysis.

Kahraman (1993) studied planetary gear trains that are also known as epicyclical gears. They have numerous advantages over simple counter-shaft gear drives, including higher torque-to-weight ratio, compactness, decreased radial bearing loads and reduced noise. In his study he proposed a simplified purely torsional model of a single stage planetary gear set. Closed form expressions for torsional natural frequencies are derived in terms of a limited number of system parameters.

Rook and Singh (1993) studied reverse idler gear system to gain a better understanding of the non-linear behavior. Results of the Galerkin method (multi-term harmonic balance) are compared with results of numerical integration techniques.

Lin et al. (1994) conducted a computer simulation to investigate the effects of both linear and parabolic tooth profile modifications on the dynamic response of low contact ratio spur gears. The effects of the total amount of modification and length of the modification zone were studied at various loads and speeds to find the optimal profile modification for minimal dynamic loading.

Litvin et al. (1995) proposed an approach for the design and generation of low-noise helical gears with localized bearing contact. The approach is applied to double circular arc helical gears and modified involute gears. The reduction of noise and vibration is achieved by application of predesigned parabolic function of transmission errors. Computerized simulation of meshing and contact of designed gears demonstrated that the proposed approach will produce a pair of gears that has a parabolic transmission error function even when misalignment is present.

Cai (1995) developed a vibration model for helical gears, assuming that there are no spacing error and no shaft run-out, in consideration of nonlinear tooth separation phenomenon. In the model, a simple modified stiffness function, including the effect of tooth numbers and addendum modification coefficients, is proposed for a helical involute tooth pair.

Blankenship and Singh (1995) developed a new model that describes mesh force transmissibility in a helical gear pair. New spectral stiffness and transmissibility matrices are developed based on linear theory, which completely characterize the steady state forced response of a helical gear pair. They concluded that additional degree of freedom must be included in the gear mesh interface model in those geared systems analyses which attempts to predict structure borne noise and casing vibration associated with power transmission systems.

Vinayak et al. (1995) developed a model for multi-mesh transmissions with external, fixed center, helical or spur gears. Each gear is modeled as a rigid body with six degrees of freedom. Excitation to the system is considered in the form of either external torque pulsation or internal static transmission error. They compared the results with finite element model results.

Yoon and Rao (1996) presented a method to minimize the STE using cubic splines for gear tooth profile. They conducted a parametric study to establish the superiority of cubic spline based gear profile over the involute profile as well as other profiles based on the use of linear and parabolic tip relieves.

Arıkan (1996) carried out a study on the effect of tooth profile modifications on spur gear dynamic loads. In his work, emphasis is placed on the addendum modification, and the effect of it on the dynamic gear loads is investigated.

Howard, Shengxiang and Wang (2001) developed a dynamic model that incorporates the effect of variations in gear tooth torsional mesh stiffness, using finite element analysis.

Vaishya and Singh (2001) studied the sliding friction induced nonlinearity and parametric effects in gear dynamics. They stated that dynamic interactions result between friction and system parameters due to the sliding resistance and meshing properties. The harmonic balance formulation is developed to predict the dynamic behavior and sub-harmonic instabilities in the system. Finally, the

dynamic effects of friction-induced non-linearity are investigated and the critical parameters are identified.

Velex and Sainsot (2002) presented an original analytical analysis of tooth friction excitations in errorless spur and helical gears based upon a Coulomb friction model. The potentially significant contribution of tooth friction to translational vibrations of pinions and gears is pointed out, particularly in the case of high contact ratio gears.

Wojnarowski and Onishchenko (2003) carried out analytical and experimental investigations of the influence of the deformation and wear on spur gear dynamics. They developed an elastic, dynamic model with worn teeth having two degrees of freedom. Results of the experiments showed that the change of the out lines of the teeth due to wear must be taken into account when calculating the durability of the gear transmission.

Yüksel and Kahraman (2004) employed a computational model of a planetary gear set to study the influence of surface wear on the dynamic behavior of a typical planetary gear set. The overall computational scheme combines a wear model that defines geometric description of contacting gear tooth surfaces having wear and a deformable-body dynamic model of a planetary gear set.

Özgüven, Maliha and Doğruer (2004) presented a new nonlinear dynamic model for a gear-shaft-disk-bearing system. A nonlinear dynamic model of a spur gear pair is coupled with linear finite element models of shafts carrying them, and with discrete models of bearings and disks. The nonlinear elasticity term resulting from backlash is expressed by a describing function, and a method developed in previous studies to determine multi harmonic responses of nonlinear multi-degree-of-freedom systems is employed for the solution. The computer code, Non-Linear Geared Rotor Dynamics (NLGRD) developed in this study is capable of calculating dynamic gear loads, dynamic bearing forces and bearing vibrations, as well as making the modal analysis of the corresponding linear system.

Velex and Ajmi (2005) introduced an original approach to the modeling of pinion–gear excitations by using a three-dimensional model of single-stage geared transmissions. In their model, shape deviations and errors on gears are considered, and the associated equations of motion account for time-varying mesh stiffness as well as torsional, flexural and axial couplings. Using an extended finite element model of a spur and helical gear test rig, the dynamic results from the formulations based on transmission errors are compared with the reference solutions.

Even though there are several mathematical models developed for gear dynamics, there are only a few extensive experimental studies that can be used to verify these models. Attia (1959) presented a set of experimental results giving the dynamic loads in spur gears. Munro (1962) used a lightly damped test rig to measure the dynamic transmission error of a spur gear at different speeds. Kubo (1972) has measured the dynamic tooth stresses in spur gears at a wide range of speeds. Also Kahraman (2004) carried various experimental studies on dynamic analysis of a multi-shaft helical gear transmission systems and experimental investigations of the influence of the lubricant viscosity and additives on gear wear.

1.3 Scope of the Thesis

In this thesis, the advanced gear-shaft-bearing model and software “Nonlinear Geared Rotor Dynamics (NLGRD)” (Özgüven, Maliha and Doğruer, 2004) are modified further to include the features summarized below.

Firstly, the nonlinear effects of the bearing clearances are taken into consideration and the mathematical model is reconstructed accordingly.

Secondly, the computer code developed is rewritten in MatLAB 7.0 to handle the change in the mathematical model and the emphasis is placed on the bearing clearances. By introducing the pre and post processors of the program, any user-error is tried to be minimized. Having completed the analyses, user can see the results graphically without terminating the interface.

Then the model is verified by carrying out some case studies and by comparing the results with available experiment results and the results of other theoretical models.

The effects of several parameters on the dynamic to static load ratio are studied by using the configuration of experimental setup of Kubo as a case study. Effects of bearing stiffness, bearing clearance and gear backlash are studied in depth. Emphasis is placed on the interaction between bearing clearance nonlinearity with the other system parameters and especially the gear backlash.

CHAPTER II

2 PROBLEM FORMULATION AND DYNAMIC MODELING OF SYSTEM ELEMENTS

2.1 Introduction

There are many mathematical models developed for the dynamic analysis of geared systems in literature. Using a single degree of freedom model considering the gear itself may be a fast and accurate approach when the effect of rotor and bearing dynamics can be ignored. Sometimes, it is unavoidable to use a complicated model to include the coupling between the mesh mode and the other modes.

Although there are many multi degree of freedom models for the dynamic analysis of geared rotors, the Finite Element Method (FEM) seems a highly efficient, flexible and accurate approach. The configuration, location and number of elements need not to be fixed when the FEM is used. However, when nonlinearities are included into the model, FEM requires considerably high computational time, which makes lumped models favorable in such cases, since the solution is obtained by numerical integration in time domain and FEM has much larger degrees of freedom. In such cases, harmonic response analysis seems more suitable since the solution is obtained in frequency domain. However, a new lumped model must be constructed each time when the configuration, location and/or number of elements are changed.

Therefore in this study, FEM is employed along with the harmonic response analysis method for nonlinear systems, which reduces the computational time drastically compared to classical FEM applied to nonlinear systems. Thus, the flexibility of FEM is retained without increasing the computational effort.

The model developed in this study is capable of handling stepped rotors, multi-disks and multi-bearings. It also includes the effects of gear-backlash, gear errors, profile modifications and clearances in bearings. While the mesh stiffness is assumed to be constant when the gear pair is in contact, the excitation effect of the mesh stiffness variation is included in the analysis through a displacement excitation at the mesh point.

In this chapter the application of the finite element technique to a non-linear geared rotor system is presented. In this study, the formulation for a geared system composed of two gears with backlash nonlinearity, two rotors, bearings and disk elements, employed in a previous study (Maliha et. al, 2004) has been used and nonlinearity due to clearances in bearings is added to the formulation.

2.2 Theory

A typical generic geared rotor system, which consists of a spur gear pair mounted on flexible shafts, supported by bearings is shown in Figure 2.1. The basic elements of such a system can be listed as follows:

- Flexible shafts
- Rigid disks
- Flexible bearings with clearance nonlinearity
- Gears with flexible teeth and backlash nonlinearity

Assuming that the axial motions of shafts are negligible, each node in the finite element model of a shaft will have five degrees of freedom. Then each finite shaft element has ten degrees of freedom. The rigid disks and gear blanks are modeled as five degrees of freedom rigid elements, whereas flexible bearings are modeled as two degrees of freedom elements having nonlinear stiffness values. Each of these elements will be discussed in detail in following sections.

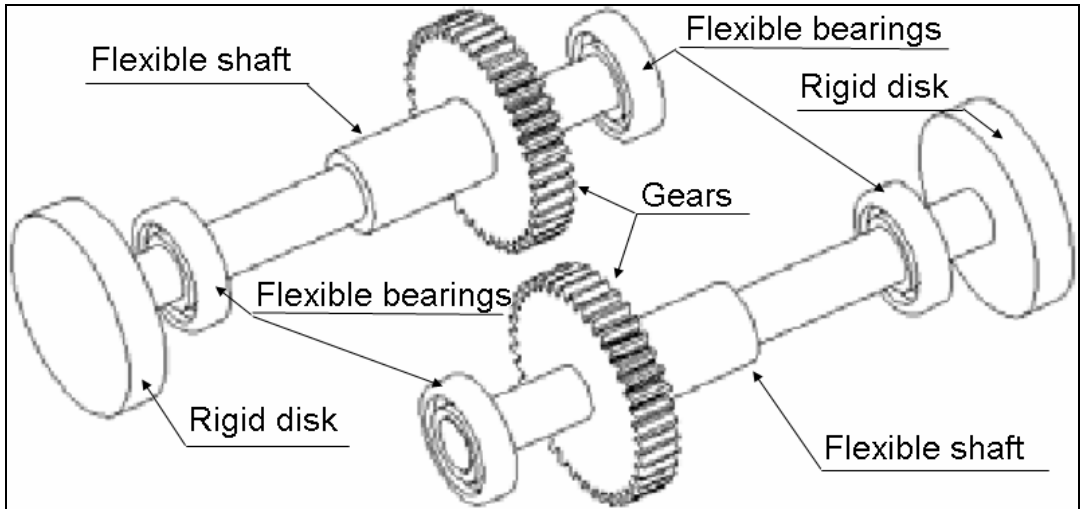


Figure 2.1 A typical geared rotor system

The individual element matrices (mass, damping and stiffness) are then assembled to form the overall system matrices. The two gears are coupled by a non-linear spring damper system. The coupling matrices are then added to the overall system matrices to give the equation of motion in the following form:

$$[M]\{\ddot{q}\} + [C]\{\dot{q}\} + [K]\{q\} + \{N\} = \{f\} \quad (2.1)$$

where $[M]$, $[C]$ and $[K]$ represent the mass, viscous damping and linear stiffness matrices respectively, $\{q\}$ is the vector of displacements and dot denotes differentiation with respect to time, $\{f\}$ and $\{N\}$ represent the external forcing and the internal non-linear forces, respectively.

2.3 Formulation of System Elements

2.3.1 Finite Element Modeling of Flexible Shafts

The shaft elements (or also called *rotor* elements) considered in this study are uniform and circular. The length of rotor element is L and the mass per unit length is m^e . The ten degrees of freedom element has four translations and six rotations as shown in Figure 2.2.

The time dependent end point displacements of the finite rotor element are indicated by $\{q^e\}$, where 10-DOFs are:

- 4 translations (2 at each side): q_1, q_2 and q_6, q_7
- 6 rotations (3 at each side): q_3, q_4, q_5 and q_8, q_9, q_{10}

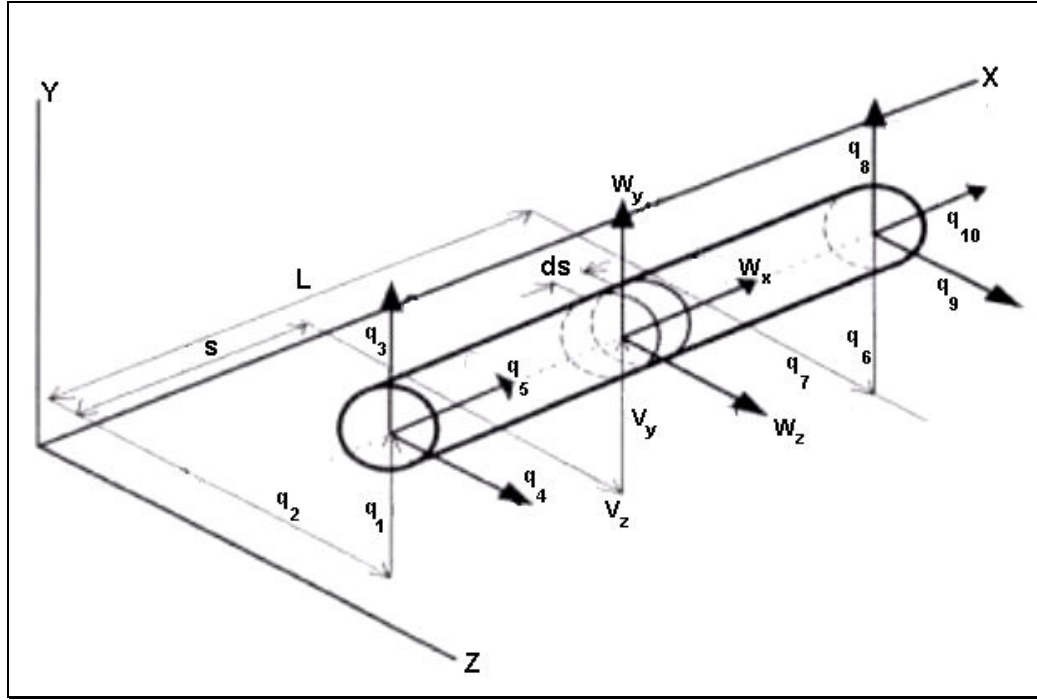


Figure 2.2 Finite Element Rotor

Using the FEM model, first the kinetic and the potential energies of the rotor element are obtained. Then applying the Lagrange equation, the equation of motion for the finite rotor element is obtained as (Özgüven and Özkan, 1984):

$$\left([M_t^e] + [M_r^e] + [M_T^e] \right) \{\ddot{q}^e\} + \left(\eta_v [K_B^e] \right) \{\dot{q}^e\} + \left(\frac{1 + \eta_H}{\sqrt{1 + \eta_H^2}} \left([K_B^e] + [K_T^e] \right) - [K_A^e] + \frac{\eta_H}{\sqrt{1 + \eta_H^2}} [K_C^e] \right) \{q^e\} = \{f^e\} \quad (2.2)$$

in this equation:

- $[K_B^e]$, $[K_T^e]$ and $[K_A^e]$ are transverse, torsional and axial incremental stiffness matrices respectively
- $[M_t^e]$, $[M_r^e]$ and $[M_T^e]$ are translational, rotational and torsional mass matrices respectively
- $[K_C^e]$ is the damping incremental stiffness matrix
- η_H and η_v are hysterical loss and viscous damping factors respectively

- $\{f^e\}$ is the external forcing vector

The elements of these matrices are given in detail in Appendix A.

2.3.2 Formulation of Rigid Disks

Disk elements are assumed to be rigid and planar. Each disk has;

- mass of m^d and diametral mass moment of inertia I_d^D
- polar mass moment of inertia I_d^P
- 5-dof associated such that 2 of them are translations in y and z directions and 3 of them are rotations about the y,z and x directions. (q_1, q_2 and q_3, q_4, q_5).

Then the equation of motion for a disk element can be obtained as:

$$\left([M_T^d] + [M_R^d] \right) \{\ddot{q}^d\} = \{f^d\} \quad (2.3)$$

in this equation:

- $[M_T^d]$ and $[M_R^d]$ are translational and rotational mass matrices respectively (elements of these matrices are given in detail in Appendix A)
- displacements $\{q^d\}^T = \{q_1, q_2, q_3, q_4, q_5\}$

2.3.3 Formulation of Nonlinear Bearings

In this study, the flexible bearings are modeled as 2-DOF elements. The schematic representation of a nonlinear bearing is shown in Figure 2.3.

As shown in the figure, bearings

- are discrete elements
- are modeled as 2-DOF elements, the DOFs being two translations: q_1, q_2
- have radial clearances
- have linear viscous damping coefficient: $C_{YY}, C_{YZ}, C_{ZY}, C_{ZZ}$
- have time invariant stiffness coefficient: $K_{YY}, K_{YZ}, K_{ZY}, K_{ZZ}$

where K_{ij} and C_{ij} are coefficients that represent the forces in i^{th} direction due to a motion in j^{th} direction.

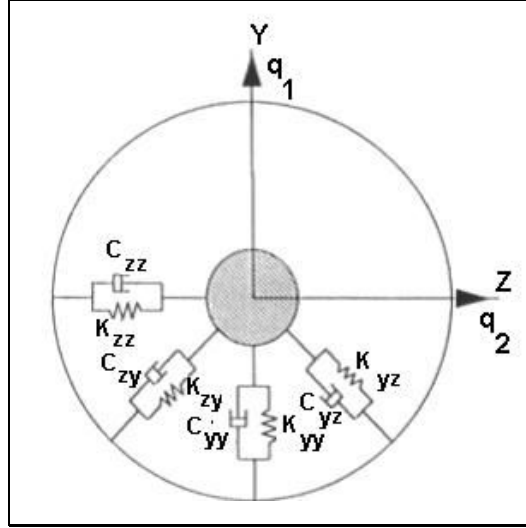


Figure 2.3 Schematic Representation of Nonlinear Bearings

As a result force displacement relation for a bearing can be written as:

$$\begin{bmatrix} C_{YY} & C_{YZ} \\ C_{ZY} & C_{ZZ} \end{bmatrix} \begin{Bmatrix} \dot{q}_1 \\ \dot{q}_2 \end{Bmatrix} + \begin{bmatrix} K_{YY} & K_{YZ} \\ K_{ZY} & K_{ZZ} \end{bmatrix} \begin{Bmatrix} f_b(q_1) \\ f_b(q_2) \end{Bmatrix} = \{f^b\} \quad (2.4)$$

2.3.3.1 Clearance Nonlinearity in Bearings

In the force displacement relation, $f_b(q_i)$ is the displacement function which represent the nonlinearity in bearing and it is defined as *clearance-type dead space function with backlash around the origin*.

$f_b(q_i)$ can be defined as (T.A. Harris, 1966; M. F. White, 1979; T. C. Lim and R. Singh, 1990):

$$f_b(q_i) = \begin{cases} \sum_{r=1}^H [q_i \cos(\alpha_r) - b_b]^n \cos(\alpha_r), & q_i > b_b \\ 0, & -b_b < q_i < b_b \\ -\sum_{r=1}^H [q_i \cos(\alpha_r) - b_b]^n \cos(\alpha_r), & q_i < -b_b \end{cases} \quad (2.5)$$

where α_r is the angular position of the r^{th} rolling element in contact, $2b_b$ is the radial clearance of the bearing, n is the power of the nonlinear force displacement

relationship ($n=1.5$ for ball bearings and $n=10/9$ for roller bearings) and H is the total number of rolling elements in contact under loaded conditions.

Figure 2.4 shows exact and approximate bearing deflection functions f_b for a pre-defined roller bearing. Note that both approximations differ in clearances b_{bA} and b_{bB} , but have the same slope as the exact bearing stiffness curve for $q_i > 3b_b$. To simplify the analysis considerably, linear approximations A and/or B can be accepted.

As a result, nonlinear bearing deflection function $f_b(q_i)$ can be approximated in the piecewise linear form as:

$$f_b(q_i) = \begin{cases} q_i - b_b, & q_i > b_b \\ 0, & -b_b < q_i < b_b \\ q_i + b_b, & q_i < -b_b \end{cases} \quad (2.6)$$

Note that $f_b(q_i) = q_i$ when the clearance (b_b) is equal to zero (i.e linear case).

Describing function method is used to represent this nonlinearity, which will be discussed in detail in the following chapter.

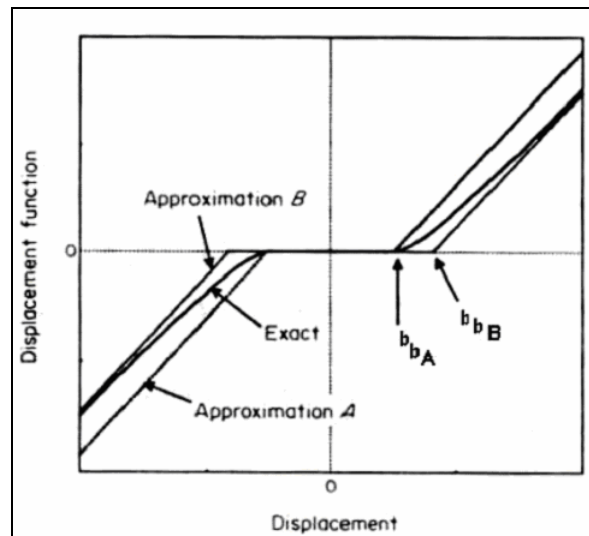


Figure 2.4 Exact and approximate bearing deflection functions

2.3.4 Formulation of Gear Mesh

The gear pair is modeled by two disks which represent the inertia of gears and by a non-linear spring damper system representing the gear mesh. The model includes the following important features:

- the excitation effect of time varying mesh stiffness
- backlash
- separation of teeth in mesh
- gear errors
- profile modifications

Figure 2.5 shows schematical representation of a non-linear gear mesh model.

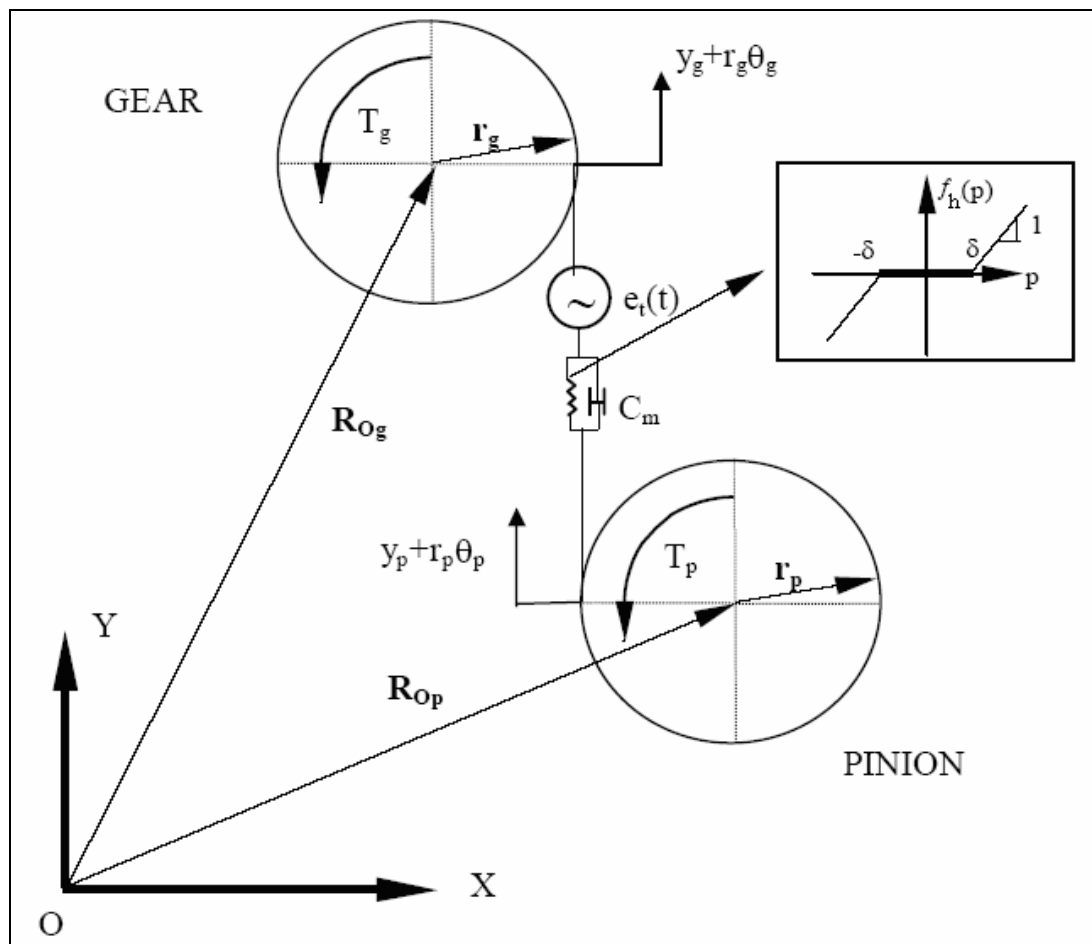


Figure 2.5 Dynamic model of a spur gear mesh interface

As it can be seen from the Figure 2.5, two gears are coupled by a nonlinear displacement function of $f_h(p)$ and viscous damping coefficient of C_m both acting along the pressure line.

Friction forces at the mesh point can be assumed to be negligible (Houser, 1988). Also the damping coefficient can be assumed to be time-invariant (Kahraman, 1999). In the gear mesh model used, the effect of tooth separation is taken into consideration but tooth impact is ignored (Kahraman et al. 1991, Maliha, 1994; Maliha et al. 2004).

Considering the mesh model shown in Figure 2.5, the relative displacement between two gears along the pressure line can be written as:

$$p=y_p - y_g + r_p\theta_p - r_g\theta_g - e_t(t) \quad (2.7)$$

and its time derivative is:

$$\dot{p}=\dot{y}_p - \dot{y}_g + r_p\dot{\theta}_p - r_g\dot{\theta}_g - \dot{e}_t(t) \quad (2.8)$$

where θ_p and θ_g are total angular rotations, r_p and r_g are base circle radii of pinion and gear, respectively and $e_t(t)$ is the loaded static transmission error which will be discussed in detail in the following section.

Then, the differential equations for translational and torsional vibrations of the gear pair can be written as:

$$m_p\ddot{y}_p + W_1 = 0 \quad (2.9)$$

$$m_g\ddot{y}_g - W_1 = 0 \quad (2.10)$$

$$I_p\ddot{\theta}_p + W_1r_p = T_p \quad (2.11)$$

$$I_g\ddot{\theta}_g - W_1r_g = -T_g \quad (2.12)$$

The mesh force W_1 in the Y-direction (along the pressure line) can be written as:

$$W_1 = C_m\dot{p} + k_h f_h(p) \quad (2.13)$$

where $f_h(p)$ is the nonlinear displacement function representing backlash (details of which will be discussed in Section 2.3.4.2), k_h is the mesh stiffness and C_m is the viscous mesh damping coefficient.

Substituting W_1 and \dot{p} expression into the equations of motion yields:

$$m_p \ddot{y}_p + C_m \dot{y}_p - C_m \dot{y}_g + C_m r_p \dot{\theta}_p - C_m r_g \dot{\theta}_g - C_m \dot{e}_t(t) + k_h f_h(p) = 0 \quad (2.14)$$

$$m_p \ddot{y}_p - C_m \dot{y}_p + C_m \dot{y}_g - C_m r_p \dot{\theta}_p + C_m r_g \dot{\theta}_g + C_m \dot{e}_t(t) - k_h f_h(p) = 0 \quad (2.15)$$

$$I_p \ddot{\theta}_p + r_p C_m \dot{y}_p - r_p C_m \dot{y}_g + r_p^2 C_m \dot{\theta}_p - r_p r_g C_m \dot{\theta}_g - r_p C_m \dot{e}_t(t) + r_p k_h f_h(p) = T_p \quad (2.16)$$

$$I_g \ddot{\theta}_g - r_g C_m \dot{y}_p + r_g C_m \dot{y}_g - r_p r_g C_m \dot{\theta}_p + r_g^2 C_m \dot{\theta}_g + r_g C_m \dot{e}_t(t) - r_g k_h f_h(p) = -T_g \quad (2.17)$$

Re-arranging in matrix form:

$$\begin{bmatrix} m_p & 0 & 0 & 0 \\ 0 & m_g & 0 & 0 \\ 0 & 0 & I_p & 0 \\ 0 & 0 & 0 & I_g \end{bmatrix} \cdot \begin{Bmatrix} \ddot{y}_p \\ \ddot{y}_p \\ \ddot{\theta}_p \\ \ddot{\theta}_g \end{Bmatrix} + \begin{bmatrix} C_m & -C_m & r_p C_m & -r_g C_m \\ -C_m & C_m & -r_p C_m & r_g C_m \\ C_m & -r_p C_m & r_p^2 C_m & -r_p r_g C_m \\ -C_m & r_g C_m & -r_p r_g C_m & r_g^2 C_m \end{bmatrix} \cdot \begin{Bmatrix} \dot{y}_p \\ \dot{y}_p \\ \dot{\theta}_p \\ \dot{\theta}_g \end{Bmatrix} + \begin{Bmatrix} k_h f_h(p) \\ -k_h f_h(p) \\ r_p k_h f_h(p) \\ -r_g k_h f_h(p) \end{Bmatrix} = \begin{Bmatrix} C_m \dot{e}_t(t) \\ -C_m \dot{e}_t(t) \\ T_p + r_p C_m \dot{e}_t(t) \\ -T_g - r_g C_m \dot{e}_t(t) \end{Bmatrix} \quad (2.18)$$

As a result, the equation of motion for the gear pair is reduced to the following form:

$$[M_h] \{\ddot{q}_h\} + [C_h] \{\dot{q}_h\} + \{N_h\} = \{f_h\} \quad (2.19)$$

where

$$[M_h] = \begin{bmatrix} m_p & 0 & 0 & 0 \\ 0 & m_g & 0 & 0 \\ 0 & 0 & I_p & 0 \\ 0 & 0 & 0 & I_g \end{bmatrix}, \quad [C_h] = \begin{bmatrix} C_m & -C_m & r_p C_m & -r_g C_m \\ -C_m & C_m & -r_p C_m & r_g C_m \\ C_m & -r_p C_m & r_p^2 C_m & -r_p r_g C_m \\ -C_m & r_g C_m & -r_p r_g C_m & r_g^2 C_m \end{bmatrix} \quad (2.20)$$

and

$$\{N_h\} = \begin{Bmatrix} k_h f_h(p) \\ -k_h f_h(p) \\ r_p k_h f_h(p) \\ -r_g k_h f_h(p) \end{Bmatrix}, \quad \{f_h\} = \begin{Bmatrix} C_m \dot{e}_t(t) \\ -C_m \dot{e}_t(t) \\ T_p + r_p C_m \dot{e}_t(t) \\ -T_g - r_g C_m \dot{e}_t(t) \end{Bmatrix}, \quad \{q_h\} = \begin{Bmatrix} y_p \\ y_p \\ \theta_p \\ \theta_g \end{Bmatrix} \quad (2.22)$$

$$\{N_h\} = \begin{Bmatrix} k_h f_h(p) \\ -k_h f_h(p) \\ r_p k_h f_h(p) \\ -r_g k_h f_h(p) \end{Bmatrix}, \quad \{f_h\} = \begin{Bmatrix} C_m \dot{e}_t(t) \\ -C_m \dot{e}_t(t) \\ T_p + r_p C_m \dot{e}_t(t) \\ -T_g - r_g C_m \dot{e}_t(t) \end{Bmatrix}, \quad \{q_h\} = \begin{Bmatrix} y_p \\ y_p \\ \theta_p \\ \theta_g \end{Bmatrix} \quad (2.23)$$

$$\{N_h\} = \begin{Bmatrix} k_h f_h(p) \\ -k_h f_h(p) \\ r_p k_h f_h(p) \\ -r_g k_h f_h(p) \end{Bmatrix}, \quad \{f_h\} = \begin{Bmatrix} C_m \dot{e}_t(t) \\ -C_m \dot{e}_t(t) \\ T_p + r_p C_m \dot{e}_t(t) \\ -T_g - r_g C_m \dot{e}_t(t) \end{Bmatrix}, \quad \{q_h\} = \begin{Bmatrix} y_p \\ y_p \\ \theta_p \\ \theta_g \end{Bmatrix} \quad (2.24)$$

Describing function method will be used to represent the nonlinear forces vector $\{N_h\}$, the details of which will be discussed in the following chapter.

2.3.4.1 Static Transmission Error Excitation

Excitation mechanism can be divided into two main groups:

- External excitation: Low frequency excitation due to rotating unbalance, geometric eccentricities and prime mover and load torque fluctuations (Houser, 1988) are external excitations and they are typically at low frequencies (the very first multiples of the input shaft speed Ω_p).
- Internal excitation: High frequency excitations caused by manufacturing related profile and spacing errors and the elastic deformation of teeth shaft can be considered as internal excitation.

All of the internal excitations stated above can be combined in an overall error function, known as *Static Transmission Error (STE)*. Static Transmission Error can be defined as the difference between the actual angular position of the driven gears and the position where it would be if the gears were perfect (Houser 1988).

Therefore in gear models, the variable mesh stiffness can be modeled as an average constant mesh stiffness and a periodic displacement excitation (STE) at the mesh point when the system is loaded (Özgüven and Houser 1988b).

There are several studies in the literature for the computation of mesh stiffness and STE. In this study *Load Distribution Program (LDP)*, which was developed at the Ohio State University and has been updated several times since its first development, is used to find mesh stiffness and STE.

A typical static transmission error function for the spur gears with no teeth errors is shown in Figure 2.6. It acts along the line of action and the period is given by $\Omega_h = N_p \Omega_p$ where N_p is the number of teeth on pinion and Ω_p is the rotational speed of pinion.

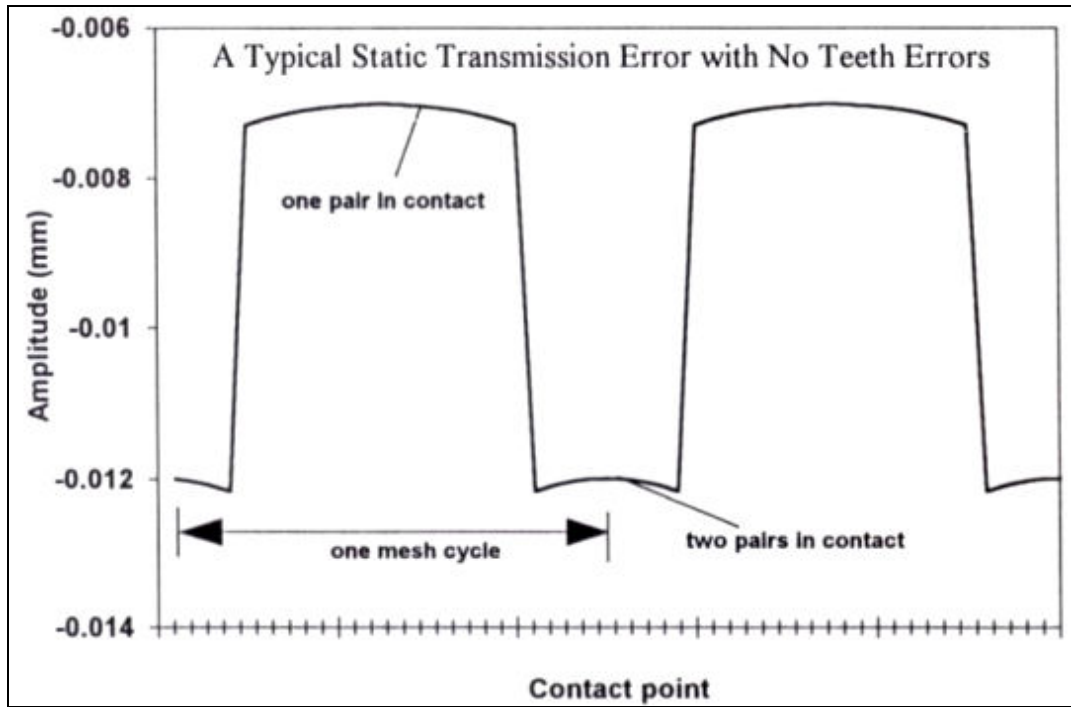


Figure 2.6 A typical static transmission error function

Although the transmission error is periodic, it is not harmonic. Therefore, direct use of it is not suitable for modal analysis. However, a periodic STE function can be defined in terms of harmonic components using *Fourier Series*.

Now consider a periodic function $f(t)$ with period T . Such a function can be represented by Fourier series of the form:

$$f(t) = \sum_{m=1}^{\infty} (a_m \cos(m\omega t) + b_m \sin(m\omega t)) \quad (2.25)$$

where $\omega = 2\pi/T$ is the fundamental frequency.

In this study, STE is approximated by the highest n harmonics and the harmonic components (a_m and b_m) are determined by using either *Rectangular Wave Approximation* or applying *Discrete Fourier Transform (DFT)* Method to the LDP output.

2.3.4.1.1 Load Distribution Program (LDP)

The Load Distribution Program is a computer program for predicting the load distribution across the zone of contact for a single pair of spur or helical gears. The gears may have an internal or an external mesh and may be mounted on shafts between centers or overhung.

The model assumes the load distribution to be a function of the elasticity of gear system and a function of errors or modifications on the gear teeth. Program considers the following effects in calculations:

- Bending deflection of gear bodies and supporting shafts
- Flexibility of bearings and housings
- Torsional deflection of gear bodies
- Bending of teeth in contact
- Local contact deflections
- Shaft misalignment
- Involute profile errors
- Lead errors
- Tooth spacing errors

In this study, LDP output is used for calculating STE, and DFT method is applied to find the harmonic components. Figure 2.7 and Figure 2.8 shows a typical input and output screens of LDP program respectively.

2.3.4.1.2 Rectangular Wave Approximation for STE Calculation

In this approach, the periodic STE is taken as a rectangular wave with the amplitude of the periodic transmission error. The coefficients a_m and b_m can be calculated analytically as:

$$a_m = \frac{-e_t}{m\pi} \left[(3 - \cos(m\omega y)) \cdot \sin\left(m\omega \frac{x}{2}\right) - \sin(m\omega y) \cdot \cos\left(m\omega \frac{x}{2}\right) \right] \quad (2.26)$$

$$b_m = \frac{-e_t}{m\pi} \left[(\cos(m\omega y) - 1) \cdot \cos\left(m\omega \frac{x}{2}\right) - \sin(m\omega y) \cdot \sin\left(m\omega \frac{x}{2}\right) \right] \quad (2.27)$$

where $(x+y)/y$ is the gear contact ratio and e_t is the amplitude of the STE function.

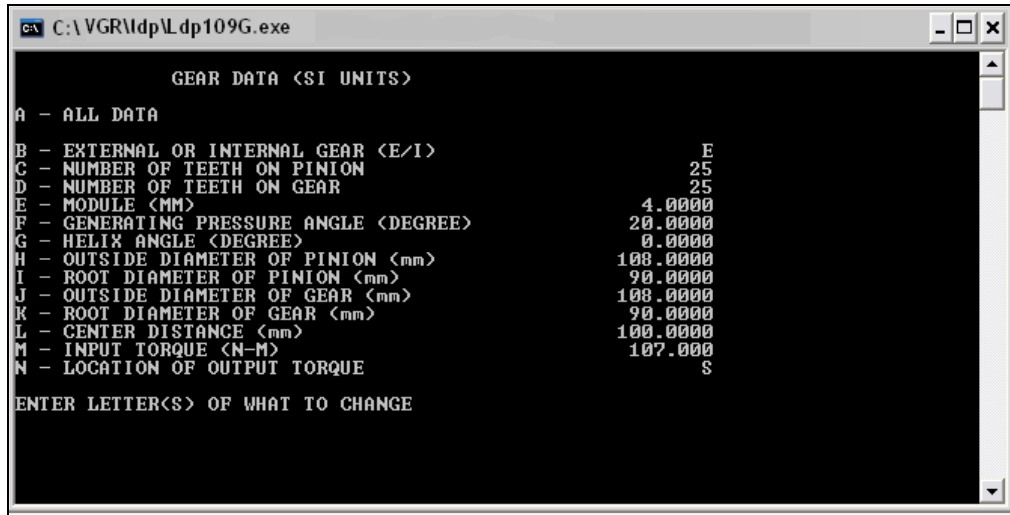


Figure 2.7 Typical input screen of LDP

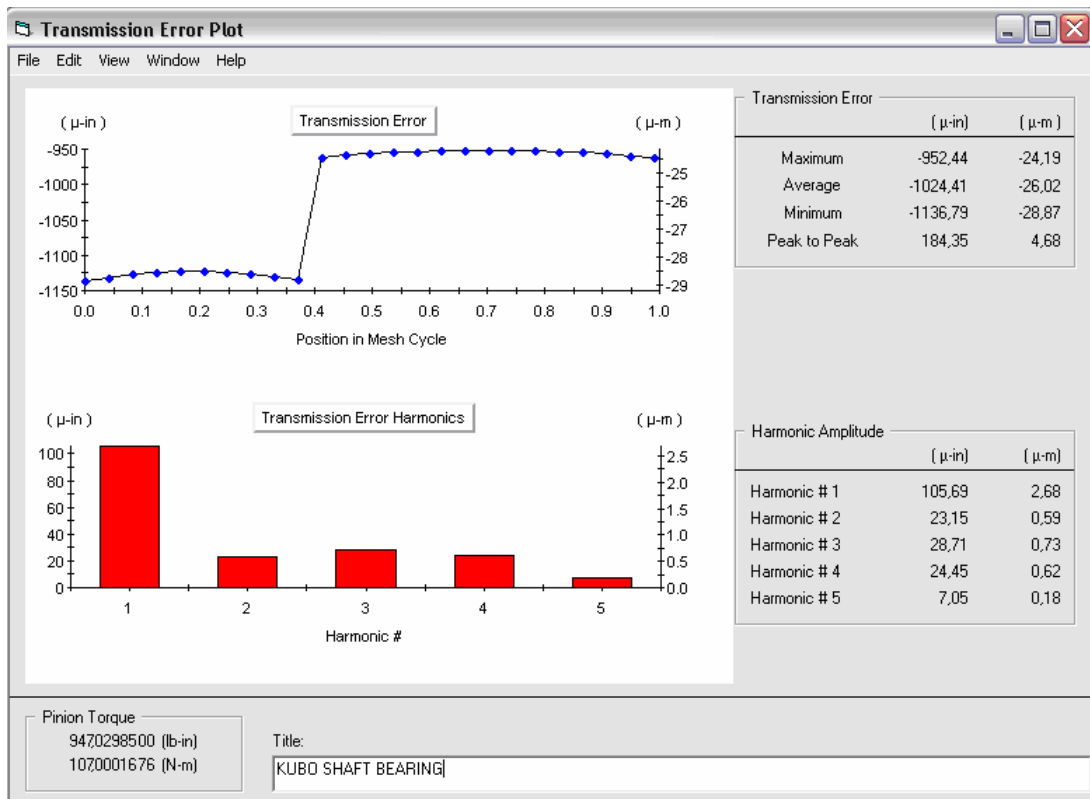


Figure 2.8 Typical output screen of LDP

This approximation for STE calculation is illustrated in Figure 2.9 with the highest 5 harmonics.

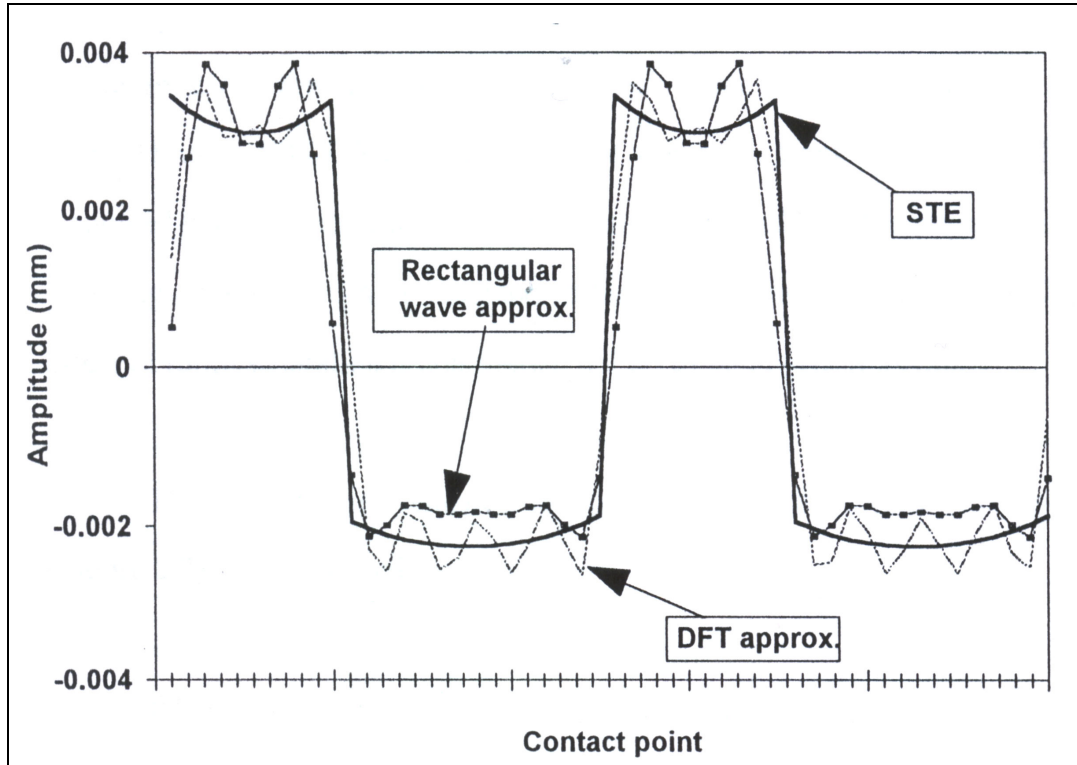


Figure 2.9 STE Approximations

2.3.4.1.3 Discrete Fourier Transform (DFT) Method for STE Calculation

The expression for Fourier coefficients in DFT is given as:

$$a_m + ib_m = \frac{1}{N} \sum_{r=0}^{N-1} x_r e^{\frac{i(2\pi mr)}{N}} \quad (2.28)$$

where N and x_r are the number and the amplitude of discrete data points obtained from LDP program respectively. It should be noted that the maximum calculated harmonics (m) should be less than $N/2$ to prevent aliasing (Newland, 1987).

This method for STE calculation is illustrated in Figure 2.9 with the highest 5 harmonics. As shown in the figure, the DFT approximation is closer to the real STE function. Nevertheless, rectangular approximation gives a satisfactory

approximation in case of no tooth profile modifications and errors. Therefore, the rectangular wave approximation can be useful if the STE data is not available. Also the rectangular approximation can be taken as the reference to see the effect of tooth profile modifications.

However, when there are profile modifications or errors on gear tooth, STE will not be in the form of rectangular wave. Consequently, LDP should be used to calculate STE function and DFT should be applied to find the Fourier components.

2.3.4.2 Backlash Nonlinearity in Gear Pairs

Backlash can be defined as the amount by which a tooth space exceeds the thickness of the mating tooth. There is always some amount of backlash in a gear pair either to provide better lubrication and to eliminate interference, or due to manufacturing errors and wear. The backlash nonlinearity may cause tooth separation and impact in geared rotor systems. Such impacts may result in extensive vibration and noise problems and large dynamic loads which may affect reliability and life of geared rotor systems (Dudley, 1984).

Previous studies have shown that the dynamic behavior of a system with discontinuous nonlinearities is quite different from the behavior of the same system with continuous nonlinearities. The gear backlash non-linearity is actually a discontinuous and non-differentiable function and it represents a strong nonlinear interaction in the governing differential equations.

In this study, the gear mesh of a spur gear pair is represented by a nonlinear spring and a linear damper. The nonlinear spring can be modeled by a dead space function with backlash of $2b$ and a time invariant mesh stiffness k_h when two gears are in contact, which is actually a similar approach explained in section 2.3.3.1.

For a relative displacement p , the nonlinear displacement function $f_h(p)$ is defined as:

$$f_h(p) = \begin{cases} 0 & \text{if } |p| \leq b \\ \text{sign}(p) \cdot (|p| - b) & \text{if } |p| > b \end{cases} \quad (2.29)$$

Figure 2.10 shows the displacement ($f_h(p)$) function versus relative displacement (p) for a gear pair.

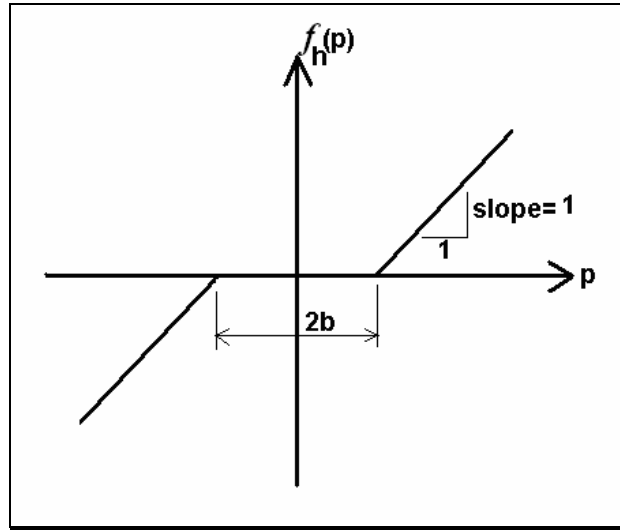


Figure 2.10 Backlash Nonlinearity in Gear Pairs

Then the nonlinear force ($F_h(p)$) on the gear mesh spring can be defined in terms of $f_h(p)$ function as:

$$F_h(p) = k_h \cdot f_h(p) \quad (2.30)$$

where k_h is the invariant gear mesh stiffness.

Note that when there is no backlash in the gear mesh (i.e $b=0$), then nonlinear displacement function reduces to $f_h(p)=p$ and the force on the mesh reduces to $F_h(p)=k_h \cdot p$ (i.e the linear case).

In this study describing function method is used to represent the nonlinear $f_h(p)$ function, details of which will be discussed in the following chapter.

CHAPTER III

3 MODELING OF NONLINEARITIES BY DESCRIBING FUNCTIONS

3.1 Introduction

In this chapter, the method suggested for the forced response analysis of geared rotor systems with backlash and clearance type nonlinearity is presented. The internal forcing that represents the static transmission error is approximated by n harmonics which have the highest amplitudes, and the response to this internal forcing is determined by applying the describing function theory.

First the describing function theory is introduced briefly and then it is used to derive the describing function for a general memory-less static nonlinear periodic force. Finally, the quasi-linear receptance matrix for geared rotor system is formed.

3.2 Theory

The main motivation for describing function (DF) techniques is the need to understand the behavior of nonlinear systems, which in turn is based on the simple fact that every system is nonlinear except in very limited operating regimes. Nonlinear effects exist in most of the systems either by design or due to manufacturing errors and/or wear. Unfortunately, the mathematics required to understand nonlinear behavior is considerably more advanced than that needed for the linear case.

The basic idea of the DF approach for modeling and studying nonlinear system behavior is to replace each nonlinear element with a quasi-linear descriptor or describing function whose gain is a function of input amplitude (Gelb and Vander Velde, 1968; Atherton, 1982). The functional form of such a descriptor is

governed by several factors: the type of input signal, which is assumed in advance, and the approximation criterion, e.g., minimization of mean squared error.

Unlike linear models, quasi-linear models put no restriction on the response amplitude. A nonlinear system has a different quasi-linear equivalent for different types of inputs. This means that a quasi-linearized model exhibits the basic characteristics of nonlinear behavior which is “dependence of response characteristics on input”.

The criterion used for approximation is to minimize the mean-squared difference between the output of that approximation and the output of the nonlinearity. Therefore, the fundamental limitation on the usage of describing functions is that the form of the signal at the input of the nonlinearity must be guessed in advance.

3.3 Sinusoidal Input Describing Functions

The sinusoidal input describing function is a quasi-linear representation for a nonlinear element subjected to a sinusoidal input. It is the most widely known and used describing function.

In this view, if a dynamic nonlinearity $y(x, \dot{x})$ is excited by a sinusoidal input of

$$x = A \cdot \sin \psi \tag{3.1}$$

where $\psi = \omega \cdot t$, then the output is expressible by the Fourier series expansion as:

$$y(A \cdot \sin \psi, A\omega \cdot \cos \psi) = \sum_{m=1}^{\infty} A_m(A, \omega) \cdot \sin(m\omega t + \varphi_m(A, \omega)) \tag{3.2}$$

In the DF analysis, usually the fundamental harmonic component of the output is considered, since the higher harmonics have often smaller amplitudes than the fundamental component (Ogata, 1990).

Then the sinusoidal input describing function, denoted by $v(A,\omega)$ is defined as:

$$v(A,\omega) = \frac{\text{phasor representation of output component at freq. } \omega}{\text{phasor representation of input component at freq. } \omega} \quad (3.3)$$

$$= \frac{A_1(A,\omega)}{A} e^{j\phi_1(A,\omega)}$$

In other words, the describing function is the complex fundamental harmonic gain of a nonlinearity in the presence of a driving sinusoid.

Manipulating equation (3.2), the general form for the sinusoidal input describing function (SIDF) can be obtained as (Gelb and Vander Velde, 1968; Atherton, 1982):

$$v(A,\omega) = \frac{A_1}{A} e^{j\phi_1} = \frac{j}{\pi A} \int_0^{2\pi} y(A \cdot \sin \psi, A\omega \cdot \cos \psi) \cdot e^{-j\psi} \cdot d\psi \quad (3.4)$$

3.4 Describing Function of Dead-Zone Element

The symmetrical dead-zone nonlinear element is shown in Figure 3.1

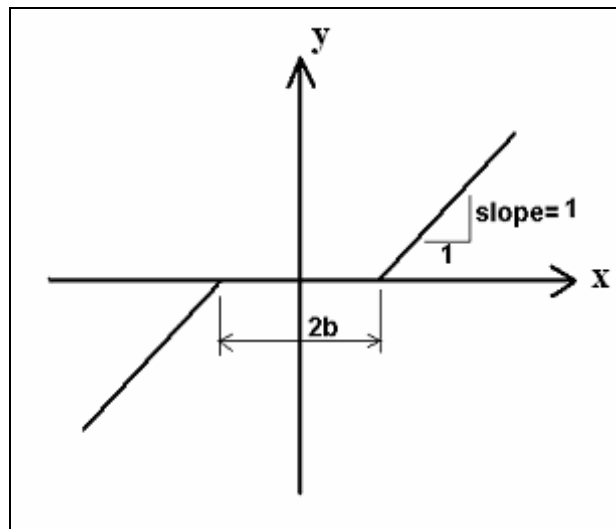


Figure 3.1 Symmetrical Dead-Zone Nonlinearity

The two regions of interest can be defined in terms of b as follows:

$$y(x)=\begin{cases} 0 & \text{if } |x| \leq b \\ \text{sign}(x) \cdot (|x| - b) & \text{if } |x| > b \end{cases} \quad (3.5)$$

The nonlinearity whose input-output characteristics have no dependence on the input derivatives ($y=y(x)$ only) is denoted as *static nonlinearity*. The dead-zone nonlinearity shown in the above equation is therefore a static one.

Moreover, for an odd nonlinearity ($y(x) = -y(-x)$), the imaginary part of the describing function vanishes. As a result, the describing function for an odd static nonlinearity can be defined as (Gelb and Vander Velde, 1968; Atherton, 1982):

$$v(A) = \frac{2}{\pi A} \int_0^{\pi} y(A \cdot \sin \psi) \cdot \sin \psi \cdot d\psi \quad (3.6)$$

Note that the type of gear backlash and the bearing clearance nonlinearity presented in chapter 2 is also odd-static.

3.5 Periodic Input Describing Functions

A periodic input that consists of a bias term and a sum of infinite number of harmonics can be defined as:

$$x = \sum_{m=0}^{\infty} X_m e^{jm\psi} = X_0 + \sum_{m=1}^{\infty} X_m e^{jm\psi} \quad (3.7)$$

The describing function for such an input depends on the bias level (X_0), the amplitudes of the sinusoids (X_m) and the frequencies ($m\omega$). The approximating gain to the bias input component for a dead-zone nonlinearity element is:

$$v_{X_0} = \frac{1}{\pi X_0} \int_0^{\pi} y(x) d\psi \quad (3.8)$$

and the gain to the sinusoidal input component is:

$$v_{X_m} = \frac{2}{\pi X_m} \int_0^{\pi} y(x) \cdot \sin(m\psi) \cdot d\psi \quad (3.9)$$

3.6 Forced Periodic Response

The equation of motion of an axisymmetric nonlinear geared rotor in which the damping is constant and the nonlinearities are involved only in the elastic part of the system can be written as (Genta and Bona, 1990):

$$[M]\{\ddot{x}\} + [C]\{\dot{x}\} + [K]\{x\} + \{N\} = \{f\} \quad (3.10)$$

where $\{N\}$ shows the nonlinear internal forces in the system.

If the external forcing is periodic, then it can be represented as a sum of infinite number of harmonics as:

$$\{f\} = \sum_{m=0}^{\infty} \{f\}_m = \text{Im} \left(\sum_{m=0}^{\infty} \{F\}_m e^{jm\psi} \right) \quad (3.11)$$

It can be assumed that in a geared rotor system, the system response is periodic when the forcing is periodic (Tanrıku et al. 1992), then the relative displacement p and the general displacement vector $\{x\}$ can be expressed as:

$$p = \sum_{m=0}^{\infty} p_m = \text{Im} \left(\sum_{m=0}^{\infty} P_m e^{jm\psi} \right) \quad (3.12)$$

$$\{x\} = \sum_{m=0}^{\infty} \{x\}_m = \text{Im} \left(\sum_{m=0}^{\infty} \{X\}_m e^{jm\psi} \right) \quad (3.13)$$

where P_m and $\{X\}_m$ are the complex amplitudes of relative displacement p and general displacement vector $\{x\}$ at $m\omega$, respectively.

Equation (3.13) allows one to transform the nonlinear differential equation (3.10) into the nonlinear algebraic equation:

$$\left(-(m\omega)^2 [M] + j(m\omega)[C] + [K] \right) \{X_m\} + \{N\}_m = \{F\}_m \quad (3.14)$$

This equation can be solved directly by using an iterative technique, which is generally very difficult.

In this study, nonlinearity is associated only with the four degrees of freedom of the dynamic gear mesh interface and the two degrees of freedom of each bearing. Therefore, if there are k number of bearings in the system, then the total number of coordinates connected to a nonlinear element will be $2*k+4$.

3.6.1 Modeling Gear Mesh Interface using Describing Functions

For the gear mesh interface, the nonlinear matrix given by equation (2.22) is:

$$\{N_h\} = \begin{Bmatrix} k_h f_h(p) \\ -k_h f_h(p) \\ r_p k_h f_h(p) \\ -r_g k_h f_h(p) \end{Bmatrix} \quad (3.15)$$

Re-representing the nonlinear function $f_h(p)$ in terms of the describing functions (equations (3.8) and (3.9)) yields:

$$\begin{aligned} f_h(p) &= \sum_{m=0}^{\infty} v_m(A) \cdot P_m \cdot e^{jm\psi} \\ &= \left(\frac{1}{\pi P_o} \int_0^{\pi} f_h(p) \cdot d\psi \right) \cdot P_o + \sum_{m=0}^{\infty} \left(\frac{2}{\pi P_m} \int_0^{\pi} f_h(p) \cdot \sin(m\psi) \cdot d\psi \right) \cdot P_m \cdot e^{jm\psi} \end{aligned} \quad (3.16)$$

and by writing $\{N_h\}_m$ in terms of describing functions, one obtains

$$\{N_h\}_m = \{G_h\}_m e^{jm\psi} \quad (3.17)$$

where

$$\{G_h\}_m = \begin{Bmatrix} v_m \cdot k_h \\ -v_m \cdot k_h \\ r_p v_m \cdot k_h \\ -r_g v_m \cdot k_h \end{Bmatrix} \cdot P_m \quad (3.18)$$

and from equation (2.7), the complex amplitude P_m is:

$$P_m = Y_{p_m} - Y_{g_m} + r_p \theta_{p_m} - r_g \theta_{g_m} - E_{t_m} \quad (3.19)$$

where E_{t_m} is the complex amplitude of the STE at frequency $m\omega$.

Substituting equation (3.19) into (3.18) gives

$$\{G_h\}_m = \begin{Bmatrix} v_m \cdot k_h \cdot (Y_{p_m} - Y_{g_m} + r_p \theta_{p_m} - r_g \theta_{g_m} - E_{t_m}) \\ -v_m \cdot k_h \cdot (Y_{p_m} - Y_{g_m} + r_p \theta_{p_m} - r_g \theta_{g_m} - E_{t_m}) \\ r_p v_m \cdot k_h \cdot (Y_{p_m} - Y_{g_m} + r_p \theta_{p_m} - r_g \theta_{g_m} - E_{t_m}) \\ -r_g v_m \cdot k_h \cdot (Y_{p_m} - Y_{g_m} + r_p \theta_{p_m} - r_g \theta_{g_m} - E_{t_m}) \end{Bmatrix} \quad (3.20)$$

which can be re-arranged in matrix form as:

$$\{G_h\}_m = \begin{bmatrix} v_m \cdot k_h & -v_m \cdot k_h & r_p v_m \cdot k_h & -r_g v_m \cdot k_h \\ -v_m \cdot k_h & v_m \cdot k_h & -r_p v_m \cdot k_h & r_g v_m \cdot k_h \\ r_p v_m \cdot k_h & -r_p v_m \cdot k_h & r_p^2 v_m \cdot k_h & -r_p r_g v_m \cdot k_h \\ -r_g v_m \cdot k_h & r_g v_m \cdot k_h & -r_p r_g v_m \cdot k_h & r_g^2 v_m \cdot k_h \end{bmatrix} \cdot \begin{Bmatrix} Y_{p_m} \\ Y_{g_m} \\ \theta_{p_m} \\ \theta_{g_m} \end{Bmatrix} + \begin{Bmatrix} -v_m \cdot k_h \\ v_m \cdot k_h \\ -r_p v_m \cdot k_h \\ r_g v_m \cdot k_h \end{Bmatrix} \cdot E_{t_m} \quad (3.21)$$

or

$$\{G_h\}_m = [\Delta]_m \cdot \{X_h\}_m + [R]_m \cdot E_{t_m} \quad (3.22)$$

$$[\Delta]_m = \begin{bmatrix} v_m \cdot k_h & -v_m \cdot k_h & r_p v_m \cdot k_h & -r_g v_m \cdot k_h \\ -v_m \cdot k_h & v_m \cdot k_h & -r_p v_m \cdot k_h & r_g v_m \cdot k_h \\ r_p v_m \cdot k_h & -r_p v_m \cdot k_h & r_p^2 v_m \cdot k_h & -r_p r_g v_m \cdot k_h \\ -r_g v_m \cdot k_h & r_g v_m \cdot k_h & -r_p r_g v_m \cdot k_h & r_g^2 v_m \cdot k_h \end{bmatrix}, \quad \{X_h\}_m = \begin{Bmatrix} Y_{p_m} \\ Y_{g_m} \\ \theta_{p_m} \\ \theta_{g_m} \end{Bmatrix} \quad (3.23)$$

$$(3.24)$$

and

$$[\mathbf{R}_m] = \begin{Bmatrix} -\mathbf{v}_m \cdot \mathbf{k}_h \\ \mathbf{v}_m \cdot \mathbf{k}_h \\ -r_p \mathbf{v}_m \cdot \mathbf{k}_h \\ r_g \mathbf{v}_m \cdot \mathbf{k}_h \end{Bmatrix} \quad (3.25)$$

Inserting equations (3.11), (3.12) and (3.17) into (2.19), the gear mesh interface differential equations can be obtained as:

$$\left(-(m\omega)^2 [\mathbf{M}_h] + j(m\omega) [\mathbf{C}_h] + [\Delta_h]_m \right) \{X_h\}_m + [\mathbf{R}]_m \cdot E_{t_m} = \{F_h\}_m \quad (3.26)$$

or

$$\left(-(m\omega)^2 [\mathbf{M}_h] + j(m\omega) [\mathbf{C}_h] + [\Delta_h]_m \right) \{X_h\}_m = \{F_h\}_m - [\mathbf{R}]_m \cdot E_{t_m} \quad (3.27)$$

Inserting the forcing vector $\{F_h\}_m$ (manipulating equation (2.18)) into the above equation yields:

$$\left(-(m\omega)^2 [\mathbf{M}_h] + j(m\omega) [\mathbf{C}_h] + [\Delta_h]_m \right) \{X_h\}_m = \begin{Bmatrix} C_m \dot{E}_{t_m} + \mathbf{v}_m \cdot \mathbf{k}_h \cdot E_{t_m} \\ -C_m \dot{E}_{t_m} - \mathbf{v}_m \cdot \mathbf{k}_h \cdot E_{t_m} \\ T_p + r_p \mathbf{v}_m \cdot \mathbf{k}_h \cdot E_{t_m} \\ -T_g - r_g \mathbf{v}_m \cdot \mathbf{k}_h \cdot E_{t_m} \end{Bmatrix} \quad (3.28)$$

where \dot{E}_{t_m} is the complex amplitude of first time derivative of STE at frequency $m\omega$.

Then $\{X_h\}_m$ can be written as:

$$\{X_h\}_m = [\alpha_h]_m \cdot \{F_q\}_m \quad (3.29)$$

where

$$[\alpha_h]_m = \left[-(m\omega)^2 [\mathbf{M}_h] + j(m\omega) [\mathbf{C}_h] + [\Delta_h]_m \right]^{-1} \quad (3.30)$$

and

$$\{F_q\}_m = \begin{Bmatrix} C_m \dot{E}_{t_m} + v_m \cdot k_h \cdot E_{t_m} \\ -C_m \dot{E}_{t_m} - v_m \cdot k_h \cdot E_{t_m} \\ T_p + r_p v_m \cdot k_h \cdot E_{t_m} \\ -T_g - r_g v_m \cdot k_h \cdot E_{t_m} \end{Bmatrix} \quad (3.31)$$

Therefore, for the gear mesh, $[\alpha_h]_m$ is the response level dependent quasi-linear receptance matrix at frequency $m\omega$. Also note that the forcing vector $\{F_q\}_m$ includes describing function terms (v_m) which are actually functions of response as well. Therefore, the forcing itself is also response level dependent. Solution of this equation is presented in the following chapter.

Note that when backlash in gear mesh is zero (i.e when the system is linear), the integral terms in equation (3.16) reduce to 1 since $f_h(p)=p$ for that case. Therefore one can find the solution for the linear case by taking $v_m = 1$ in above equations.

3.6.2 Modeling Bearing Clearances using Describing Functions

Force displacement relationship for a bearing was given as

$$\begin{bmatrix} C_{YY} & C_{YZ} \\ C_{ZY} & C_{ZZ} \end{bmatrix} \begin{Bmatrix} \dot{q}_1 \\ \dot{q}_2 \end{Bmatrix} + \begin{bmatrix} K_{YY} & K_{YZ} \\ K_{ZY} & K_{ZZ} \end{bmatrix} \begin{Bmatrix} f_b(q_1) \\ f_b(q_2) \end{Bmatrix} = \{0\} \quad (2.4)$$

Let us define the nonlinear bearing forcing vector $\{N_b\}$ as:

$$\{N_b\} = \begin{bmatrix} K_{YY} & K_{YZ} \\ K_{ZY} & K_{ZZ} \end{bmatrix} \begin{Bmatrix} f_b(q_1) \\ f_b(q_2) \end{Bmatrix} \quad (3.32)$$

Then equation (2.4) becomes:

$$\begin{bmatrix} C_{YY} & C_{YZ} \\ C_{ZY} & C_{ZZ} \end{bmatrix} \begin{Bmatrix} \dot{q}_1 \\ \dot{q}_2 \end{Bmatrix} + \{N_b\} = \{0\} \quad (3.33)$$

where

$$\{N_b\} = \begin{bmatrix} K_{YY} & K_{YZ} \\ K_{ZY} & K_{ZZ} \end{bmatrix} \begin{Bmatrix} f_b(q_1) \\ f_b(q_2) \end{Bmatrix} = \begin{Bmatrix} K_{YY}f_b(q_1) + K_{YZ}f_b(q_2) \\ K_{ZY}f_b(q_1) + K_{ZZ}f_b(q_2) \end{Bmatrix} \quad (3.34)$$

Since the nonlinearity type for the bearings is the same that of as gear mesh (dead-zone), the approach explained in section 3.6.1 can be used for quasi-linearization.

Similar to the equations (3.8) and (3.9), DF terms for the bearing displacements can be written as:

$$v_{Q_o} = \frac{1}{\pi Q_o} \int_0^\pi y(q) \cdot d\psi \quad (3.35)$$

$$v_{Q_m} = \frac{2}{\pi Q_m} \int_0^\pi y(q) \cdot \sin(m\psi) \cdot d\psi \quad (3.36)$$

Since the response is periodic, displacement of a bearing (q) can be expressed as:

$$q = \sum_{m=0}^{\infty} q_m = \text{Im} \left(\sum_{m=0}^{\infty} Q_m e^{jm\psi} \right) \quad (3.37)$$

where Q_m is the complex amplitude of the bearing displacement at frequency $m\omega$.

Re-representing the nonlinear function $f_b(q)$ in terms of the above describing functions, one can obtain:

$$\begin{aligned} f_b(q) &= \sum_{m=0}^{\infty} v_m \cdot Q_m \cdot e^{jm\psi} \\ &= \left(\frac{1}{\pi Q_o} \int_0^\pi f_b(q) \cdot d\psi \right) \cdot Q_o + \sum_{m=0}^{\infty} \left(\frac{2}{\pi Q_m} \int_0^\pi f_b(q) \cdot \sin(m\psi) \cdot d\psi \right) \cdot Q_m \cdot e^{jm\psi} \end{aligned} \quad (3.38)$$

By writing $\{N_b\}_m$ in terms of describing functions, one obtains

$$\{N_b\}_m = \{G_b\}_m e^{jm\psi} \quad (3.39)$$

where

$$\{\mathbf{G}_b\}_m = \begin{bmatrix} \mathbf{K}_{YY}v_m(q_1) & \mathbf{K}_{YZ}v_m(q_2) \\ \mathbf{K}_{ZY}v_m(q_1) & \mathbf{K}_{ZZ}v_m(q_2) \end{bmatrix} \cdot \begin{Bmatrix} Q_{1m} \\ Q_{2m} \end{Bmatrix} \quad (3.40)$$

or

$$\{\mathbf{G}_b\}_m = [\Delta_b]_m \cdot \begin{Bmatrix} Q_{1m} \\ Q_{2m} \end{Bmatrix} \quad (3.41)$$

$$\text{where } [\Delta_b]_m = \begin{bmatrix} \mathbf{K}_{YY}v_m(q_1) & \mathbf{K}_{YZ}v_m(q_2) \\ \mathbf{K}_{ZY}v_m(q_1) & \mathbf{K}_{ZZ}v_m(q_2) \end{bmatrix} \quad (3.42)$$

Inserting equations (3.39), (3.41) and (3.44) into (2.4) yields

$$[j(m\omega)[C_b] + [\Delta_b]_m] \{\mathbf{X}_b\}_m = \{0\} \quad (3.43)$$

where

$$[\Delta_b]_m = \begin{bmatrix} \mathbf{K}_{YY}v_m(q_1) & \mathbf{K}_{YZ}v_m(q_2) \\ \mathbf{K}_{ZY}v_m(q_1) & \mathbf{K}_{ZZ}v_m(q_2) \end{bmatrix} \quad (3.44)$$

$$\text{and } \{\mathbf{X}_b\}_m = \begin{bmatrix} Q_{1m} \\ Q_{2m} \end{bmatrix} \quad (3.45)$$

define the quasi-linear receptance matrix such that

$$[\alpha_b]_m = [j(m\omega)[C_b] + [\Delta_b]_m]^{-1} \quad (3.46)$$

which represents the response level dependent quasi-linear receptance matrix at frequency $m\omega$ for the bearings.

Note that when clearance in a bearing is zero (i.e when the system is linear), the integral terms in equation (3.38) reduce to 1 since $f_h(p)=p$ for that case. Therefore one can find the solution for the linear case by taking $v_m = 1$ in above equations.

After calculating $[\Delta_h]_m$ and $[\Delta_b]_m$ matrices, $[\Delta]_m$ matrix is created for the entire system and the overall equation for harmonic response is formed as:

$$(-(m\omega)^2 [M] + j(m\omega)[C] + [K] + [\Delta]_m) \{X\}_m = \{F\}_m \quad (3.47)$$

Let us define the linear dynamic stiffness matrix $[\beta]_m$ and rearrange equation (3.47) as:

$$[\beta]_m \cdot \{X\}_m + \{G\}_m = \{F\}_m \quad (3.48)$$

where

$$[\beta]_m = [-(m\omega)^2 [M] + j(m\omega)[C] + [K]] \quad (3.49)$$

which represent the linear dynamic stiffness matrix at frequency $m\omega$ for the linear part of the system.

The solution of equation (3.47) will be discussed in the following chapter.

CHAPTER IV

4 SOLUTION TECHNIQUE AND COMPUTER PROGRAM NLGRD V3.0

4.1 Solution Technique

The quasi-linear theory presented in previous chapter converts a set of differential equations into a set of nonlinear complex algebraic equations. However, since the DF terms are functions of the response, an iterative process is required. To reduce the computational effort, one can separate the nonlinear equations from the linear ones as suggested in previous studies (Tanrikulu et al. 1992, Maliha et al. 2004). Then the iteration process is applied only for the nonlinear set of equations rather than the whole system.

In this study, the nonlinearity is associated only with the gear mesh and the bearings. If the number of bearings in the system is k , then the total number of nonlinear equations associated with the bearings are $2*k$ since the bearings are modeled as 2 DOF elements.

From the previous section we know that, the nonlinear equations associated with the gear mesh are 4. As a result, total number of nonlinear equations are $2*k+4$. Therefore, one should separate $2*k+4$ nonlinear equations from the linear ones first. Then the iteration process can be applied as follows:

From the previous chapter, equation (3.48) was:

$$[\beta]_m \cdot \{X\}_m + \{G\}_m = \{F\}_m \quad (4.1)$$

Then this equation can be written as:

$$\begin{bmatrix} [\beta_{11}] & [\beta_{12}] \\ [\beta_{21}] & [\beta_{22}] \end{bmatrix} \cdot \begin{Bmatrix} \{X_1\} \\ \{X_2\} \end{Bmatrix} + \begin{Bmatrix} \{G_1\} \\ \mathbf{0} \end{Bmatrix} = \begin{Bmatrix} \{F_1\} \\ \{F_2\} \end{Bmatrix} \quad (4.2)$$

such that $\{X_1\}$ is the displacement vector for the coordinates with nonlinear elements and $\{X_2\}$ is the displacement vector for the remaining ones. Note that subscript m is dropped for simplicity.

Equation (4.2) can be expanded as

$$[\beta_{11}] \cdot \{X_1\} + [\beta_{12}] \cdot \{X_2\} + \{G_1\} = \{F_1\} \quad (4.3)$$

$$[\beta_{21}] \cdot \{X_1\} + [\beta_{22}] \cdot \{X_2\} = \{F_2\} \quad (4.4)$$

Solving equation (4.4) for $\{X_2\}$ gives

$$\{X_2\} = [\beta_{22}]^{-1} \cdot [\{F_2\} - [\beta_{21}] \cdot \{X_1\}] \quad (4.5)$$

Substituting equation (4.5) into (4.3) and noting that $\{G_1\} = [\Delta_{11}] \cdot \{X_1\}$ gives:

$$\{X_1\} = \left[[\beta_{11}] + [\Delta_{11}] - [\beta_{12}] \cdot [\beta_{22}]^{-1} \cdot [\beta_{21}] \right]^{-1} \cdot \left\{ \{F_1\} - [\beta_{12}] \cdot [\beta_{22}]^{-1} \cdot \{F_2\} \right\} \quad (4.6)$$

As shown in equation (4.6), the right hand side contains the nonlinearity matrix $[\Delta_{11}]$ and nonlinear forcing vector $\{F_1\}$ whose elements are written by using DFs and therefore they are the functions of the response vector $\{X_1\}$. Then an iterative solution is required. $\{X_1\}$ should be recalculated in each iteration step in the solution process until convergence.

By using this technique, only the nonlinear coordinates are updated in the iteration procedure rather than all coordinates and this reduces the computational time considerably.

In this study, no external force is taken on the system, and therefore the only excitation is due to the internal mesh force. Therefore $\{F_2\}=0$. Moreover, if the periodic forcing is approximated by the first n harmonics equation (4.6) further simplifies to:

$$\{X_1\}_m = \left[[\gamma]_m + [\Delta_{11}]_m \right]^{-1} \cdot \{F_1\}_m \quad m=0,1,2\dots n \quad (4.7)$$

where

$$[\gamma]_m = \left[[\beta_{11}]_m - [\beta_{12}]_m \cdot [\beta_{22}]_m^{-1} \cdot [\beta_{21}]_m \right] \quad (4.8)$$

Note that equation (4.7) represents $(2*k+4)*(n+1)$ set of nonlinear equations which are coupled by describing functions and have to be solved simultaneously. The coupling terms are functions of vectors $\{X_1\}_0, \{X_1\}_1, \{X_1\}_2, \dots \{X_1\}_n$. The nonlinear set of equations are solved by finding these vectors iteratively and substituting them in the nonlinear DF terms to form the nonlinearity matrix $[\Delta_{11}]$. In order to form the nonlinearity matrix in the first iteration, linear response is used.

The procedure used for solution is summarized below:

- The $(2*k+4)*(n+1)$ set of equations (4.7) are decomposed into $n+1$ set of equations having $2*k+4$ unknowns in $2*k+4$ equations (i.e the vector $\{X_1\}_m$)
- Initially, each vector $\{X_1\}_m$ is calculated by inverting the matrix $\left[[\gamma]_m + [\Delta_{11}]_m \right]$ where the nonlinear terms in $[\Delta_{11}]$ matrix are neglected (i.e. linear response is found).
- After solving for the whole set of vectors $\{X_1\}_m$, the nonlinear terms in matrix $[\Delta_{11}]$ and $\{F_1\}$ are evaluated using the computed vector $\{X_1\}$.
- The previous steps are repeated using the new nonlinearity matrix in each step until obtaining an acceptable convergence for the vector $\{X_1\}$.

Thus matrices of order $2*k+4$ are inverted $n+1$ times instead of inverting a matrix of order N (N is the order of the entire system). Therefore, this reduces the computational time and improves the accuracy and convergence.

The detailed iteration scheme used for calculating the harmonic response amplitudes at a given frequency ω is given below:

1. The system matrices are assembled and mass, damping and stiffness matrices (each of order N) are formed.
2. System coordinates are renumbered such that first 4 coordinates are gear mesh coordinates (equation (2.24)) and following $2 \cdot k$ coordinates are bearing coordinates (where k is the total number of bearings in the system).
3. The quasi linear dynamic stiffness matrix $[\beta]_m$ is formed for the m-th harmonic for the linear part of the system by using equation (3.49)
4. $[\beta]_m$ matrix is separated into $[\beta_{11}]$, $[\beta_{12}]$, $[\beta_{21}]$ and $[\beta_{22}]$ matrices by using the method explained above (equations (4.3) and (4.4)).
5. $[[\gamma]_m + [\Delta_{11}]_m]$ matrix is calculated by using equation (4.8) and by neglecting the nonlinear describing function terms in $[\Delta_{11}]_m$ (i.e letting $v_m = 1$).
6. Excitation vector $\{F_1\}_m$ is calculated using equation (3.31) by neglecting the nonlinear describing function terms (i.e letting $v_m = 1$).
7. Steps 3 to 6 are repeated for $m=0,1,2,\dots,n$ to form $[\gamma]_0, [\gamma]_1, \dots, [\gamma]_n$ and $\{F_1\}_0, \{F_1\}_1, \dots, \{F_1\}_n$
8. The complex displacement amplitude vectors $\{X_1\}_m^i$ are calculated by using equation (4.7).
9. The describing function terms (v_m) are calculated by using $\{X_1\}_m^i$, and $[\Delta_{11}]_0, [\Delta_{11}]_1, \dots, [\Delta_{11}]_n$ matrices are formed by using the method explained in Chapter 3.
10. Steps 5 to 7 are repeated, but this time, describing function terms (v_m) and $[\Delta_{11}]_m$ matrices found in step 9 are used.
11. The complex displacement amplitude vectors at the $(i+1)^{th}$ iteration (i.e. $\{X_1\}_m^{i+1}$) are determined by using equation (4.7).
12. Since the system is highly nonlinear, the new $(i+1)^{th}$ displacement amplitude vectors are updated by applying a relaxation factor (R) as follows:

$$\{X_1\}_m^{i+1} = \{X_1\}_m^{i+1} + R \cdot (\{X_1\}_m^{i+1} - \{X_1\}_m^i) \quad (4.9)$$

13. The iteration is carried until the root mean square error of displacement

$$E_{\text{rms}} = \sqrt{\sum_{m=0}^n \left| \frac{\{X_1\}_m^{i+1} - \{X_1\}_m^i}{\{X_1\}_m^i} \right|^2} \quad (4.10)$$

drops below a certain selected value.

Figure 4.1 shows the iteration scheme at a particular frequency.

4.2 Computer Program

NLGRD V3.0 is a computer program prepared for analyzing the dynamic response of a geared rotor system. NLGRD is a general purpose program which is used to calculate the dynamic to static load ratio (DSLRL), the dynamic transmission error (DTE), bearing forces and the modal properties (natural frequencies and mode shapes) for the linear part of the system, for any two shafts coupled by a spur gear pair and mounted on flexible bearings with clearance.

The program is capable of handling stepped shafts, multi-bearings and multi-disks. It also takes into account the excitation effect of variable mesh stiffness, gear errors and profile modifications, backlash and bearing clearance. The main computer program is composed of two main parts.

The graphical user interface, which is written in Visual Basic 6.0, is named as VGR 3.0 (Visual Geared Rotors) and it is used to form the system from the chosen components, and prepare input files for the second part of the program. In this respect, the emphasis is placed on user friendliness in VGR 3.0. The graphical drawing of the geared rotor system is formed while the user adds new items to the system. Therefore, any user dependent error is minimized. VGR 3.0 is capable of preparing input files for both NLGRD 3.0 and LDP.

The second part of the program, which is written in MatLAB 7.0, is called NLGRD 3.0 and it contains the main solution procedure. The code approximates the STE by the highest n Fourier coefficients.

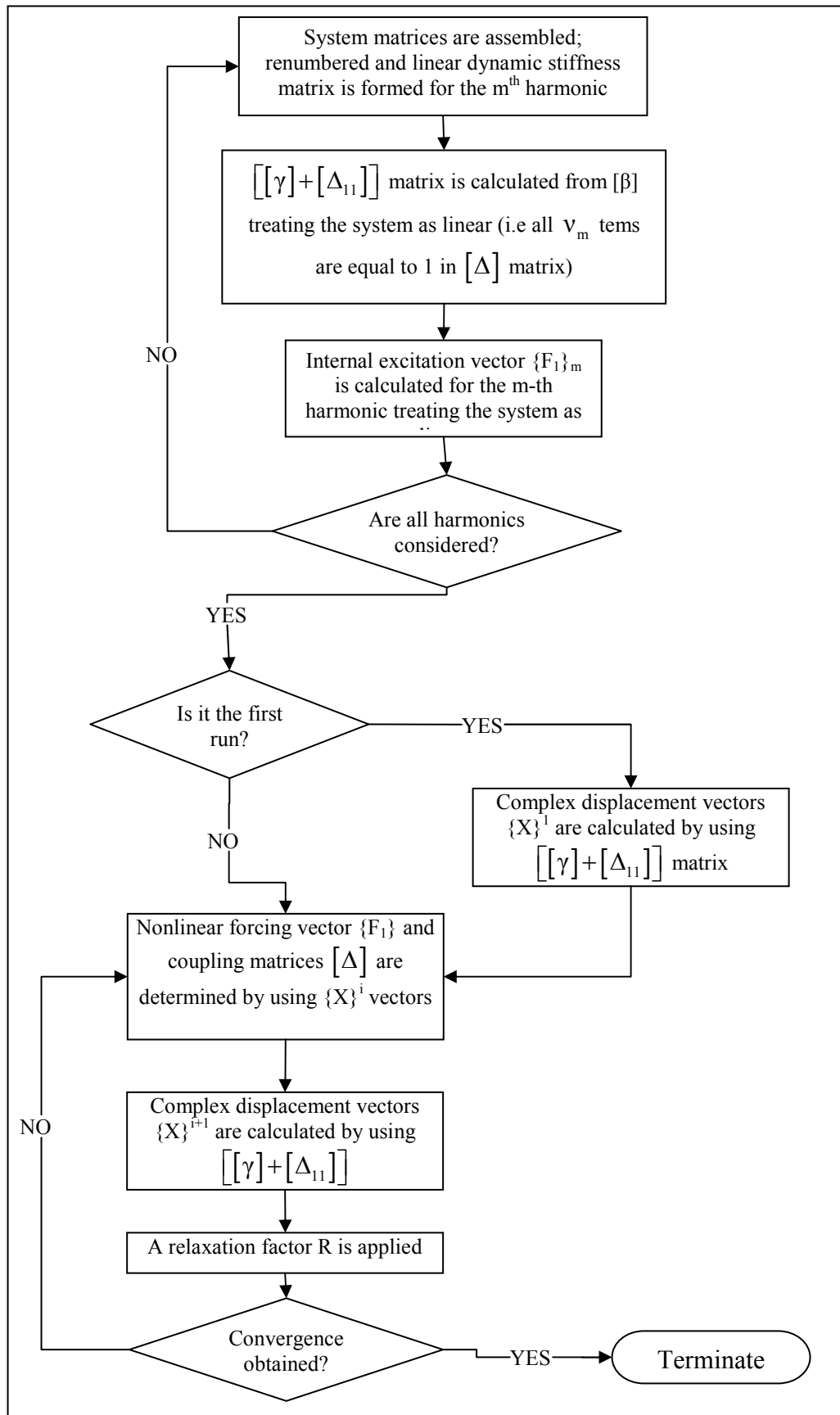


Figure 4.1 Iteration scheme used for calculating $\{X\}$ at a particular frequency

The Fourier series expansion of internal periodic forcing can be obtained analytically if a rectangular wave is assumed or by the Discrete Fourier Transform (DFT) method if the static transmission error data is obtained by using Load Distribution Program (LDP).

In this study, the graphical user interface (VGR) is modified slightly to enable the user to enter the radial clearance values of the bearings. Besides this change, no modification is made to VGR and the same code is used with the previous study (Doğruer, 1999). However, the solution code NGRD V3.0 is a completely new computer code which is written in MatLAB 7.0, and using a new mathematical formulation. In this aspect, the previous solution code (NGRD V2.0), which was written in Fortran 77, is used only as guidance.

4.2.1 Pre-Processor VGR 3.0

Connectivity of the system is formed while the user clicks the basic item buttons. Positions of the items are irrelevant to connectivity. Figure 4.3 shows the main window of user interface VGR 3.0.

However, items must be loaded from left to right and top to bottom. Therefore user must first construct the first shaft from left to right then click stop button. Then start constructing the second shaft and click stop button when finished. The construction of a typical geared rotor system is shown in Figure 4.4.

Loaded items can be dragged anywhere on the screen after clicking the move button.

Geometric properties of the items can be defined by double clicking the item then entering the geometric properties through data windows.

Detailed information about entering the system elements and using VGR 3.0 can be found in Appendix B and in the study carried by Doğruer (Doğruer, 1999).

4.2.2 Processor NLGRD V3.0

After the system is formed through VGR 3.0, solver button is clicked to create the necessary files for the solution code NLGRD 3.0.

By clicking the solver button, MatLAB 7.0 opens automatically and analyzes the system. Therefore, MatLAB 7.0 must be installed to use NLGRD 3.0. After solving the system equations, NLGRD 3.0 creates the output files for the post processor.

NLGRD 3.0 consists of a set of subroutines linked together and uses the dynamic arrays for efficient utilization of memory. The main routine of NLGRD 3.0 is named as *solve.m* and it is the driver of the solution subroutines which solve the system equations by utilizing the algorithm explained in the previous section. *solve.m* also forms the complex receptance matrix and then computes the displacement vectors by iteration.

The important subroutines driven by *solve.m* can be explained in brief as follows:

- *force.m* subroutine calculates the highest n harmonics of a rectangular wave for a given STE amplitude and a gear contact ratio.
- *inforc.m* subroutine reads the STE output file produced by the program LDP and calculates the highest n harmonics by using DFT subroutine.
- *grmesh.m* subroutine forms the mesh stiffness and damping matrices of the gear pair.
- *deltas.m* subroutine forms the $[\Delta]$ matrices after calling *descf.m* subroutine which calculates the describing functions. The number and amplitudes of harmonics and the harmonic order for the describing functions are specified in *solution.m* subroutine.
- *dynf.m* subroutine is used to calculate the maximum dynamic force for a given frequency. Then the dynamic to static load ratio (DSL_R) and the dynamic transmission error (DTE) are calculated.

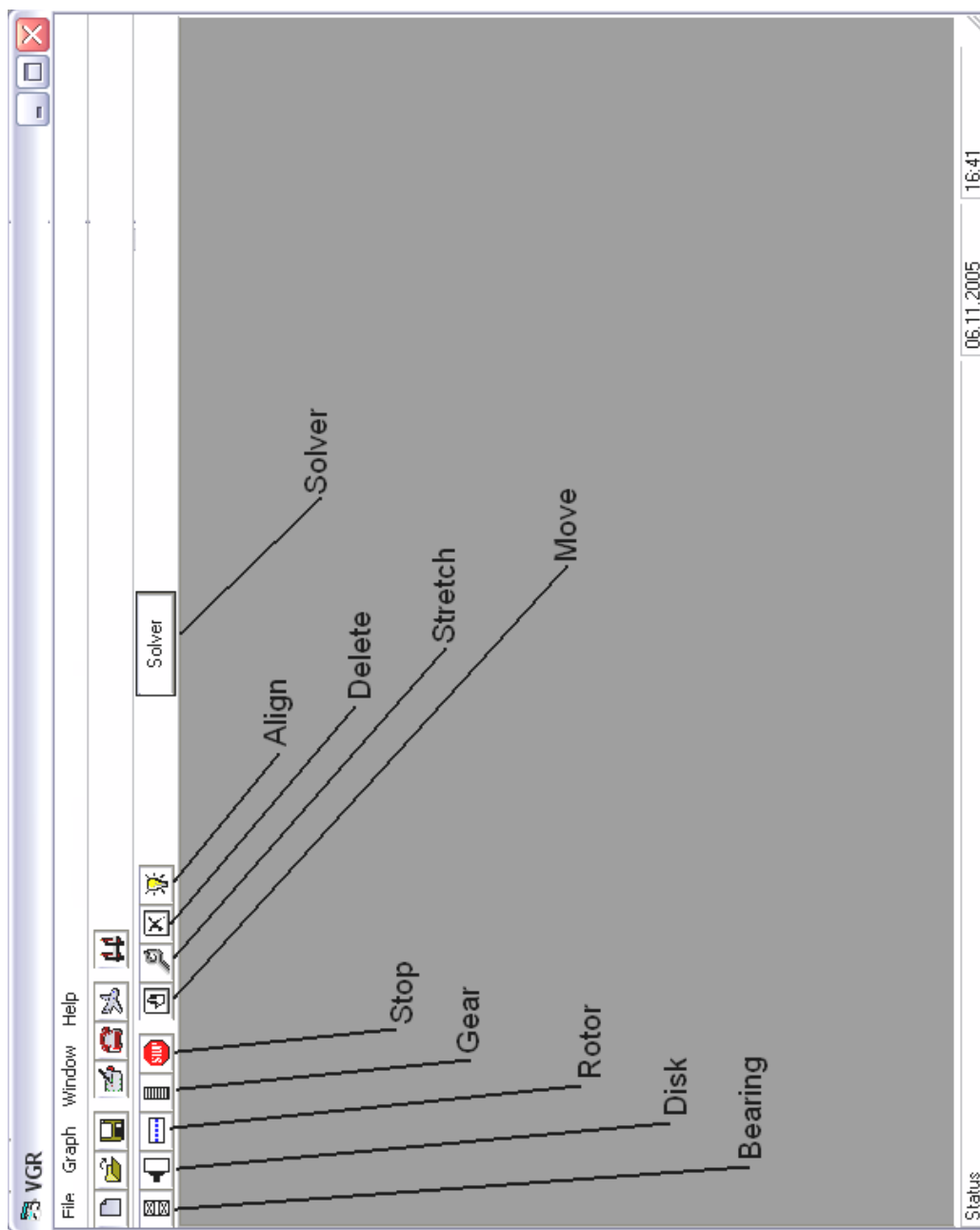


Figure 4.2 Main Window of user interface

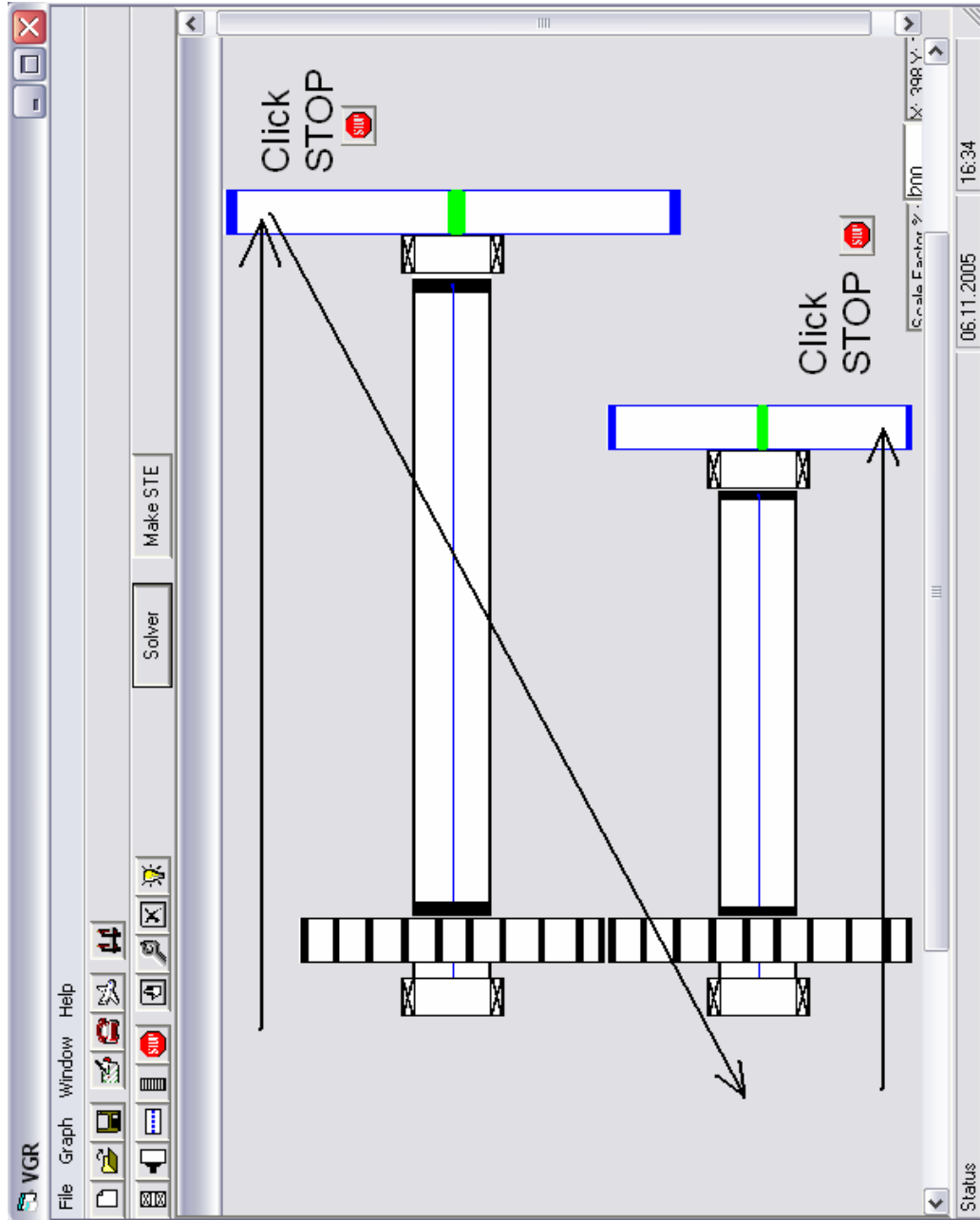


Figure 4.3 Assembly order of a geared rotor system

- *dynf.m* subroutine is used to calculate the maximum dynamic force for a given frequency. Then the dynamic to static load ratio (DSLRL) and the dynamic transmission error (DTE) are calculated.
- *bearing.m* subroutine is used to calculate the bearing forces using the bearing displacements found by the subroutine *solve.m*.

4.2.3 Post Processor VGR 3.0

After NLGRD version 3.0 solves the system equations, results can be seen through user interface graphically. The post processor window is shown in Figure 4.4. User can control the graph window by changing the parameters of control window. For example X and Y axis scale can be changed through the *graph properties* window. The user can take the advantage of seeing both the results and the model itself at the same time.

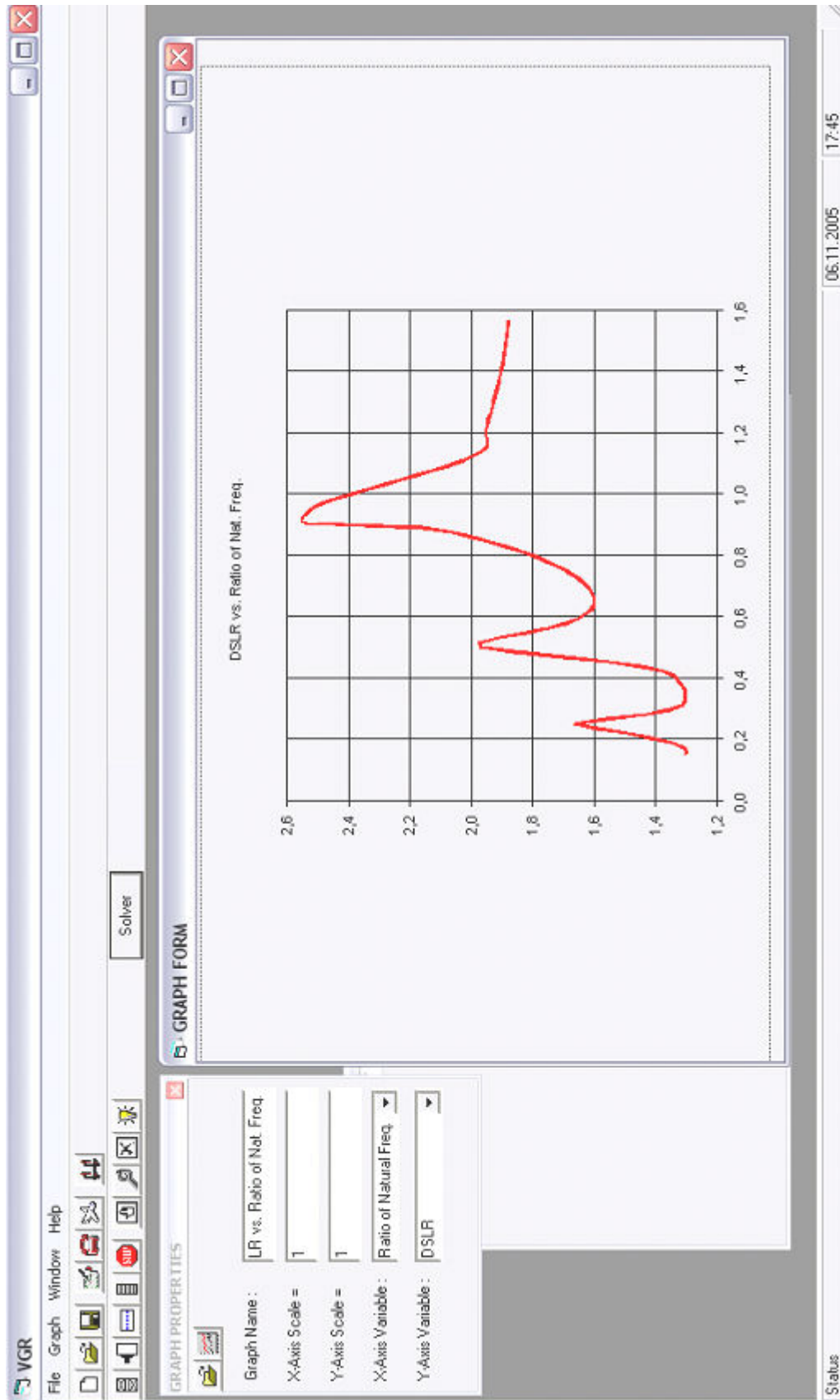


Figure 4.4 Post processor window

CHAPTER V

5 VERIFICATION AND COMPARISON

5.1 Introduction

In this chapter, the nonlinear model developed in this study is verified by comparing the theoretical results obtained by using NGRD V3.0 with the experimental results available, and also with those of the previously tested nonlinear mathematical models.

Firstly, the results of the model are validated by comparing them with the experimental results of Kubo (1972) and Munro (1962).

Then the results of the model suggested is compared with the linear model GRD (Kahraman et al., 1992) and the nonlinear models DYTE (Özgüven and Houser, 1988b), DYTEM (Özgüven, 1991a), Kahraman 1-D model (Kahraman and Singh, 1990) and Kahraman 3-D model (Kahraman and Singh, 1991).

5.2 Experimental Validation

5.2.1 Verification by Kubo's Experimental Setup

Kubo has presented results of extensive experimental studies on the dynamic stresses in spur gears. He used a heavily damped four-square test rig for which the configuration and parameters are shown in Figure 5.1 and Table 5.1, respectively.

Kubo measured the dynamic factor as the ratio of the dynamic to static tooth stress. However in this study, the dynamic factor is defined as the dynamic to static force (or load) ratio (DSLRL). This ratio is equivalent to the dynamic factor

calculation based on the stress analysis under the assumption that the change in the moment arm due to changes in contact point is negligible. Since this assumption cannot be justified, the comparison should be made carefully. Therefore, dynamic factors calculated by NLGRD V3.0 are not expected to exactly match with the experimental values.

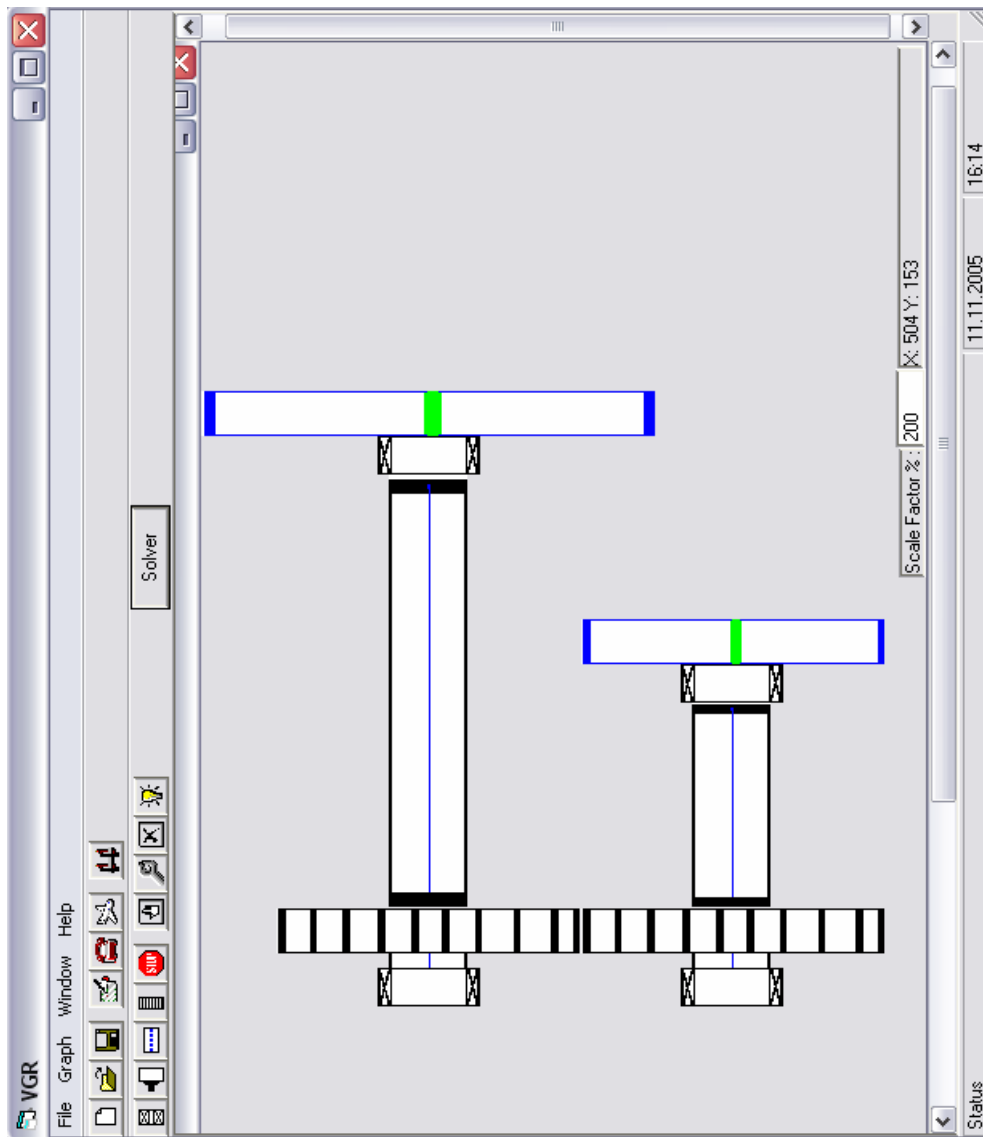


Figure 5.1 Configuration of Kubo's Setup

Table 5.1 Parameters of Kubo's Setup

Module (mm)	4
Number of teeth	25/25
Base diameter (mm)	94
Outside diameter (mm)	108
Rotor diameter (mm)	90
Pitch diameter (mm)	100
Face width (mm)	15
Backlash (mm)	0.1
Pressure angle (deg)	20
Contact ratio	1.56
Mesh stiffness (N/m)	$2.587 \cdot 10^8$
Mesh damping ratio*	0.1
Amplitude of STE (m)	$2.479 \cdot 10^{-6}$
Drive and load torque (N.m)	107.9
Static Load (N)	2295
I_p (kg.m ²)	$1.152 \cdot 10^{-3}$
I_g (kg.m ²)	$1.152 \cdot 10^{-3}$
I_L (kg.m ²)	$1.152 \cdot 10^{-3}$
I_M (kg.m ²)	$5.762 \cdot 10^{-3}$
Bearing stiffness (N/m)	$3.503 \cdot 10^{12}$
Bearing Damping (Ns/m)	$3.503 \cdot 10^5$
Shaft damping ratio	0.005
Length of shaft-1* (mm)	210
Length of shaft-2* (mm)	140

* estimated data

Moreover, Kubo's experimental setup was designed to investigate the standalone effects of gear pair. To achieve this, Kubo used very stiff shafts and bearings to support the gear pair to simulate rigid supports and to decouple mesh mode from the other modes. However, NLGRD V3.0 is developed for analyzing more flexible systems in order to see the coupling effect of mesh mode with other modes by changing system properties such as bearing compliances or rotor properties. In this respect, the simpler models may be sufficient to give accurate results for Kubo's system. However, when the bearings and rotors are more flexible, then NGRD V3.0 is still capable of analyzing the system whereas simpler models cannot take these effects into account.

Nevertheless, the change of dynamic forces with rotating speed can be compared in a qualitative manner rather than a quantitative manner. Comparison of the results of NLGRD V3.0 and Kubo's experiment are shown in Figure 5.2.

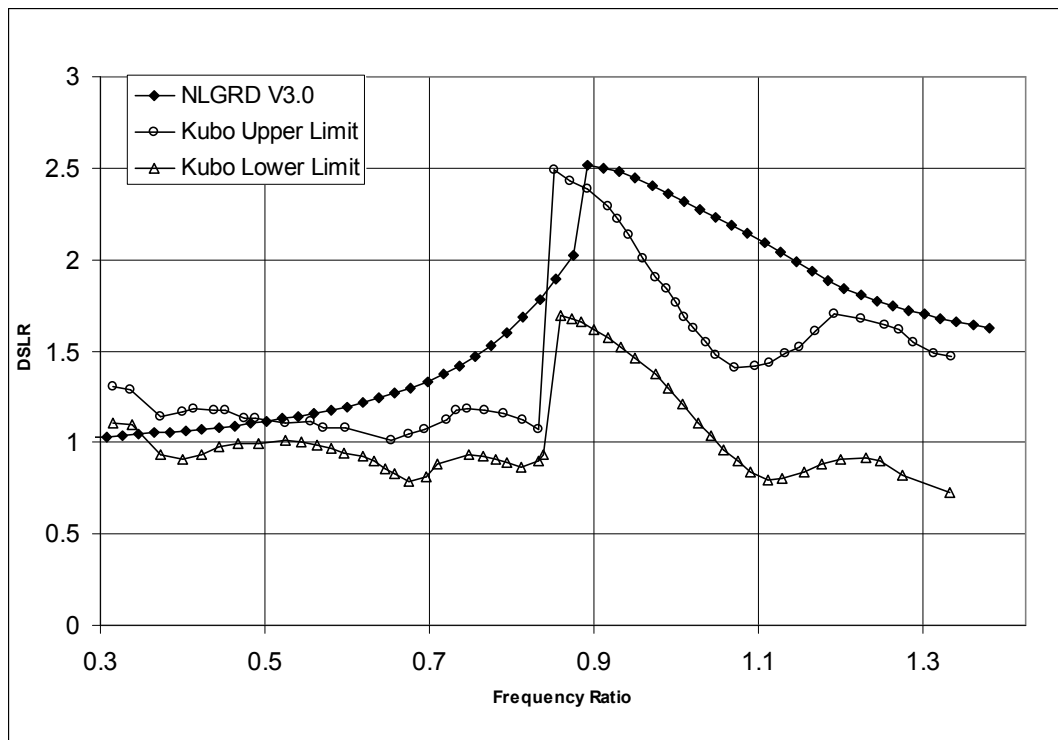


Figure 5.2 Comparison of NLGRD results with Kubo's Experiment

As shown in the figure, the DSLR values calculated by NLGRD V3.0 predict the important features of the experimental results. The jump at the resonant frequency is clearly distinguished whereas the location of the jump is slightly shifted compared to the experimental results. Note that the frequency ratio on the x-axis is defined as the ratio of rotational speed to torsional natural frequency at the mesh mode.

The trend of the dynamic factor is in general in good agreement with Kubo's results. The difference between the experimental results and the calculated ones is mainly due to comparing dynamic factors based on stresses with those based on forces.

5.2.2 Verification by Munro's Experimental Setup

As a second example case, experimental results of Munro (1962) are compared with those of the model developed. Munro used a four-square test rig to measure dynamic transmission error of a spur gear pair for which the configuration and parameters are shown in Figure 5.3 and Table 5.2, respectively.

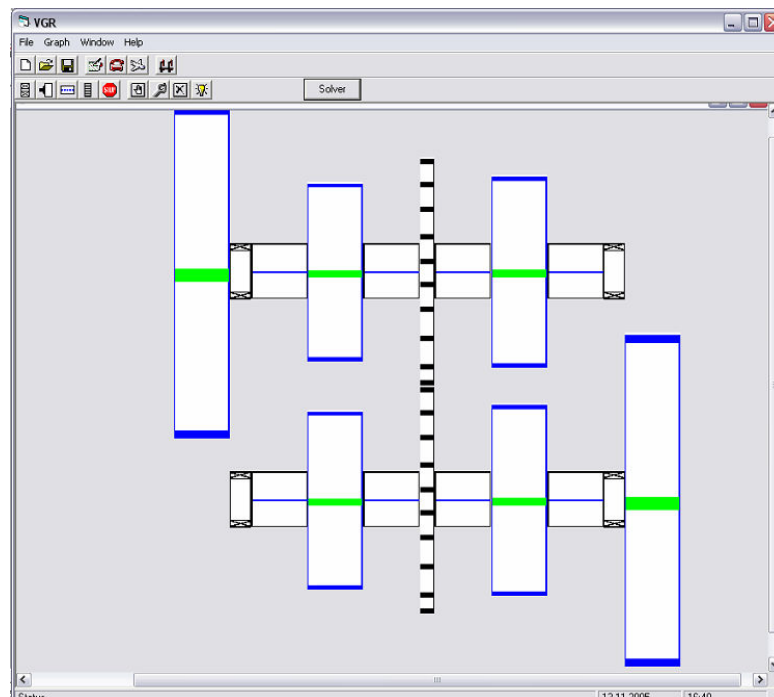


Figure 5.3 Configuration of Munro's System

Table 5.2 Parameters of Munro's Setup

Diametral pitch	4
Number of teeth	32/32
Pitch diameter (mm)	204.8
Face width (mm)	12.7
Backlash (mm)	0.12
Contact ratio*	1.60
Mesh stiffness (N/m)	$3.44 \cdot 10^9$
Mesh damping ratio	0.0175
Amplitude of STE (m)	$1.143 \cdot 10^{-6}$
Static Load (N)	3782
$I_1 = I_3$ (kg.m ²)	0.02563
$I_2 = I_4$ (kg.m ²)	0.03426
I_L^* (kg.m ²)	0.67
I_M^* (kg.m ²)	0.60
Bearing stiffness (N/m)	$5.8 \cdot 10^8$
Bearing Damping (Ns/m)	$5.8 \cdot 10^4$
Shaft damping ratio	0.005
Length of shafts* (mm)	204.8

* Estimated data

Munro selected high precision spur gear with manufacturing errors much smaller than tooth deflections were selected. Tooth profile modifications were applied to obtain a minimum (but not zero) STE at design load (DL) of 3780 N. Other components of the setup (shafts, bearings and casing) were made as rigid as possible.

However, some of the key parameters were not specified by Munro in his publication. For example, it was stated that some additional inertias were added to gears to shift the primary resonant frequency within the operational speed range, but the specific values of such inertias were not given. Moreover, backlash was not

measured or reported explicitly. Therefore, some of the system parameters are estimated from the schematic figures in Munro's publications (Munro, 1962).

The measured and predicted maximum dynamic transmission error (DTE) at the design load and $\frac{3}{4}$ design load are compared in Figure 5.4 and Figure 5.5, respectively.

As it can be seen in Figure 5.4, the subharmonic and resonance frequencies are predicted correctly. However, NGRD V3.0 predicts lower amplitude for the main resonance. This may mainly because of the estimated system parameters. Even though the changes in these parameters seem to be slight, the effects may be more.

As shown in Figure 5.5, NGRD V3.0 predicts the first and the second resonant peak amplitudes very close to the experimental values with a slight shift in the frequency values.

As a result, the whole trend of the results obtained by NGRD V3.0 follow the trend of Munro's experimental results. The jump at the main resonance and the subresonance whose frequency is half of the main resonance are predicted successfully.

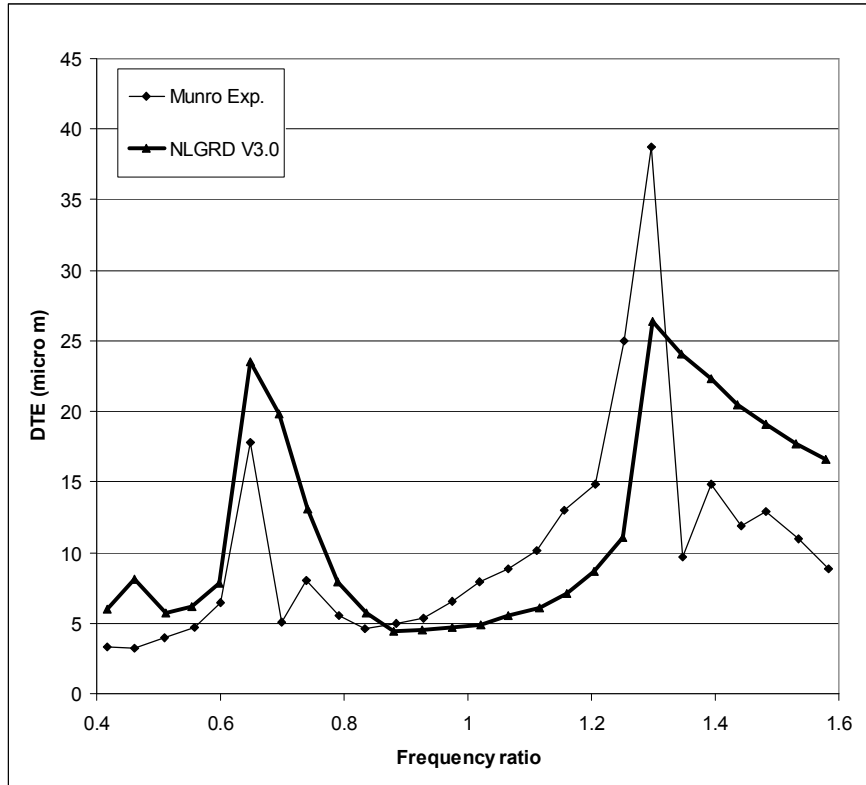


Figure 5.4 Comparison with Munro's experiment at design load (DL)

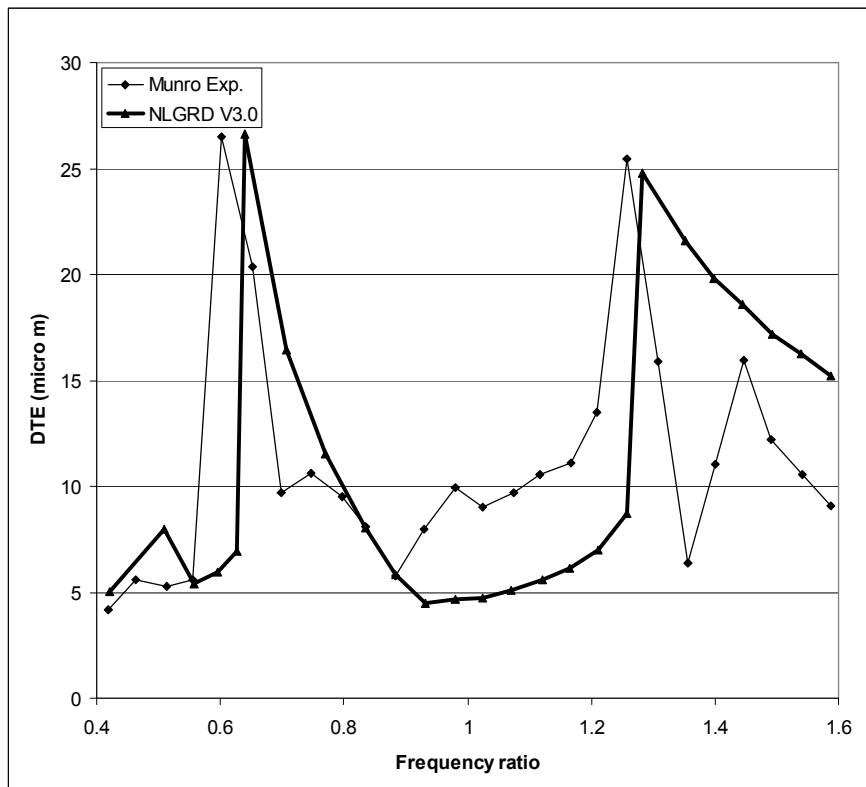


Figure 5.5 Comparison with Munro's experiment at 3/4 DL

5.3 Comparison with Other Mathematical Models

5.3.1 Comparison with DYTE and DYTEM

Özgüven and Houser (1988b) proposed a single degree of freedom nonlinear model which consists of two disks representing the inertia of gears and a spring-damper system representing the gear mesh. The computer program DYTE (Dynamic Transmission Error Program) and the solution were based on the basic assumption that the torsional vibrations of a gear pair can be decoupled from other vibration modes. This assumption is valid when the gear pair is mounted on stiff bearings and the gear shafts have much higher torsional stiffness values compared to mesh stiffness.

The effects of variable mesh stiffness and nonlinearities due to backlash and tooth impact are included in the model.

Later, Özgüven (1991a) improved the model by including the shaft and bearing dynamics. The six degree of freedom model includes a spur gear pair, two shafts, inertias of the prime mover and load, and bearings. The computer program developed is DYTEM (Dynamic Transmission Error Program Multi-DOF).

Both DYTE and DYTEM use two different methods to find the dynamic factors. In the first method, the effect of variable mesh stiffness is included without any approximation, whereas in the second method, variable mesh stiffness is modeled with a constant mesh stiffness value and an internal excitation function (STE), which is actually the same approximation used in NGRD V3.0. Therefore, the second method is used to compare the results obtained from DYTE and DYTEM with NGRD V3.0.

Figure 5.6 shows the dynamic factors obtained by NGRD V3.0 and DYTE for Kubo's gear system given in Table 5.1. As shown in the figure, the results have generally the same shape and trend.

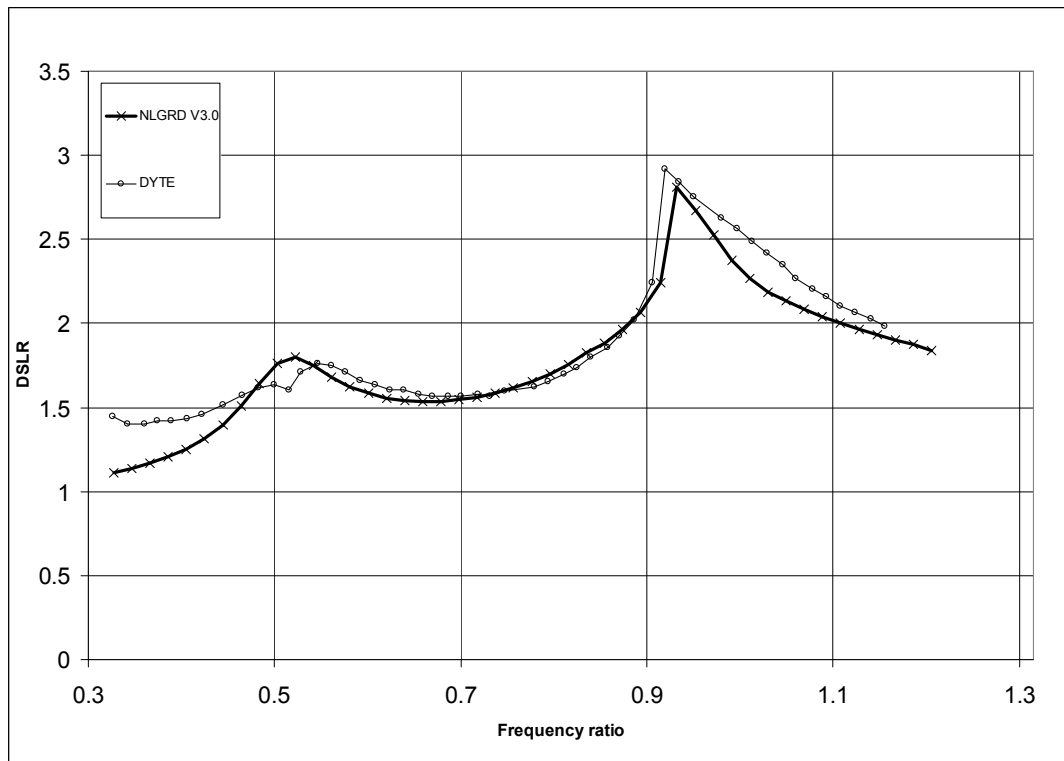


Figure 5.6 Comparison between NLGRD V3.0 and DYTE

The comparison of the dynamic factors calculated by NGRD V3.0 and DYTE shows that they are very close to each other and the frequencies where the jump occurs are almost matching. The slight shift in resonance for NGRD V3.0 is due to the coupling between the vibration modes of gear mesh and shafts.

The results of both NGRD V3.0 and DYTEM are shown in Figure 5.7. As it is seen from the figure, both programs predict the subharmonic resonance at the same frequency value, whereas DSLR value obtained by NGRD V3.0 is higher than the value obtained by DYTEM at the subharmonic resonance.

Figure 5.7 also shows that dynamic factors calculated by NGRD V3.0 and DYTEM at the mesh resonance are close to each other. However, there is a shift in the resonance frequency for the NGRD V3.0 results. Nevertheless, the results of NGRD V3.0 are in good agreement with the results of DYTEM.

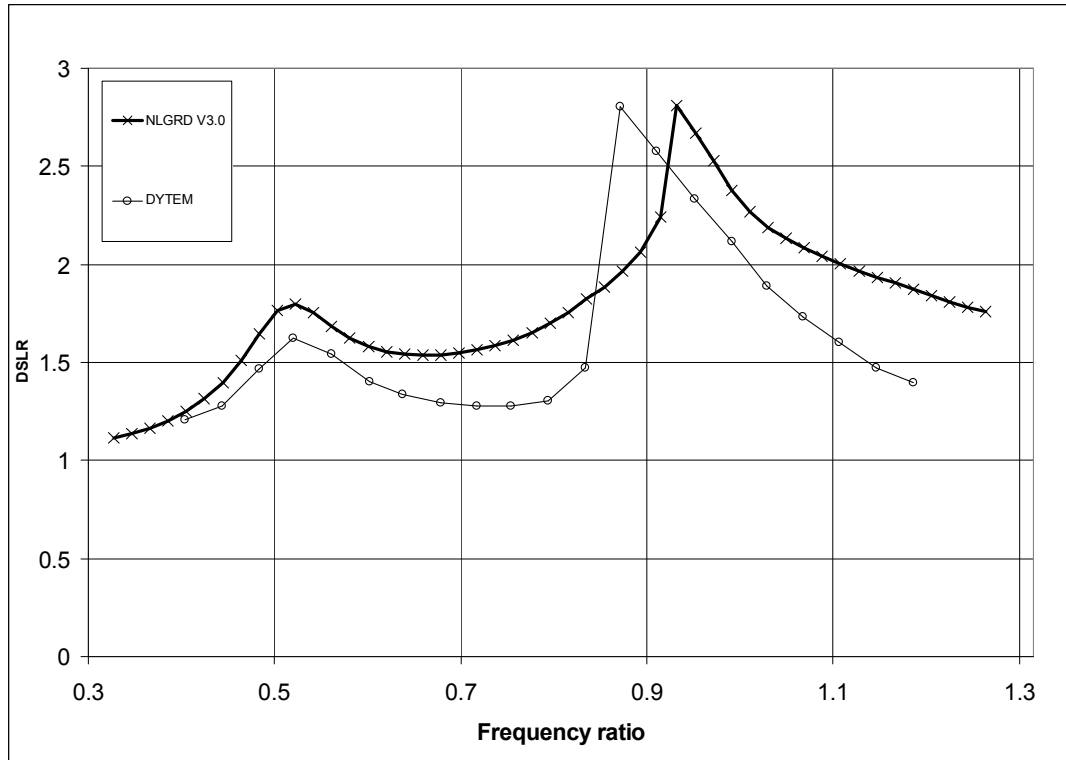


Figure 5.7 Comparison between NGRD V3.0 and DYTEM

5.3.2 Comparison with Kahraman's Models

Kahraman and Singh (1990) developed a single degree of freedom semi definite model of spur gear pair with rotary inertia. The shafts and the bearings are assumed to be rigid and the degree of freedom is associated with the relative displacement along the pressure line (same as equation (2.7)). In their model, the gear mesh is modeled by a constant stiffness with a backlash and a time invariant viscous damping. However, the excitation effect of varying stiffness is considered through a periodic internal excitation (STE) function. Digital simulation technique (5th-6th order Runge-Kutta numerical integration) is used to solve the problem. In the solution procedure, they first considered only the fundamental harmonic component of STE. Then higher harmonics were included in the solution.

Figure 5.8 shows the DSLR values calculated by NGRD V3.0 and Kahraman's 1-DOF model (in which only the fundamental component of STE is considered) for the system described in their publication (Kahraman and Singh, 1990).

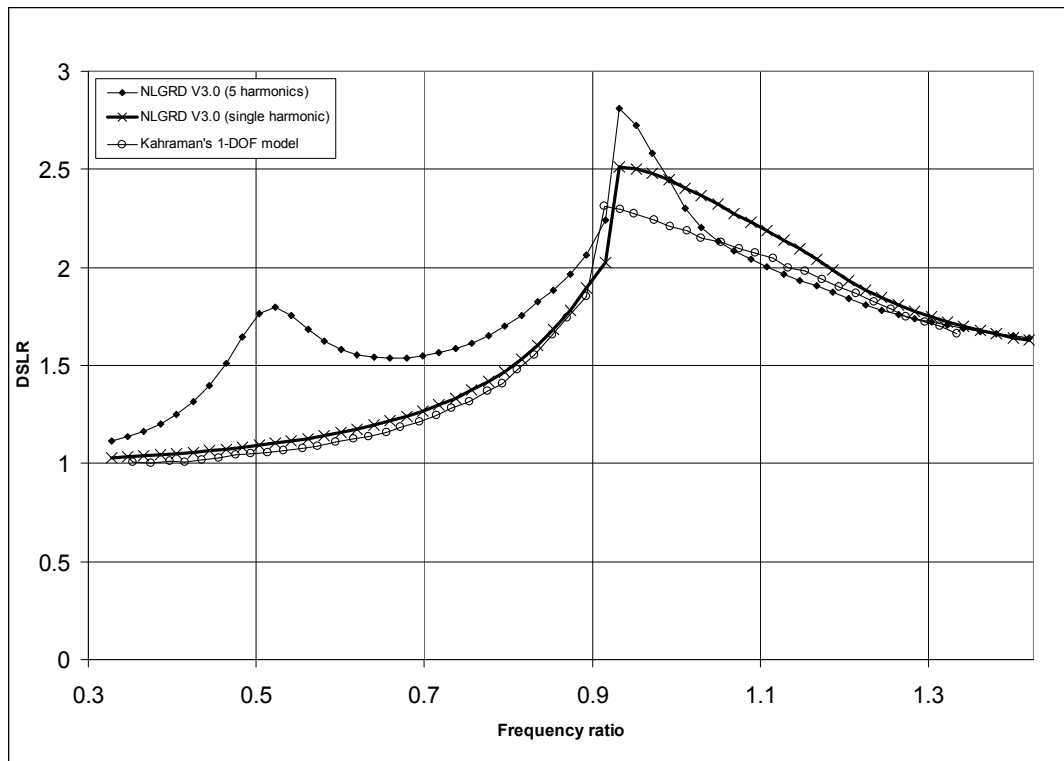


Figure 5.8 Comparison between NGRD V3.0 and Kahraman's 1-DOF model

As shown in the figure, results of Kahraman's model and NGRD V3.0 with single harmonic have exactly the same shape except a slight difference around the resonance region. With NGRD V3.0, resonance frequency is estimated slightly higher when compared with Kahraman's 1-DOF model. This is mainly due to the coupling effect of vibration modes of mesh and rotors.

However, since Kahraman's 1-DOF model considers only the fundamental harmonic component of STE, it cannot predict the subharmonic resonances. In this case NGRD V3.0 gave better results when compared with Kahraman's 1-DOF model.

Figure 5.8 also shows that DSLR value calculated with NGRD V3.0 with single harmonic at mesh resonance is higher than that calculated by 1-DOF model. Nevertheless, the results of NGRD V3.0 are in good agreement with the results of Kahraman's 1-DOF model.

Later, Kahraman and Singh (1991) extended the 1-DOF model to include the bearing dynamics and came up with a 3-DOF model in which the gear mesh is modeled with a time variable mesh stiffness with backlash and bearings is modeled with clearance type nonlinearities. The model is excited by the STE and the governing equations are solved using digital simulation technique.

The comparison of the dynamic factors calculated by Kahraman's 3-DOF model and NGRD V3.0 for the gear system in the publication of Kahraman and Singh (1991) is shown in Figure 5.9.

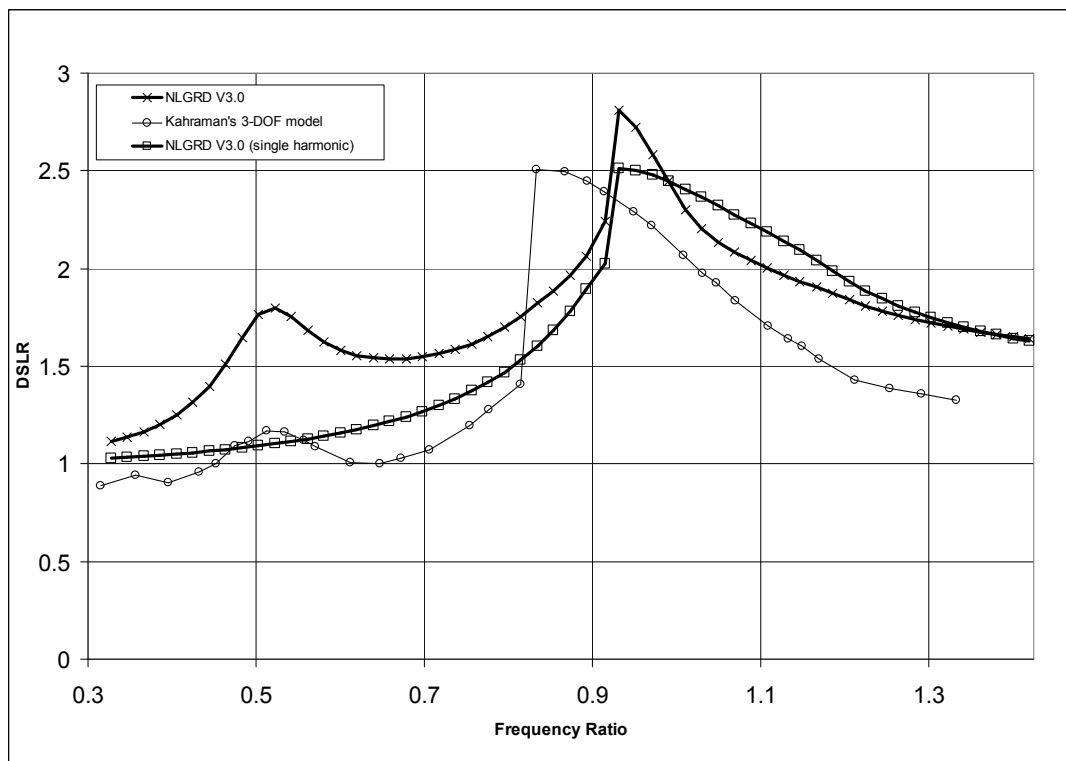


Figure 5.9 Comparison between NGRD V3.0 and Kahraman's 3-DOF model

As shown in the figure, the dynamic factor curves have the same trend and the same order of magnitude around the resonance peak with a shift of the frequency where the jump occurs. The deviation of this frequency is again mainly because of coupling between the vibration modes.

However, the main difference between 3-DOF model and NGRD V3.0 is that 3-DOF model represents the gear mesh with a time varying stiffness ($k_h(t)$) in

addition to the STE function; whereas in NGRD V3.0, mesh stiffness is taken to be constant (k_h) and its excitation effect is considered through loaded STE. This may be one of the reasons for the slight difference in the amplitudes of the dynamic factors at main resonance.

The amplitudes of the subharmonics of STE used by Kahraman are not given; hence the dynamic factors at the subharmonic region cannot be compared.

As it can be seen from the comparisons, NGRD V3.0 gives successful results. Note that the solution techniques used in the previous mathematical models employed in this chapter for comparison are completely different from the solution technique used in the present study. Most of them use digital simulation technique and obtain the solution in time domain. However, in the model presented here, describing function approach is used and the solution is obtained in frequency domain.

Therefore, close match of the results obtained by NGRD V3.0 with those obtained by other models validates the describing function approach and the solution technique used in this study.

CHAPTER VI

6 PARAMETRIC STUDY AND DISCUSSION

6.1 Introduction

In this chapter, the mesh and bearing forces in a geared rotor system with backlash and clearance type nonlinearity are studied for a range of rotor speed. The effects of gear and bearing properties on the dynamic behavior of spur gears on flexible rotors and nonlinear bearings are investigated. Several key issues such as the interaction of gear backlash or bearing clearance nonlinearity with system parameters are studied and the effects of these changes on the dynamic factor and bearing forces are examined.

In the case studies, the configuration of experimental spur gear system of Kubo (1972) is used. Furthermore, a wide range of values is used for some parameters so that coupling between modes can be studied. The system configuration and the parameters used in 4 different systems are given in Figure 5.1 and Table 5.1, respectively.

At the end of each parametric study, a detailed discussion about the results is given.

6.2 Effect of Bearing Properties

6.2.1 Effect of Bearing Stiffness

To study the effect of bearing stiffness on the dynamics of a spur gear pair, the stiffness values of the bearings for the experimental set of Kubo are varied while keeping all other parameters fixed. These system parameters are given in

Table 6.1. Here, k_h is mesh stiffness, k_b is bearing stiffness and C_b is bearing damping.

Note that system I has the original system parameters of the experimental setup of Kubo where the mesh mode is uncoupled from the other vibration modes (Özgüven, 1991a).

Table 6.1 Bearing Properties of Systems I, II, III, IV and V.

System	k_h (N/m)	k_b (N/m)	C_b (N.s/m)	Bearing clearance (mm)	k_b/k_h
I	$2.587 \cdot 10^8$	$3.503 \cdot 10^{12}$	$3.503 \cdot 10^{12}$	0	>1000
II	$2.587 \cdot 10^8$	$2.587 \cdot 10^{10}$	$8.758 \cdot 10^3$	0	100
III	$2.587 \cdot 10^8$	$2.587 \cdot 10^9$	$8.758 \cdot 10^3$	0	10
IV	$2.587 \cdot 10^8$	$2.587 \cdot 10^8$	$8.758 \cdot 10^3$	0	1

The effect of bearing stiffness on the dynamic factor can be seen in Figure 6.1. It is observed that lowering the bearing stiffness causes a decrease in the DSLR values for $k_b/k_h \geq 10$ (system I and III). However, when k_b is much higher than k_h , changing the bearing stiffness does not affect the dynamic factors considerably (system I and II). Another important observation is that as the bearing stiffness decreases, the speed where the sudden jump occur decreases.

When k_b/k_h is decreased further to 1 (system IV), the dynamic factor decreases further. Figure 6.2 shows the comparison between system I and IV. It is also observed that there is no jump at the mesh resonance frequency in system IV as can be seen in the figure. Moreover, while the mesh resonance frequency is expected to decrease, it is increased. If Figure 6.3 is analyzed, then it can be seen that coupling occurs for $1 < k_b/k_h < 10$ and a second peak is observed when k_b/k_h approaches to 1.

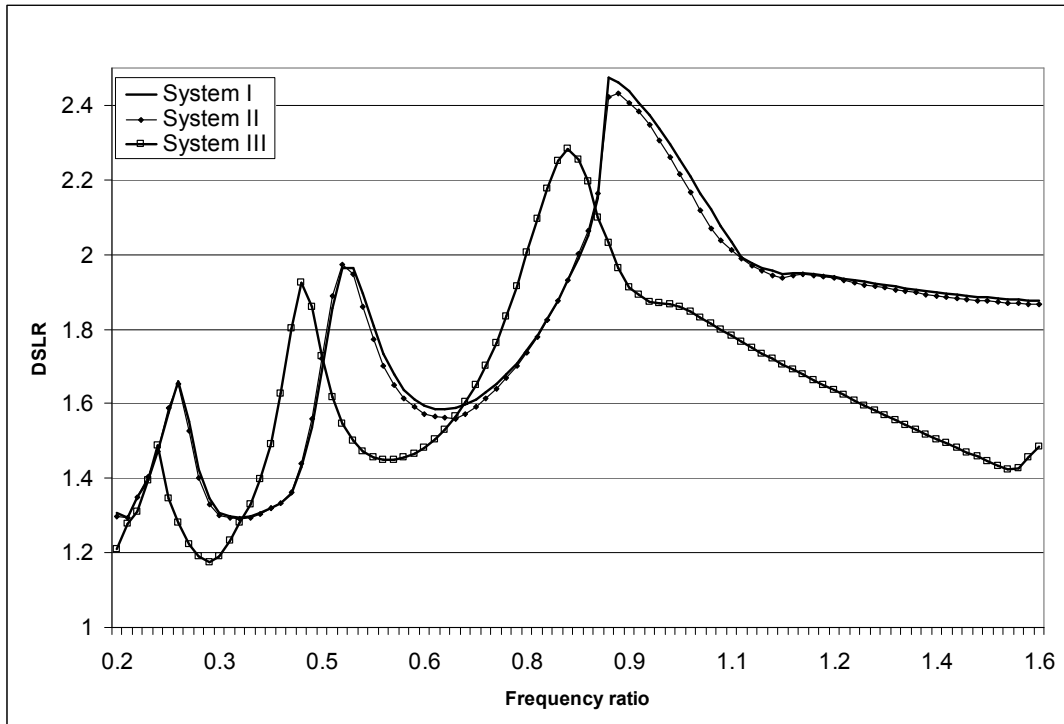


Figure 6.1 Effect of Bearing Stiffness on DSLR (System I, II and III)

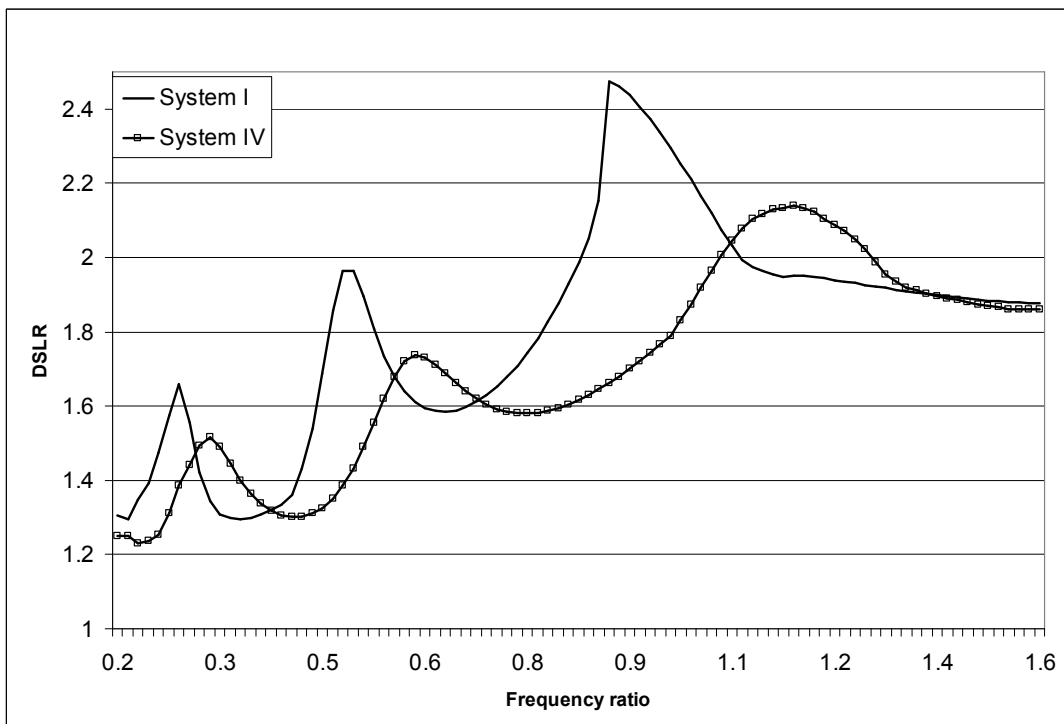


Figure 6.2 Effect of Bearing Stiffness on DSLR (System I and IV)

In order to see the detailed effect of bearing stiffness on the resonance frequencies of the system, DSLR values are calculated for different k_b/k_h values and the results are given in Figure 6.3.

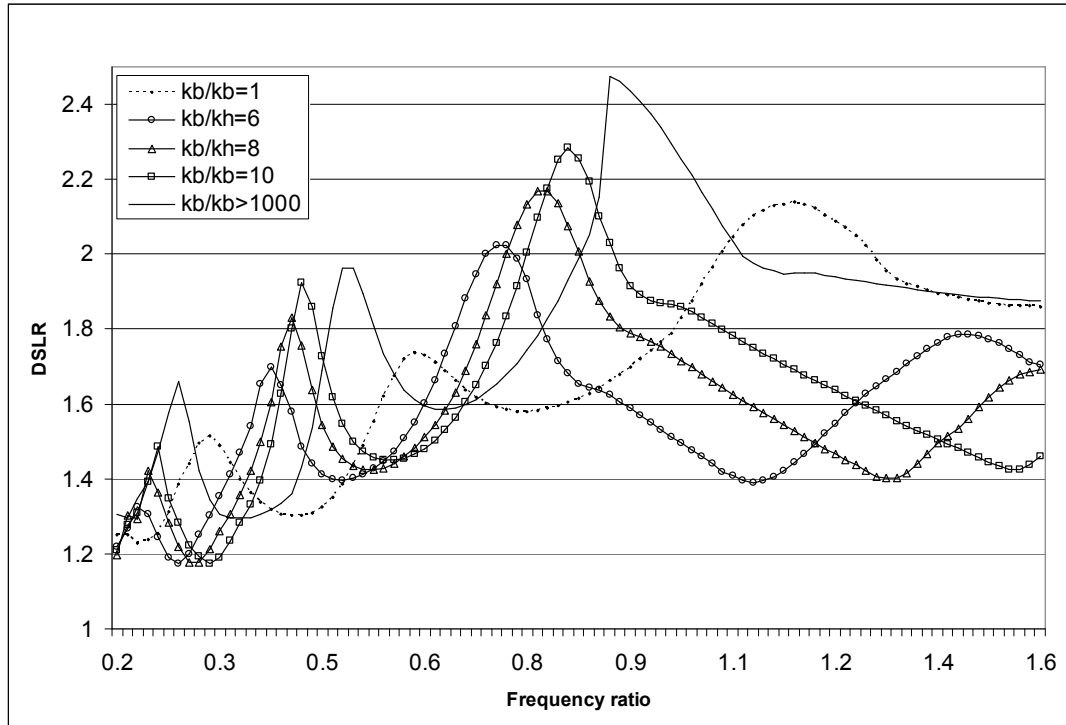


Figure 6.3 Effect of Bearing Stiffness on DSLR for Different k_b/k_h Ratios.

Analyzing Figure 6.1, Figure 6.2 and Figure 6.3, the following conclusions can be obtained:

- Decreasing the bearing stiffness decreases the dynamic factor.
- For a very high k_b/k_h ratio (in this case, it is 100), the bearing stiffness does not affect the gear dynamics significantly.
- Decreasing the bearing stiffness decreases all resonance frequencies. For high k_b/k_h ratios (>10) the resonance is mainly governed by gear mesh stiffness while for low k_b/k_h ratios (<1), the resonance is mainly governed by bearing stiffness.
- For $1 < k_b/k_h < 10$, the transverse and torsional vibrations are completely coupled. Two separate resonance peaks can be observed around the mesh resonance frequency. The lower one is governed by gear mesh stiffness and it is dominant when k_b/k_h increases whereas the second peak is governed by

the bearing stiffness and it is dominant when k_b/k_h decreases. Therefore, slight changes in bearing stiffness affect dynamic factors considerably.

- As the bearing stiffness decreases, sudden jump in DSLR values, which is due to the existence of backlash, diminishes. The complete effect of backlash will be discussed in detail in the following sections.

6.2.2 Effect of Bearing Clearance

To study the effect of bearing clearance on dynamic factor, backlash value is taken as zero and clearance value is increased gradually and DSLR values are calculated for different k_b/k_h ratios starting from 0.01 to 1000. It was observed that the clearance does not affect the dynamic factor except for a specific range of k_b/k_h ratios. Figure 6.4 shows dynamic factors calculated for Kubo's setup in which k_b/k_h ratio is greater than 1000.

Figure 6.4 shows an example case in which clearance value does not affect the dynamic factor in frequency range of interest at all.

However, when k_b/k_h ratio is selected so that the vibration modes of the mesh and bearings are coupled, then a considerable change in DSLR values are observed.

For Kubo's system, coupling effect of mesh and bearings are best observed for $k_b/k_h=13$ and the effect of clearance is studied for that value. Figure 6.5 shows DSLR plots for different clearance values when $k_b/k_h=13$.

As shown in the figure, when the clearance is increased, dynamic factor decreases. Moreover, the mesh resonance frequency shifts to lower values. This may be explained as follows. When the bearings have some amount of clearance, a zero stiffness region occurs for the coordinates associated with bearings. Therefore the resistive effect of bearing decreases. When there is coupling, as a result of this softening effect, resonance frequency shifts to lower values.

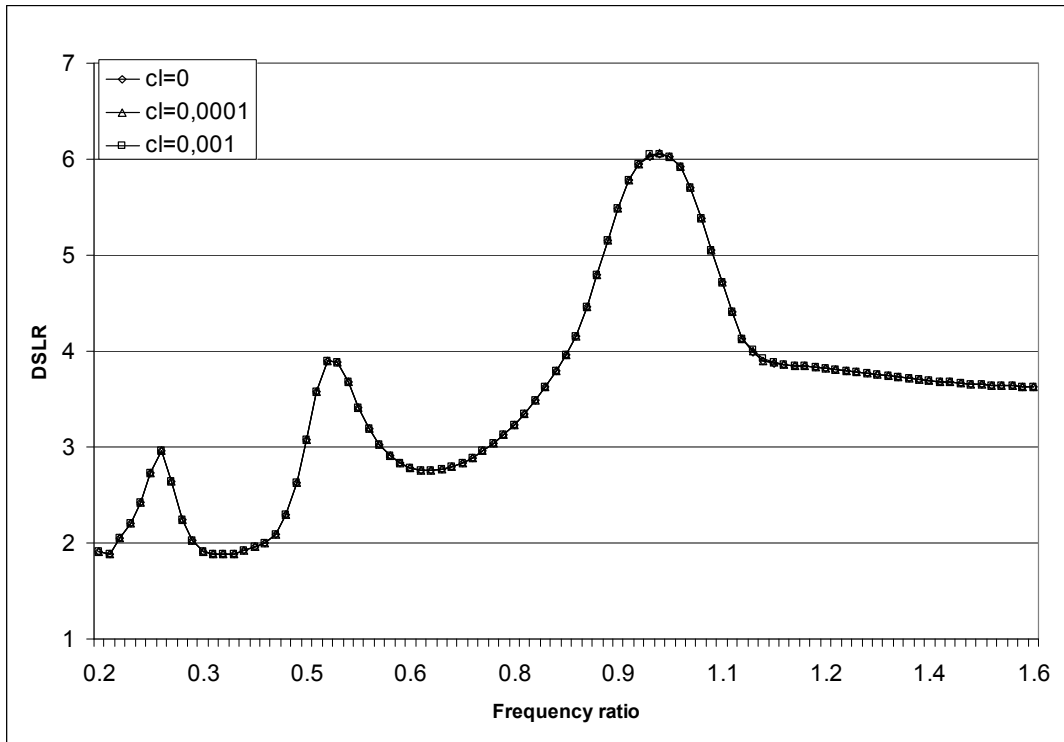


Figure 6.4 Effect of Bearing Clearance on DSLR for Kubo's Setup (backlash=0)

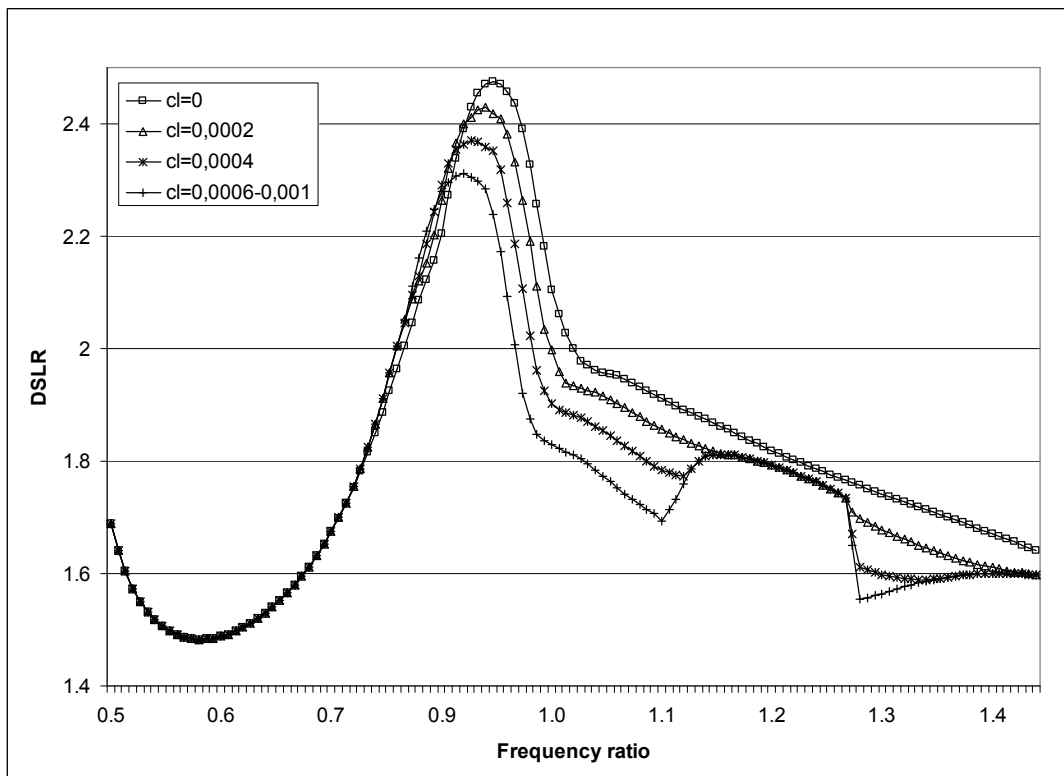


Figure 6.5 Effect of Bearing Clearance on DSLR for $k_b/k_i=13$ (backlash=0)

Another observation in Figure 6.5 is that when clearance is introduced for the bearings, a jump occurs around the frequency ratio of 1.2. In other words, introducing clearance for bearings creates a new peak at a frequency larger than mesh resonance frequency. This may be due to the insufficient clamping effect of bearings when there is clearance, which may cause tooth separation in gear mesh resulting in vibro-impacts. Due to these impacts, a jump in the mesh force is observed. The amount of jump depends on the clearance value but the location of the jump depends only on the system parameters. Figure 6.5 also shows that after a certain value, there is no change on the dynamic factor even though the clearance value is increased.

In order to study the effect of bearing clearance on the bearing forces, clearance is gradually increased and maximum the bearing force at excitation frequency is plotted for $k_b/k_h=13$. Figure 6.6 shows the change in bearing force with increasing clearance value.

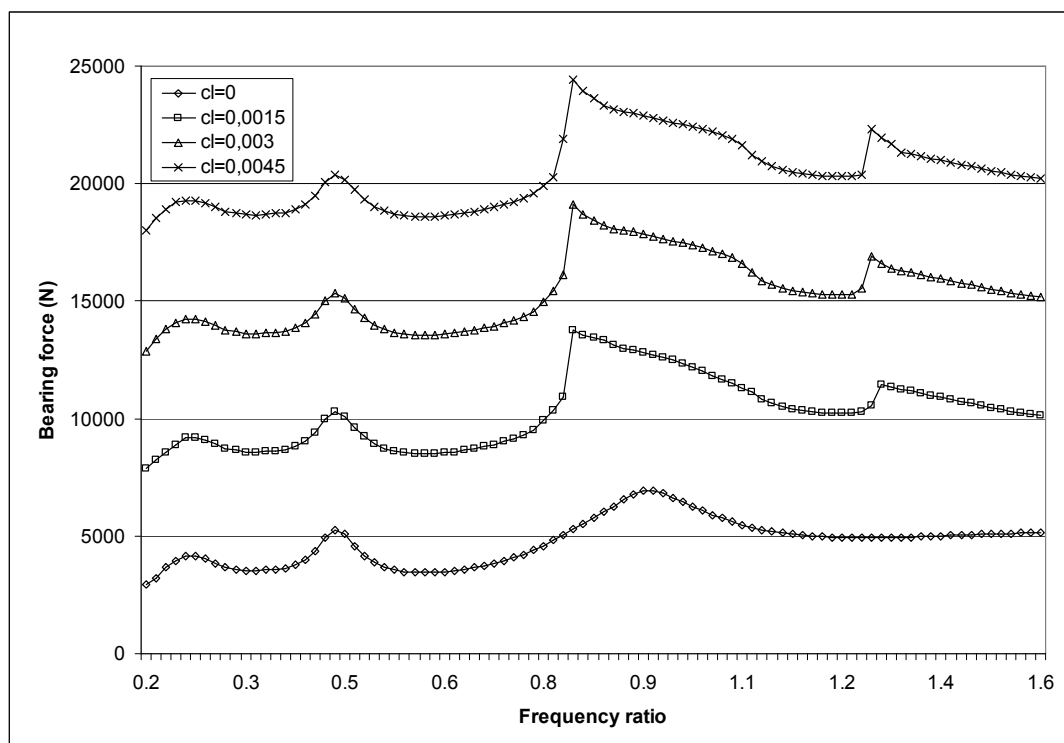


Figure 6.6 Effect of Bearing Clearance on Maximum Bearing Force ($k_b/k_h=13$, backlash=0)

As shown in the figure, there are three effects of bearing clearance on the bearing forces. First, increasing clearance value shifts the force plots upward. Second, introducing clearance for the bearings causes a sudden jump in bearing force at the mesh resonance frequency as well as at the resonance frequency of transverse vibration mode associated with the bearing. Third, the amount of jump depends only on the clearance value where the frequency of jump depends on the system properties.

6.2.3 Interaction Between Bearing Stiffness and Clearance

In this section, interaction between bearing stiffness and bearing clearance is investigated. For this purpose, the maximum bearing force for different k_b/k_h ratios are studied by first taking no clearance and then by taking a clearance of 0.003 mm. Note that gear backlash is taken as zero in these cases.

Figure 6.8 and Figure 6.7 show the effect of bearing stiffness on the maximum bearing force with and without the existence of bearing clearance, respectively. Figure 6.9 shows the effect of clearance on bearing force for a selected k_b/k_h ratio of 50.

As shown in the first two figures, there are drastic changes in bearing forces when a bearing clearance is introduced. First of all, introducing clearance increases the maximum bearing force at any frequency as stated in section 6.2.2. Moreover, increasing k_b/k_h for both systems (with or without clearance) also increases the bearing forces. In addition, introducing clearance creates jumps at the resonance frequencies associated with the bearings, which is also the conclusion stated in section 6.2.2.

However, as shown in Figure 6.7 and Figure 6.8, increasing k_b/k_h in the system with no clearance does not increase the maximum bearing force as it does for the system with clearance. This shows that there is a strong interaction between the bearing stiffness and clearance values.

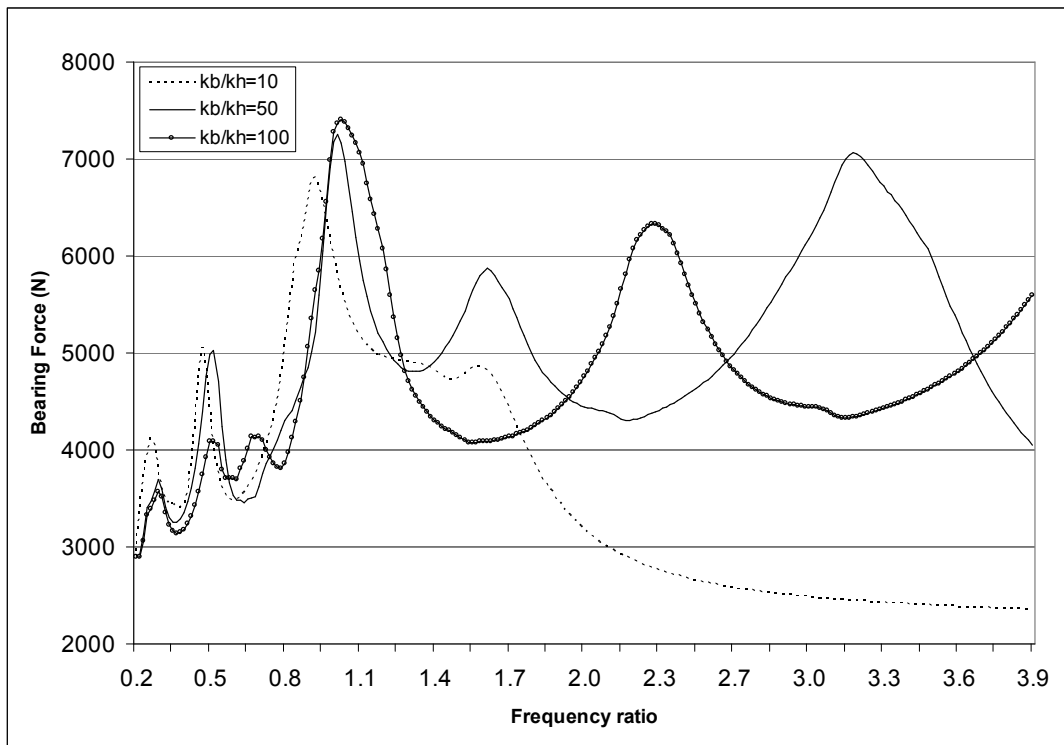


Figure 6.7 Effect of k_b/k_h on Max. Bearing Force (with no bearing clearance)

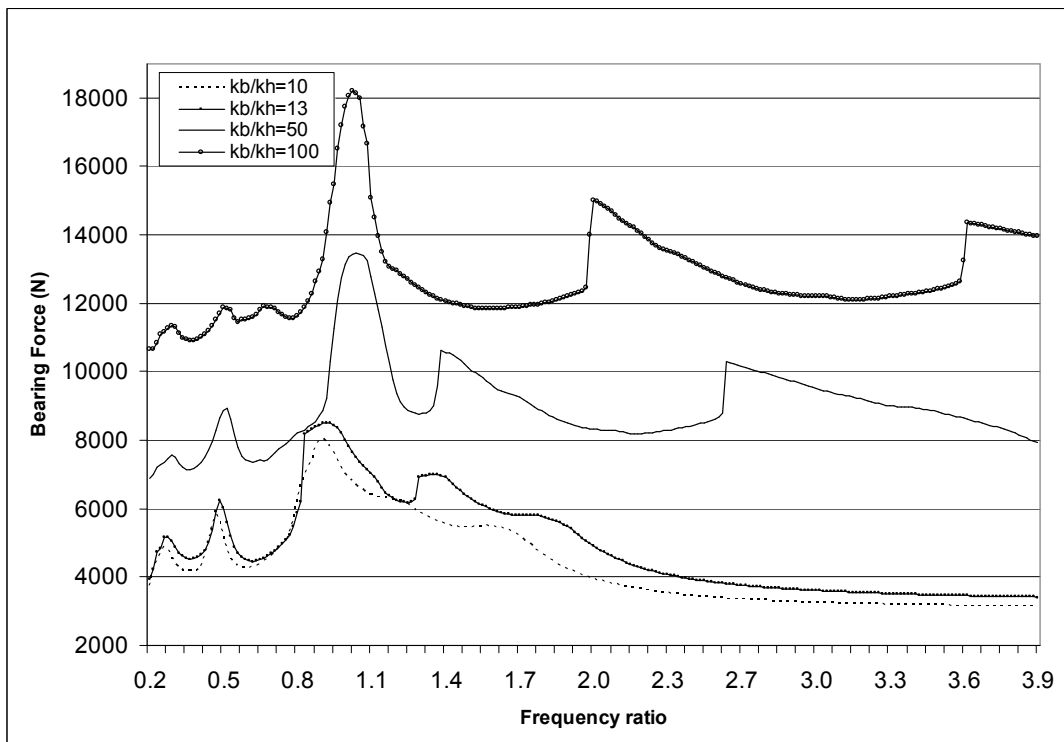


Figure 6.8 Effect of k_b/k_h on Max. Bearing Force (with clearance of 0.003 mm)

Second effect of increasing bearing stiffness is an increase in the resonance frequency associated with the transverse vibration mode of bearings. This is quite an expected result since the resonance frequency associated with bearing displacements is directly affected by the bearing stiffness values. Indeed, when there is no coupling between the mesh mode, the change in resonance frequency of bearing is supposed to be proportional to the square root of bearing stiffness.

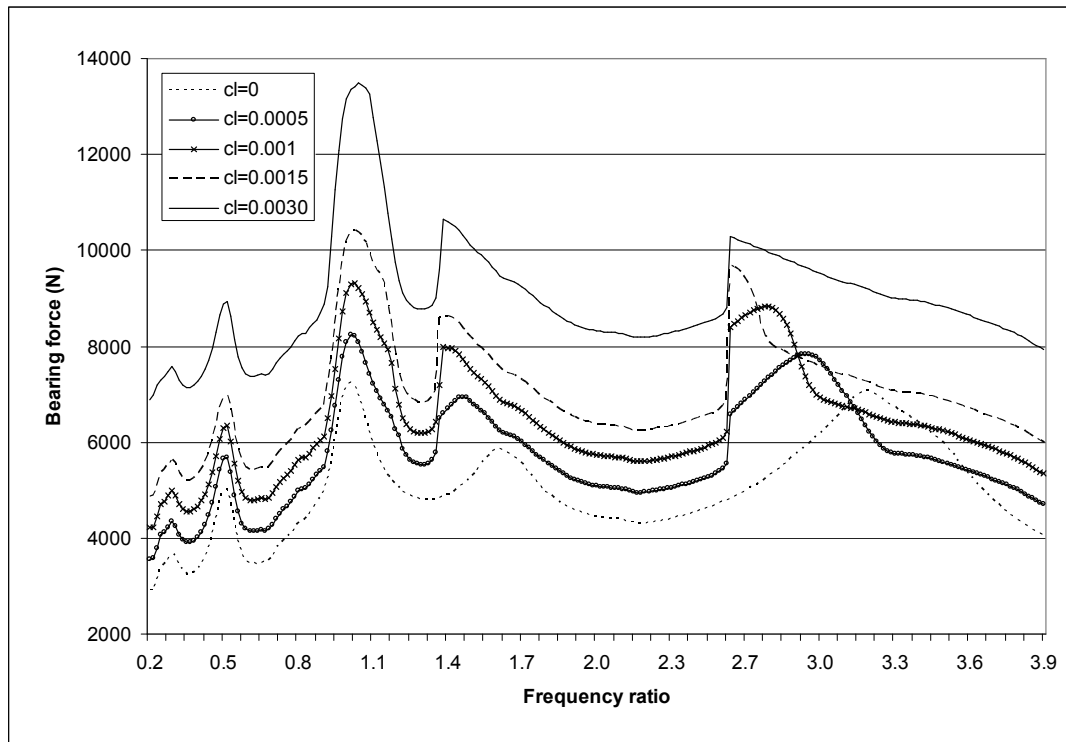


Figure 6.9 Effect of Bearing Clearance on Max. Bearing Force (for $k_b/k_h=50$)

As shown in Figure 6.8, for $k_b/k_h=50$ the first resonance associated with transverse vibration of bearing displacement is around the frequency ratio of 1.4 which corresponds to the frequency of 18000 rpm. In the same figure, when k_b/k_h is increased to 100, corresponding resonance shifts to the ratio about 2.0 which is the frequency ratio for 25800 rpm. It can be seen that the ratio of frequency increase is about 1.42 ($=2/1.4$) which is equal to the value of $\sqrt{2}$. This shows that the frequency of bearing resonance is proportional to the square root of bearing stiffness.

As stated in section 6.2.2, another effect of bearing clearance is that it creates sudden jumps in bearing forces around the bearing resonance regions as shown in Figure 6.8 and Figure 6.9. Moreover, when there is coupling between the vibration modes of the gear mesh and bearings (in this case, coupling occurs when $k_b/k_h=13$), a jump in the mesh resonance is also observed when there is bearing clearance as shown in Figure 6.8. It is also seen that as the bearing clearance increases for the same k_b/k_h ratio, the resonance frequency of bearings decrease as shown in Figure 6.9.

However, Figure 6.8 shows that the jump in the maximum bearing force is also related to k_b/k_h ratio. Up to a certain k_b/k_h ratio (10 in this case) no jump is observed in the maximum bearing force even there is some amount of bearing clearance. When bearing stiffness is increased (when $k_b/k_h=13$), only one jump occurs at the first resonance frequency of transverse mode associated with bearing (which is at the frequency ratio of 1.3). When k_b/k_h is increased further ($k_b/k_h=50$ for example), another jump occurs at the frequency ratio of 2.6.

From the above observations the following conclusions can be obtained:

- Increasing bearing clearance always increases the bearing forces regardless of k_b/k_h ratio.
- Introducing bearing clearance for a fixed k_b/k_h ratio creates sudden jumps in the maximum bearing force at the resonance frequencies of transverse vibrations associated with bearings. However, existence of jumps depends on the k_b/k_h ratio. If k_b/k_h ratio is less than a certain value, or greater than a certain value, either no jump or two jumps occur at the resonance frequencies associated with bearing displacements. These upper and lower k_b/k_h values are determined by the bearing stiffness.
- If k_b/k_h is selected such that there is coupling between gear mesh mode and bearing modes (e.g., $k_b/k_h=13$ in this case), then a sudden jump in the force is also observed at the gear mesh resonance frequency. The amount of jump depends only on the amount of clearance, and the jump frequency depends on the system properties (especially the bearing stiffness).

- When clearance in bearings is increased for a fixed k_b/k_h ratio, in addition to the increase in the maximum bearing force, resonance frequencies of bearing modes decrease (Figure 6.9). This means that for a fixed bearing stiffness value, clearance creates a softening-like effect, shifting the resonance frequency to lower values. Therefore, as the amount of clearance in bearings increases, due to wear for example, since the resonance frequencies shift to lower values (to the frequencies of interest), high vibration and noise levels may result.
- Increasing bearing stiffness increases the maximum bearing force at any frequency. However, existence of clearance in bearings strongly affects the amount of increase in the force. Moreover, increasing bearing stiffness also increases the resonance frequencies of bearings regardless of existence of clearance. If there is no coupling between gear mesh mode and bearing modes, the shift in this frequency is proportional to the square root of increase in the bearing stiffness.
- If there is no clearance in bearings, maximum bearing force around the gear mesh resonance frequency is mainly determined by gear mesh stiffness and it does not change considerably with increasing bearing stiffness (Figure 6.7) if there is no coupling. However, when there is coupling between vibration modes of gear mesh and bearings (i.e. when k_b/k_h ratio is around 10), then maximum bearing force at the gear mesh resonance frequency is slightly decreased (Figure 6.7).
- If there is clearance in bearings, increasing bearing stiffness increases the maximum bearing force more, compared to the case with no clearance.

6.3 Effect of Gear Backlash

Gear backlash can be defined as the amount by which a tooth space exceeds the thickness of the mating tooth. A gear pair may have some amount of backlash either designed to provide better lubrication and eliminate interference or due to manufacturing errors and wear. The backlash may cause tooth separation and impacts in geared rotor systems which produces high stresses and noise radiation.

To study the effect of backlash, DSLR values at different backlash values are obtained for system I (see Table 6.1). Figure 6.10 shows the effect of gear backlash (in millimeters) on the dynamic factor at the gear mesh. The following important conclusions can be extracted from the study of the figure:

- As the backlash increases, the amplitude of the dynamic factor decreases at the gear mesh frequency and at its subharmonic. The amount of decrease depends on the clearance value.
- Introducing backlash causes a sudden jump at the mesh resonance frequency and its subharmonics. The amount of jump depends on the backlash value but the location of jump depends only on the system parameters.
- Increasing backlash causes a left-shift on the mesh resonance frequency and its subharmonics. The shift depends on the backlash value.
- After a certain backlash value, there is no change on the dynamic factor even though the backlash is increased further.

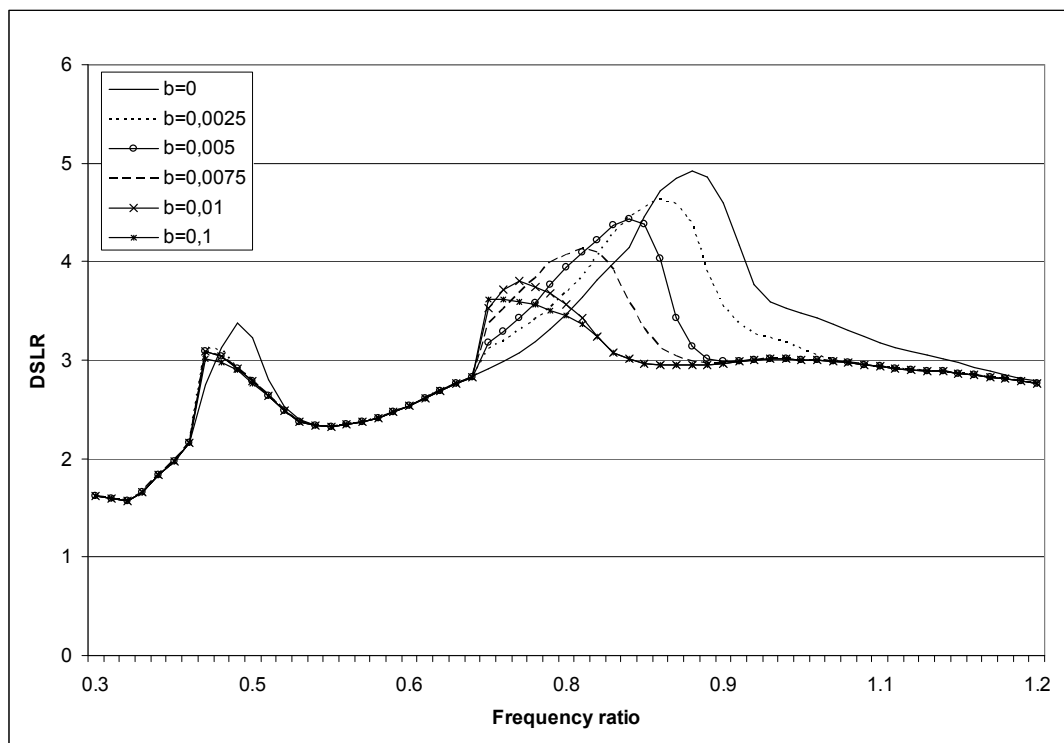


Figure 6.10 Effect of Gear Backlash on DSLR for $k_b/k_h > 1000$ (b is in mm)

In order to study the effect of gear backlash on bearing forces, the change in the maximum bearing force with increasing backlash is studied in two cases. It is observed that changing backlash value does not affect the bearing forces at all except for a special k_b/k_h ratio (13 in this case). Note that a similar result was obtained in 6.2.2 for the effect of bearing clearance on dynamic factor.

Figure 6.11 and Figure 6.12 show the effect of gear backlash on maximum bearing force for $k_b/k_h > 1000$ and $k_b/k_h = 13$, respectively.

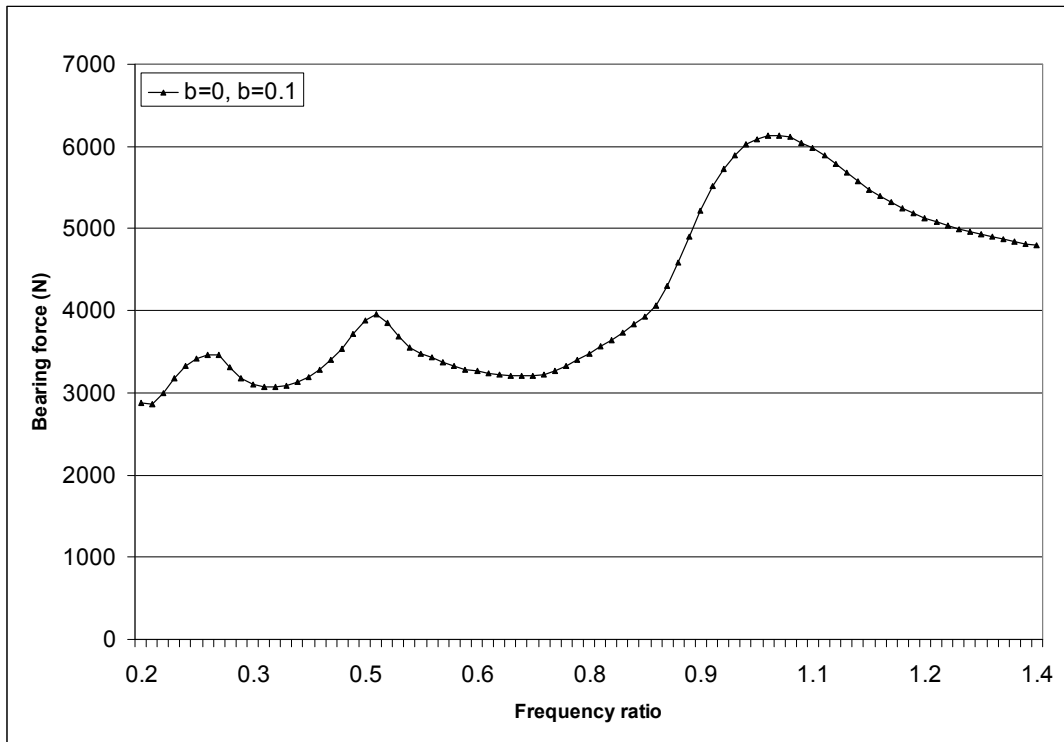


Figure 6.11 Effect of Gear Backlash on Maximum Bearing Force (for $k_b/k_h > 1000$)

Figure 6.11 is an example case in which backlash value does not affect the maximum bearing force at all in the frequency range of interest.

However, when k_b/k_h is so selected that there is coupling between the gear mesh mode and bearing mode, then a slight change in bearing force is observed as shown in Figure 6.12. As the backlash is increased for the coupled case, the dynamic factor decreases around the gear mesh resonance frequency. Moreover, introducing backlash for gear mesh creates a sudden jump in the maximum bearing

force at the mesh resonance frequency. Amount of jump is affected by the backlash value. Also after a certain backlash limit, there is no change in the maximum bearing force even though the backlash is increased further.

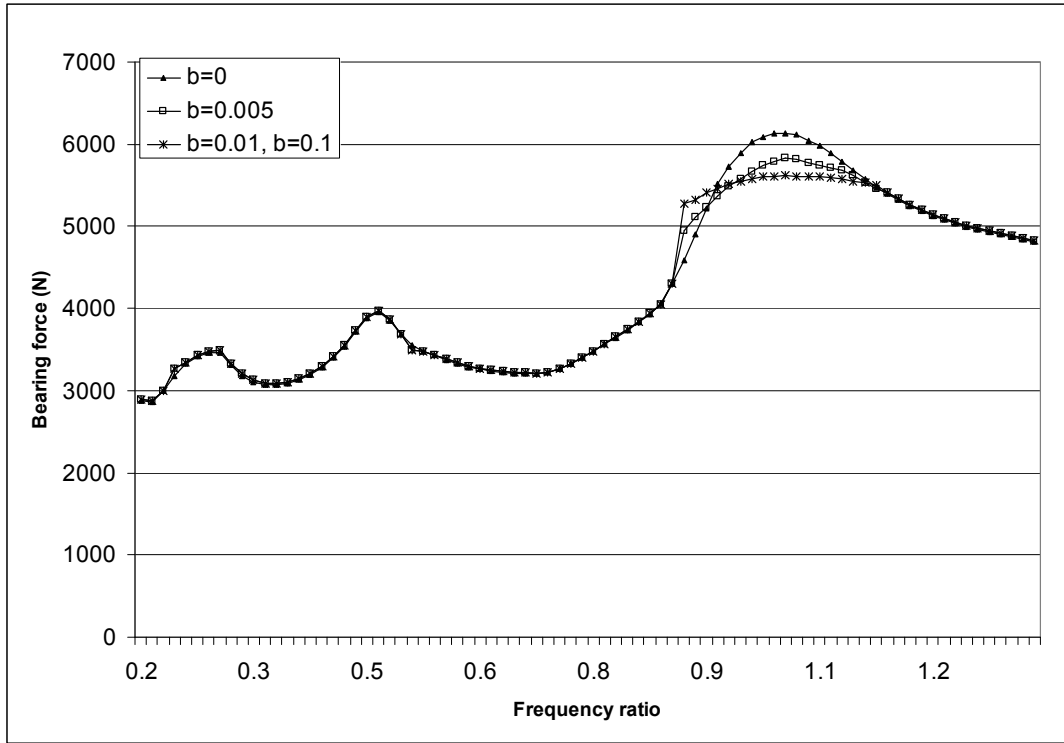


Figure 6.12 Effect of Gear Backlash on Maximum Bearing Force (for $k_b/k_h=13$)

6.4 Interaction Between Gear Backlash and Bearing Clearance

To see the interaction between gear backlash and bearing clearance, several plots were obtained for different k_b/k_h ratios by changing either backlash for a constant bearing clearance value or clearance for a constant gear backlash. It was observed that increasing bearing clearance value for a system with gear backlash and for a system without gear backlash makes the same difference in both dynamic factors and bearing forces. In other words, the same changes in section 6.2 were obtained when the gear backlash is introduced.

Similarly, it was observed that increasing backlash value gives the same changes in results when there is clearance in bearings. In other words, it can be concluded that standalone effects of gear backlash and bearing clearance on the

dynamic factor and maximum bearing force are superposed on top of each other when there is both gear backlash and bearing clearance. This means that there is a weak interaction between gear backlash and bearing clearance. Figure 6.13 shows the effect of gear backlash for different bearing clearances on maximum bearing force for $k_b/k_h=13$. Note that k_b/k_h is deliberately selected as 13 in order to see the effect of gear backlash on bearing force.

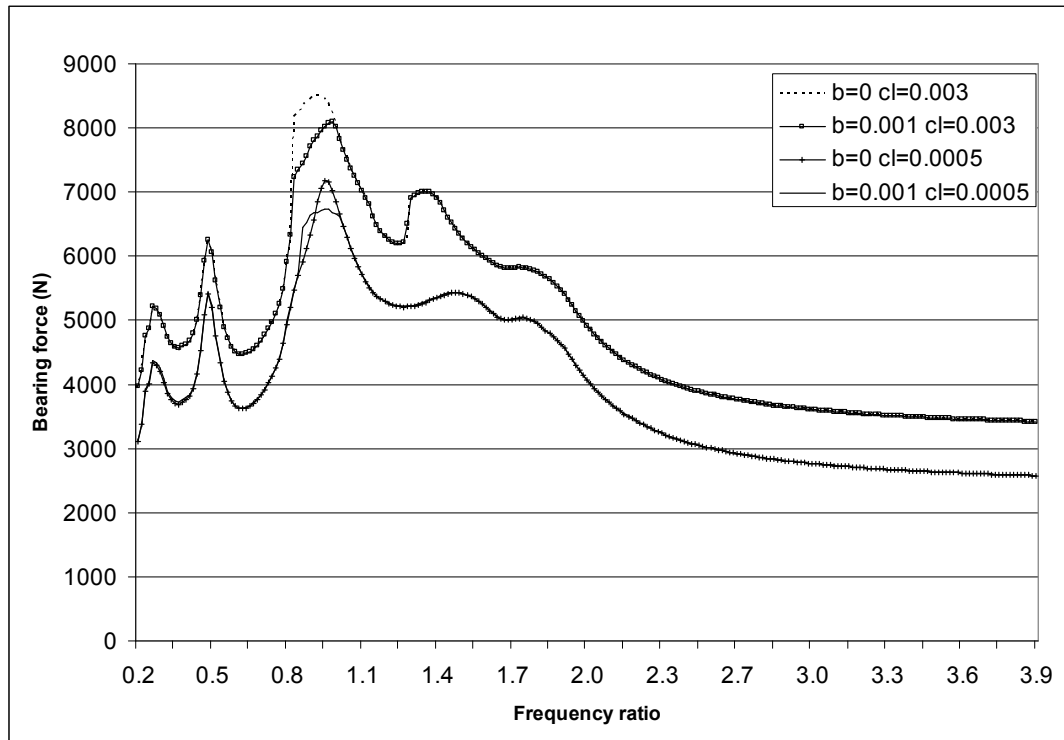


Figure 6.13 Effect of Gear Backlash for Different Bearing Clearances on Maximum Bearing Force for $k_b/k_h=13$

As can be seen in Figure 6.13, introducing gear backlash for a system with bearing clearances makes the same effect on the results as explained in section 6.3.

CHAPTER VII

7 CONCLUSIONS AND RECOMMENDATIONS

7.1 Conclusions

In this study, a nonlinear mathematical model is developed for nonlinear dynamic analysis of gear-shaft-bearing systems. The model combines the flexibility of the finite element method and the rigorous treatment of the nonlinear effect of gear backlash and bearing clearance on the dynamics of geared rotor systems. In other words, finite element modeling allows one to analyze any possible configuration for a single stage gear mesh such as a gear pair on simply supported shafts or overhung shafts.

The model includes the transverse and rotary inertia of shaft elements, the axial loading on shafts, material damping of shafts, damping and stiffness of spur gear pair and nonlinear bearings which have radial clearances. The coupling between torsional and transverse vibrations is included into the model. The model also includes the effects of gear backlash, tooth separation and gear errors. Although a constant mesh stiffness is used in this model, the excitation effect of time varying mesh stiffness is indirectly included in the analysis through a periodic displacement representing loaded static transmission error (STE). STE input is represented by the highest n harmonic terms of the Fourier series representation of the measured or calculated data.

Then a computer code for the solution of the system equations is developed using MatLAB 7.0. Therefore it is highly flexible and open to further developments. The program calculates dynamic to static load ratio, dynamic transmission error, reaction forces and displacements at bearings.

Another important feature of the code is the solution technique. Backlash and clearance type nonlinearities associated with $2*k+4$ degrees of freedom (k

being the total number of bearings) are modeled by describing functions which enable to express the dynamic equations of a nonlinear system in frequency domain. Since only a limited number of coordinates are affected from nonlinearity, system matrices are partitioned and a new method suggested in a previous study is used to reduce the size of the problem to the number of nonlinear coordinates and solve them with an iterative process. This method reduces the computational time considerably.

The computer code developed (NGRD V3.0) is capable of calculating the dynamic factor (DSL_R), dynamic transmission error (DTE) and bearing forces. Also the modal analysis of the linear part of the system can be made by using NGRD V3.0.

The results obtained by NGRD V3.0 are validated by comparing them with experimental results of Kubo and Munro. The results are found to be in good agreement with the experimental results although some deviations are observed. Reasons for these deviations are explained in related sections.

The results obtained by NGRD V3.0 are then compared with those of previously developed nonlinear models of Özgüven (1988b, 1991a) and Kahraman and Singh (1990, 1991). The change of dynamic to static load ratio with rotating speed is found to be similar. Even though completely different solution techniques are used for these models, close results are obtained which validate the use of describing function method and frequency domain solution technique.

The model and the software developed in this study has the advantage of being very flexible, compared to previous models, so that a configuration for a single gear pair system on flexible shafts and bearings can be easily handled.

In the last part of the thesis, several parametric studies are performed to understand the effects of several parameters on dynamic behavior of geared rotor systems, such as bearing stiffness, clearance in bearings and gear backlash. The interaction of bearing clearance with other system parameters is also investigated.

In this study, the following conclusions are drawn:

- In the nonlinear dynamic analysis of geared rotor systems, time varying mesh stiffness can be satisfactorily approximated by an average mesh stiffness and a periodic displacement excitation representing loaded STE.
- Bearing stiffness have the following effects on dynamic factor:
 - For a very high bearing stiffness compared to mesh stiffness, the bearing stiffness has no effect on the dynamic factor.
 - Decreasing the bearing stiffness decreases all resonance frequencies for dynamic factor. For high k_b/k_h ratios (>10) the resonances are mainly governed by gear mesh stiffness while for low k_b/k_h ratios (<1), the resonances are mainly governed by bearing stiffness.
 - For $1 < k_b/k_h < 10$, the transverse and torsional vibrations are completely coupled. Therefore, slight changes in bearing stiffness affect dynamic factors considerably.
- Interaction of bearing clearance with bearing stiffness and effects on the system dynamics are as follows:
 - Increasing clearance does not affect the dynamic factor unless there is coupling between mesh and bearing modes. When there is coupling, increasing clearance decreases the dynamic factor. However, the maximum decrease is about 7-8%. After a certain limit, increasing clearance further does not affect DSLR values.
 - Increasing clearance always increases the maximum bearing force at any frequency. To be more specific, maximum increase in bearing force in a frequency range is about 30% when the clearance is doubled.
 - Including the bearing clearance in analysis may cause sudden jumps in the bearing forces at the resonance frequencies of transverse vibration modes associated with bearings. Existence and the number of jumps within the frequency range of interest are determined by bearing stiffness (i.e. k_b/k_h ratio).
 - If there is coupling between gear mesh mode and the bearing modes, then an additional jump in the bearing force at the gear mesh resonance

frequency is also observed. Amount of jump is determined by the value of clearance.

- Increasing clearance causes a decrease in the resonance frequencies of bearing modes.
- Increasing bearing stiffness increases the maximum bearing force. When there is no clearance in bearings, doubling the bearing stiffness causes an increase of 5% in maximum bearing force in the frequency range of interest. However when there is clearance, this change may go up to 40% for the same change in bearing stiffness.
- Increasing bearing stiffness increases the resonance frequencies of bearing modes. If there is no coupling between the mesh and bearing modes, the change in the bearing mode resonance frequencies is proportional to the square root of bearing stiffness, as expected.
- Effect of gear backlash and interaction with bearing clearance are as follows:
 - Including the gear backlash nonlinearity in geared rotor systems causes a sudden jump at the mesh resonance frequency and its subharmonics in dynamic factor. Increasing backlash also decreases the mesh resonance frequency.
 - Including gear backlash does not affect the maximum bearing force unless there is coupling between the torsional and transverse modes of gear mesh and bearings. When there is coupling, increasing gear backlash decreases the maximum bearing force at mesh resonance frequency and causes a jump at the same frequency.
 - A strong interaction between bearing stiffness and clearance nonlinearity is observed.
 - A weak interaction between gear backlash and bearing clearance is observed. In other words, existence of bearing clearance in the systems with gear backlash makes the same effect as in the case when there is no gear backlash.

7.2 Recommendation for Future Work

The main objective of this study was to improve a previous study by including clearance type of nonlinearities in bearing dynamics. In this study, the average mesh stiffness is used, but the excitation effect of time varying stiffness is included through a displacement excitation taken as loaded STE. Gear backlash is also considered.

For future work, the model can be extended to include the time varying mesh stiffness directly, in order to study the effect of the approximation used in this study. Moreover, nonlinear damping between the spur gear pair can be considered. Furthermore, the mathematical model can be improved for transient response analysis.

Recommendations for further study may be listed as:

- Time varying mesh stiffness can be included directly into the analysis.
- Solution can be solved by a digital simulation technique in time domain to obtain transient analysis.
- Eccentricity and external forces can be included in the model.
- Tooth collision can be included in the model.
- Model may be extended to analyze helical gears.
- The user interface (VGR 3.0) can be extended to show the mode shapes of geared rotor system graphically.

REFERENCES

Arıkan, M.A.S., 1996. "Effect of Addendum Modification on Spur Gear Dynamic Loads", Proceedings of the ASME 7th Power Transmission and Gearing Conference, DE-Vol.88, pp. 1-8. San Diego, USA, October 6-9.

Blankenship, G. W. and Kahraman, A., 1995a. "Steady State Forced Response of a Mechanical Oscillator with Combined Parametric Excitation and Clearance Type Nonlinearity", Journal of Sound and Vibration, Vol. 185, No. 5, pp. 743-765.

Blankenship, G. W. and Singh, R., 1995b. "Analytical Solution for Modulation Sidebands Associated with A Class of Mechanical Oscillators", Journal of Sound and Vibration, Vol. 30, pp. 13-36.

Blankenship, G. W. and Singh, R., 1995c. "A New Gear Mesh Interface Dynamic Model to Predict Multi Dimensional Force Coupling and Excitation", Mechanism and Machine Theory, Vol. 30, pp. 43-57.

Blankenship, G. W. and Singh, R., 1995d. "Dynamic Force Transmissibility in Helical Gear Pairs", Mechanism and Machine Theory, Vol. 30, pp. 323-339.

Atherton, D.P., 1982. Non-linear Control Engineering. Van Nostrand Rein hold, London.

Azar, R.C. and Crossley, F.R.E., 1977. "Digital Simulation of Impact Phenomenon in Spur Gear System", Journal of Engineering for Industry, Transaction ASME, Vol. 99, pp. 792-798.

Choy, F.K., Ruan, Y.K., Zakrajsek, J.J., and Townsend, D.P., 1991. "Model Analysis of Multistage Gear Systems Coupled With Gearbox Vibrations", NASA Technical Report 90-C-033.

Cai, Y., 1995. "Simulation on the Rotational Vibration of Helical Gears in Consideration of the Tooth Separation Phenomenon (A New Stiffness Function Helical Involute Tooth Pair)", Transactions of ASME, Vol. 117, pp. 460-468.

David, J.W., and Mitchell, L.D., 1985. "Dynamic Coupling in Geared Rotor Systems", Journal of Vibration, Acoustics, Stress and Reliability in Design, Transactions of the ASME, Paper No. 85-DET-11.

Doğruer, C.U., 1999. "Dynamic Analysis of Spur Gears", M.S. Thesis, Middle East Technical University, Ankara, Türkiye

Dudely, D., 1984. Handbook of Practical Gear Design, McGraw-Hill, New York.

Faires, V.M., 1965. Design of Machine Elements, Forth Edition, Collier-Macmillan, New York.

Fisher, A., 1968. "Factors in Calculating the Load Carrying Capacity of Helical Gears", Machinery, Vol. 98, pp. 545-552.

Gelb, A., and Vander Velde, W.E., 1968. Multiple-Input Describing Functions and Non-linear System Design, McGraw-Hill, New York.

Gifford, S.J., and Tomlinson, G.P., 1989. "Recent Advances in the Application of Functional Series", Journal of Sound and Vibration, Vol. 135, No. 2, pp. 289-317.

Gregory, R. W., Harris, S. L., and Munro, R. G., 1963-1964. "Dynamic Behavior of Spur Gears", Proceedings of the Institution of Mechanical Engineers, Vol. 178, pp. 207-226.

Harris, S.L., 1958. "Dynamic Loads on the Teeth of Spur Gears", Proceedings, of the institution of Mechanical Engineers, Vol. 172, pp. 87-112.

Houser, D.R., 1988. "Gear Noise State of the Art", Proceedings, Inter-Noise 88, pp. 601-606.

Howard, I., Shengxiang, J. and Wang, J., 2001. "The Dynamic Modeling Of A Spur Gear In Mesh Including Friction And A Crack", Mechanical Systems and Signal Processing, Vol. 15, pp. 831-853.

Iida, H., Tamura, A., Kikuch, K., and Agata, H., 1980. "Coupled Torsional-Flexural Vibration of A Shaft in A Geared System of Rotors (1st report)", Bulletin of the Japanese Society of Mechanical Engineers, Vol. 23, pp. 2111-2117.

Iwatsubo, T., Arii, S., and Kawai, P., 1984. "Coupled Lateral-torsional Vibration of Rotor System Trained by Gears (1. Analysis by Transfer-matrix Method)", Bulletin of Japanese Society of Mechanical Engineers, Vol. 27, pp. 271-277.

Iwatsubo, T., Arii, S. and Kawai, P., 1984. "The Coupled Lateral Torsional Vibration of a Geared Rotor System", Proceedings of the Third International Conference on Vibration in Rotating Machinery, Institution of Mechanical Engineers, pp. 59-66.

Jordan, D.W., and Smith, P., 1987. Non-linear Ordinary Differential Equations, Oxford University Press.

Kahraman, A., 1990. "Non-linear Dynamic Analysis of Geared Systems", Ph.D. Dissertation, The Ohio State University, Ohio.

Kahraman, A., and Singh, R., 1990. "Non-Linear Dynamics of A Spur Gear Pair", Journal of Sound and Vibration, Vol. 142, pp. 49-75.

Kahraman, A., and Singh, R., 1991a. "Non-Linear Dynamics of A Geared Rotor-Bearing System with Multiple Clearances", Journal of Sound and Vibration. Vol. 144, pp. 469-506.

Kahraman, A., and Singh, R., 1991b. "Interactions Between Time-Varying Mesh Stiffness and Clearance Non-Linearities in A Geared System", Journal of Sound and Vibration, Vol. 146, pp. 135-156.

Kahraman, A., 1991. "Effect of Axial Vibrations on the Dynamics of a Helical Gear Pair", General Motors, Technical Report.

Kahraman, A., Özgüven, H.N., Houser, D.R., and Zakrajsek, J.J., 1992. "Dynamic Analysis of Geared Rotors by Finite Elements", Journal of Mechanical Design, Transactions of the ASME, Vol. 114, pp 507-514.

Kahraman, A. and Krantz, T., 2004. "An Experimental Investigation of the Influence of the Lubricant Viscosity and Additives on Gear Wear," Tribology Transactions, 47, 138-148, 2004.

Kahraman, A., Kubur, M, Zini, D., and Kienzle, K., 2004. "Dynamic Analysis of a Multi-shaft Helical Gear Transmission by Finite Elements: Model and Experiment," accepted for publication, ASME Journal of Vibrations and Acoustics.

Kesan, M., and Özgüven, H.N., 1992. "Dynamic Response of Geared Rotors to Internal Excitation by Using A Finite Element Model", Proceedings of Third World Congress on Gearing and Power Transmission, Paris, France.

Kesan, M., 1992. "Dynamic Modeling and Analysis of Spur and Helical Gears on Flexible Rotors", M.Sc. Thesis, Middle East Technical University, Ankara, Turkey.

Kisher, B., 1979. "Effect of Gear Errors on Non-Linear Vibrations of a Gear Train System", Proceedings of the International of the Federation Theory Machines and Mechanisms Fifth World Congress, pp. 1122-1125.

Kohler, H.K., Pratt, A., and Thomson, A.M., 1970. "Dynamic and Noise of Parallel Axis Gearing", Proceedings of the institution of Mechanical Engineers, Vol. 84, pp. 111-121.

Kubo, A. and Kiyono, S., 1980. "Vibration Excitation of Cylindrical Involute Gears Due to Tooth Form Error", Bulletin of the Japanese Society of Mechanical Engineers, Vol. 23, pp. 1536-1543.

Kubo, A. Yamada, K., Aida, T., Sato, S., and Harino, M., "Research on Super High Speed Gearing (5th Report, Dynamic Behavior of Helical Gears)", Transactions of Japanese Society of Mechanical Engineers, Vol. 39, no. 321, pp. 1682-1689.

Küçükay, F., 1984. "Dynamic Behavior of High Speed Gears", Proceedings of the Third International Conference on Vibration Rotating Machinery of the Institution of Mechanical Engineers, pp. 81-90.

Kohler, H. K., Pratt, A. and Thomson, A. M., 1970. "Dynamics and Noise of Parallel Axis Gearing", Proceedings of the Institution of Mechanical Engineers, Vol. 184, pp. 111-121.

Lin, H., Huston, R.L., and Coy, J.J., 1984. "Dynamic Analysis of Straight and Involute Tooth Forms", ASME Paper, No. 84-DET-226.

Lin, H.H., and Huston, R., 1986. "Dynamic Loading on Parallel Shaft Gears", NASA CR 179473.

Lin, H.H., et. al, 1994. "Dynamic Loading of Spur Gears with Linear or Parabolic Tooth Profile Modifications", Mechanism and Machine Theory, Vol. 29, No. 8, pp. 1115-1129.

Litvin, F. L., et. al, 1995. "Computerized Design and Generation of Low Noise Helical Gears with Modified Surface Topology", Transactions of ASME, Vol. 117, pp. 254-261.

Maliha, R., 1994. "Nonlinear Dynamic Analysis of Geared Rotors to Internal Excitation by Using Describing Functions and Finite Element Method", PhD Thesis, Middle East Technical University, Ankara, Türkiye

Mark, W.D., 1982. "Transfer Function Method for Gear System Dynamics Applied to Conventional and Minimum Excitation Gearing Designs", NASA CR 3626.

Mark, W.D., 1987. "Use of the Generalized Transmission Error in the Equations of Motion of Gear Systems", Journal of Mechanisms, Transmissions and Automation in Design, Transactions of ASME, Vol. 109, pp. 283-291.

Mitchell, L.D., and Mellen, D.M., 1975. "Torsional-lateral Coupling in a Geared High-speed Rotor System", ASME Paper No. 75-DET-75.

Mitchell, L.D., and Daws, J.M., 1983. "A Basic Approach to Gearbox Noise Prediction", Society of Automotive Engineers, Transactions, Vol. 9, pp. 3366-3379.

Mitchell, L.D., and David J.W., 1985. "Proposed Solution Methodology for the Dynamically Coupled Non-linear Geared Rotor Mechanics Equation", Journal of Vibration Stress Reliability in Design, Transactions of the ASME, Vol. 107, pp. 112-116.

Nakamura, K., 1967. "Tooth Separations and Abnormal Noise on Power Transmission Gears", Bulletin of the Japanese Society of Mechanical Engineers, Vol. 10, pp. 846-854.

Nelson, H.D., and Mcvaugh, J.M., 1976. "The Dynamics of Rotor-bearing Systems Using Finite Elements", Journal of Engineering for Industry, Transaction ASME, Vol. 98, pp. 593-600.

Nelson, H.D., 1980. "A Finite Rotating Shaft Element Using Timoshenko Beam Theory", Journal of Mechanical Design, Transactions of the ASME, Vol. 102, pp. 793-803.

Neriya, S.V., Bhat, R.B., and Sanker, T.S., 1985. "Coupled Torsional-flexural Vibration of a Geared Shaft System Using Finite Element Analysis", The Shock and Vibration Bulletin, Vol. 55, pp. 13-25.

Newland, D.E., 1987. An introduction to Random Vibration and Spectral Analysis.

Ogata, K., 1990. Modern Control Engineering, Prentice-Hall, Inc., Englewood Cliffs, New Jersey.

Ostachowics, W., 1990. "A Discrete Linear Beam Model to Investigate the Nonlinear Effects of Slip Friction", Computers and Structures, Vol. 36, pp. 721-728.

Oswald, B., Rebbechi, B., Zakrajsek, J.J., Townsend, D.P., and Lin, H.H., 1991. "Comparison of Analysis and Experiment for Dynamics of Low-Contact-ratio Spur Gears", NASA Technical Report 90-C-017.

Özgüven, H.N., and Özkan, Z.L., 1984. "Whirl Speeds and Unbalance Response of Multi-bearing Rotors Using Finite Elements", Journal of Vibration, Acoustics, Stress and Reliability in Design, Transactions of the ASME, Vol. 106, pp. 72-79.

Özgüven, H.N., and Houser, D.R., 1988a. "Mathematical Models Used in Gear Dynamics - A Review", Journal of Sound and Vibration, Vol. 121, pp. 383-411.

Özgüven, H.N., and Houser, D.R., 1988b. "Dynamic Analysis of High Speed Gears by Using Loaded Static Transmission Error", Journal Sound and Vibration, Vol. 125, pp. 71-83.

Özgüven, H.N., 1991a. "A Non-linear Mathematical Model for Dynamic Analysis of Spur Gears Including Shaft and Bearing Dynamics", Journal of Sound and Vibration, Vol. 145, pp. 239-260.

Özgüven, H.N., 1991b. "Assessment of Some Recently Developed Mathematical Models", Proceedings of the Eighth World Congress on the Theory of Machines and Mechanisms, Prague, Czechoslovakia, pp. 605-608.

Özgüven, H.N., Maliha, R. and Doğruer, C. U., 2004. "Nonlinear Dynamic Modeling of Gear-Shaft-Bearing Systems Using Finite Elements and Describing Functions", Transactions of ASME, Vol. 126, pp. 534-541.

Özkan, Z.L., 1983. "Whirling Speeds and Unbalance Responses of Rotating Shafts Using Finite Element Method", M.Sc. Thesis, Middle East Technical University, Ankara, Turkey.

Remmers, E.P., 1971. "The Dynamics of Gear Pair System", ASME Paper, 71-DE-23.

Remmers, E.P., 1978. "Gear Mesh Exciting Spectra for Arbitrary Tooth Spacing Errors, Load, and Design Contact ratio", Journal of Mechanical Design, Transactions of the ASME, Vol. 10, pp. 715-722.

Reswick, J.B., 1955. "Dynamic Loads on Spur and Helical Gear Teeth", Transactions of the ASME, Vol. 77, pp. 635-644.

Rettig, H., 1975. "Vibrations in Gear Drives; Test Results and Calculation Method for Dynamic Tooth Forces", Proceedings of the International Federation of the Theory of Machines and Mechanisms 4th World Congress, Newcastle.

Seireg, A., and Houser, D.R., 1970. "Evaluation of Dynamic Factors for Spur and Helical Gears", Journal of Engineering for Industry, Transactions of the ASME, Vol. 192, pp. 504-515.

Şener, Ö.S., and Özgüven, H.N., 1990 "Critical Speeds of Geared Rotors by Including Mesh Stiffness and Using a Continuous system Model", Proceedings of the ASME Design Automation Conference, DE-Vol. 23-2, pp. 429-435.

Şener, Ö.S., and Özgüven, H.N., 1993 "Dynamic Analysis of Geared Shaft Systems by Using A continuous System Model", Journal of Sound and Vibration, Vol. 166, pp. 539-556.

Shain, T.N. and Jean, A.N., 1990. "Prediction of Periodic Response of Flexible Mechanical Systems with Non-linear Characteristics", Journal of Vibration and Acoustics, Vol. 112, pp. 501-507.

Shigiley, J.E., 1963. Mechanical Engineering Design, McGraw-Hill, Inc., Tokyo, Japan.

Tanrikulu, Ö., 1991. "Forced Periodic Response Analysis of Non-Linear Structures", M.Sc. Thesis, University of London, Imperial College of Science, Technology and Medicine, London, England.

Tanrikulu, Ö., Kuran, B., Özgüven, H.N., and İmregün, M., 1993. "Forced Harmonic Response Analysis of Non-Linear Structures Using Describing Functions", AIAA Journal, v.31, n.7, pp. 1313-1320.

Tobe, T., Sato, K., and Takatsu, N., 1976. "Statistical Analysis of Dynamic Loads on Spur Gear Teeth (Effect on Shaft Stiffness)" Bulletin of the Japanese Society Mechanical Engineers, Vol. 19, pp. 808-813.

Toda, A., and Tordion, G.V., 1979. "Dynamic Behavior of a Mechanical System with Gear Transmission Error", Proceedings of the International of the Federation Theory Machines and Mechanisms Fifth World Congress, Montreal, pp.1130-1133.

Troeder, C, Peeken, H., Laschet, A., and Tooten, K., 1983. "Causes and Effect of Torque Change in Hammering of Toothed Gears" Proceedings of the International Federation of the Theory of Machines and Mechanisms sixth World Congress, New Delhi, Vol. 2, pp. 936-943.

Tucker, A.I., 1971. "Dynamic Loads on Gear Teeth, Design Applications", ASME Paper No. 71-DE-1.

Tucker, A.I., 1971. "Gear Design: Dynamic Loads", Mechanical Engineering, pp.29-33.

Tuplin, W.A., 1950. "Gear Tooth Stresses at High Speed", Proceedings of the institution of Mechanical Engineers, Vol.. 16, pp. 162-167.

Tuplin, W.A., 1958. "Dynamic Load on Gear Teeth", Proceedings of International Conference on Gearing, Institution of Mechanical Engineers, pp. 24-30.

Utagawa, M., and Harada, T., 1961. "Dynamic Loads on Spur Gear Teeth at High Speed (Influence of the Pressure Angle Errors and Comparison between the Reduction Gear and the Speed-up Gears)", Bulletin of the Japanese Society of Mechanical Engineers, Vol. 4, pp. 706-713.

Utagawa, M., and Harada T., 1962. "Dynamic Loads on spur gear teeth having pitch errors at high speed", Bulletin of the Japanese Society of Mechanical Engineers, Vol. 5, pp. 374-381.

Vaishya, M., and Singh, R., 2001, "Sliding Friction-Induced Non-Linearity And Parametric Effects In Gear Dynamics", Journal of Sound Vibration, Vol.248, pp. 671-694.

Velex, P. and Sainsot, P., 2002. "An Analytical Study of Tooth Friction Excitations In Errorless Spur And Helical Gears", Mechanism and Machine Theory, Vol. 37, pp. 641-658.

Velex, P. and Ajmi, M., 2005. "On The Modelling Of Excitations In Geared Systems By Transmission Errors", Journal of Sound and Vibration, Article in Press (available online 24 August 2005).

Vinayak, H. et. al, 1995. "Linear Dynamic Analysis of Multi Mesh Transmissions Containing External Rigid Gears", Journal of Sound and Vibration, Vol. 185, pp. 1-32.

W. T. Thomson, 1997. Theory and Vibration with Applications, 4th Edition, Chapman&Hall.

Wang, S.M., and Morse, I.E., 1972. "Torsional Response of A Gear Train System", Journal of Engineering for Industry, Transactions of the ASME, Vol. 94, pp. 583-594.

Wang, S.M., 1974. "Analysis of Non-linear Transient Motion of A Geared Torsional" Journal of Engineering for Industry, Transactions of the ASME, Vol. 96, pp. 51-59.

Wallace, D.B., and Seireg, A., 1973. "Computer Simulation of Dynamic Stress, Deformation and Fracture of Gear Teeth", Journal of Engineering for Industry, Transactions of the ASME, Vol. 95, pp 1108-1115.

W. Doebling, C. R. Farrar, M. B. Prime and D. W. Shevitz, 1996. “Damage Identification and Health Monitoring of Structural and Mechanical Systems from Changes In Their Vibration Characteristics; a Literature Review”, Reporter No: LA-13070-MS, Los Alamos National Laboratory.

W. M. Ostachowicz and M. Krawczuk, 2000. “Vibration Analysis of a Cracked Beam”, Computers and Structures, 36, 245-250.

W. M. Ostachowicz and M. Krawczuk, 1991. “Analysis of the Effect of Cracks on the Natural Frequencies of a Cantilever Beam”, Journal of Sound and Vibration, 150,191-201.

Wojnarowski, J. and Onishchenko, V., 2003. “Tooth Wear Effects On Spur Gear Dynamics”, Mechanism and Machine Theory, Vol. 38, pp. 161-178

Y.H. Chong, M. İmregün, 2000. “Use of Reciprocal Modal Vectors for Nonlinearity Detection, Archive of Applied Mechanics, 70, 453-462.

Y. P. Pu, 2002. “Quasi-Periodic Vibration of Cracked Rotor On Flexible Bearings”, Journal of Sound and Vibration, 251, 875-890.

Yoon, K. Y. and Rao, S. S., 1996. “Dynamic Load Analysis of Spur Gears Using a New Tooth Profile”, Journal of Mechanical Design, Vol. 116, pp. 1-6.

Yüksel, C. and Kahraman, A., 2004, “Dynamic Tooth Loads Of Planetary Gear Sets Having Tooth Profile Wear”, Mechanism and Machine Theory, Vol. 39, pp. 695-715.

Zorzi, E.S., and Nelson, H.D., 1977. "Finite Element Simulation of Rotor-bearing Systems With Internal Damping", Journal Engineers Power, Transaction ASME, Vol. 99, pp. 71-76.

APPENDIX A

A FINITE ELEMENT MATRICES FOR ROTORS AND RIGID DISKS

A.1 Rotor Element Matrices

A.1.1 Translational Mass Matrix: $[M_t^e]$

$$[M_t^e] = \frac{m^e L}{420} [M]_1$$

where

$$[M]_1 = \begin{bmatrix} 156 & & & & & & & & & & \\ 0 & 156 & & & & & & & & & \\ 0 & -22L & 4L^2 & & & & & & & & \\ 22L & 0 & 0 & 4L^2 & & & & & & & \\ 0 & 0 & 0 & 0 & 0 & & & & & & \\ 54 & 0 & 0 & 13L & 0 & 156 & & & & & \\ 0 & 54 & -13L & 0 & 0 & 0 & 156 & & & & \\ 0 & 13L & -3L^2 & 0 & 0 & 0 & 22L & 4L^2 & & & \\ -13L & 0 & 0 & -3L^2 & 0 & -22L & 0 & 0 & 4L^2 & & \\ 0 & 0 & 0 & 0 & 0 & 0 & 0 & 0 & 0 & 0 & 0 \end{bmatrix}$$

A.1.2 Rotational Mass Matrix: $[M_r^e]$

$$[M_r^e] = \frac{I_D^e}{30L} [M]_2, \text{ where } I_D^e = \frac{m^e r^2}{4}$$

and

$$[M]_2 = \begin{bmatrix} 36 & & & & & & & & & & \\ 0 & 36 & & & & & & & & & \\ 0 & -3L & 4L^2 & & & & & & & & \\ 3L & 0 & 0 & 4L^2 & & & & & & & \\ 0 & 0 & 0 & 0 & 0 & & & & & & \\ -36 & 0 & 0 & -3L & 0 & 36 & & & & & \\ 0 & -36 & 3L & 0 & 0 & 0 & 36 & & & & \\ 0 & -3L & -L^2 & 0 & 0 & 0 & 3L & 4L^2 & & & \\ 3L & 0 & 0 & -L^2 & 0 & -3L & 0 & 0 & 4L^2 & & \\ 0 & 0 & 0 & 0 & 0 & 0 & 0 & 0 & 0 & 0 & 0 \end{bmatrix}$$

A.1.5 Transverse Stiffness Matrix: $[K_B^e]$

$$[K_B^e] = \frac{EI}{L^3} [K]_2$$

where

$$[K]_2 = \begin{bmatrix} 12 & & & & & & & & & \\ 0 & 12 & & & & & & & & \\ 0 & -6L & 4L^2 & & & & & & & \\ 6L & 0 & 0 & 4L^2 & & & & & & \\ 0 & 0 & 0 & 0 & 0 & & & & & \\ -12 & 0 & 0 & -6L & 0 & 12 & & & & \\ 0 & -12 & 6L & 0 & 0 & 0 & 12 & & & \\ 0 & -6L & 2L^2 & 0 & 0 & 0 & 6L & 4L^2 & & \\ 6L & 0 & 0 & 2L^2 & 0 & -6L & 0 & 0 & 4L^2 & \\ 0 & 0 & 0 & 0 & 0 & 0 & 0 & 0 & 0 & 0 \end{bmatrix}$$

A.1.6 Damping Incremental Stiffness Matrix: $[K_C^e]$

$$[K_C^e] = \frac{EI}{L^3} [K]_3$$

where

$$[K]_3 = \begin{bmatrix} 0 & & & & & & & & & \\ -12 & 0 & & & & & & & & \\ 0 & 0 & 0 & & & & & & & \\ 6L & 6L & -4L^2 & 0 & & & & & & \\ 0 & 0 & 0 & 0 & 0 & & & & & \\ 0 & -12 & 6L & 0 & 0 & 0 & & & & \\ 0 & 0 & 0 & 6L & 0 & -12 & 0 & & & \\ 6L & 0 & 0 & 2L^2 & 0 & -6L & 0 & 0 & & \\ 0 & 6L & -2L^2 & 0 & 0 & 0 & -6L & -4L^2 & 0 & \\ 0 & 0 & 0 & 0 & 0 & 0 & 0 & 0 & 0 & 0 \end{bmatrix}$$

APPENDIX B

B INSTALLATION

B.1 Installation

The VGR version 3.0 is a user friendly interface which controls several sub codes. These codes are:

- NLGRD version 3.0 (Non-Linear Geared Rotor Dynamics)
- LDP version 10.9G (Load Distribution Program)
- Pine version 1.0

NLGRD version 3.0 is written in MatLAB 7.0 and it is a finite element program which computes the dynamic to static load ratio, dynamic transmission error, bearing forces and natural frequencies of a geared rotor system.

LDP version 10.9G computes the several key issues of gears by static analysis, of which the loaded static transmission error has the most significance for this study.

Pine version 1.0 converts the output of VGR version 3.0 to the format of LDP version 10.9G.

The four computer codes, VGR, NLGRD, LDP and Pine must be installed properly to run the VGR version 3.0.

The VGR version 3.0 must be installed under the directory named:

C:\VGR\Vgr30.exe

The NLGRD version 3.0 files (i.e. MatLAB m-files) must be installed under the directory named:

C:\VGR\NLGRD\MatLAB

The LDP version 10.9G must be installed under the directory named:

C:\VGR\LDP\Ldp109G.exe

The Pine version 10 must be installed under the directory named:

C:\VGR\PINE\Pine10.exe

B.2 Visual Geared Rotors 3.0 (VGR 3.0)

The VGR 3.0 is able to prepare input data for both NGRD V3.0 and LDP 10.9G. The LDP part of the program is placed in frames named LDP and the NLGRD part of the program is placed in frames named NLGRD. The parts which are common to LDP and NLGRD are placed in frames named NLGRD/LDP. All units are in SI standards. The units of the input data are indicated next to the input boxes.

Before going further, firstly user must construct the system geometrically, because the computer code, VGR 3.0, could not automatically detect the order and type of the basic elements if the system is constructed in a wrong way. For instance if clicking the stop button is forgotten, shaft one and two cannot be differentiated or gear and pinion have the same code number which may result in wrong matching of the input data.

When the user saves the program files, VGR automatically creates the following files:

- *.vgr
- *.ldp
- *.shp

*.vgr file holds the input data which is necessary for NLGRD version 3.0 to run, basically the material and geometric properties of the basic elements that are present in the system.

*.ldp file holds the input data which is necessary for Pine.exe to run. When Pine.exe is executed, *.inp file is created which is the standard input files for LDP version 10.9G

*.shp file holds the dimensions and place of basic object pictures in it. Thus when an existent file is opened VGR is able to construct the system graphically.

NLGRD version 3.0 creates the following files:

- *.mod (holds the modal analysis output)
- *.dsl (holds the dynamic to static load ratio data)
- *.brf (holds the bearing forces)
- *.brd (holds the bearing displacements)
- *.msh (holds the dynamic transmission error data)

When the user run the Pine version 1.0, File.pin is automatically created under the directory in which Pine version 1.0 is placed. It contains the source and the target file names. Pine version 1.0 automatically opens this file.

APPENDIX C

C USER MANUAL

C.1 Introduction

NLGRD V3.0 user interface - pre-processor and post-processor - is written in VB 6.0. The emphasis is placed on user-friendliness. The graphical drawing of the geared rotor system is formed while the user adds new items to the system. Thus any user dependent error is minimized. The program is capable of making more than one analysis at the same time.

The user interface, Visual Geared Rotors (VGR 3.0), could prepare input file for both NLGRD V3.0 and LDP version 10.9G. There are four basic items in the program:

- Bearing elements
- Weight elements
- Rotor elements
- Gear elements

Every time user clicks one of these buttons, VGR 3.0 interface loads a new item on the CAD form. Material, geometric and other types of data can be entered by just double clicking the items.

Beside these elements there are:

- Stop button
- Move button
- Delete Button

The main window of VGR 3.0 interface is shown in Figure C.1. Having formed the system, user can make analysis by clicking the *Solver* button.

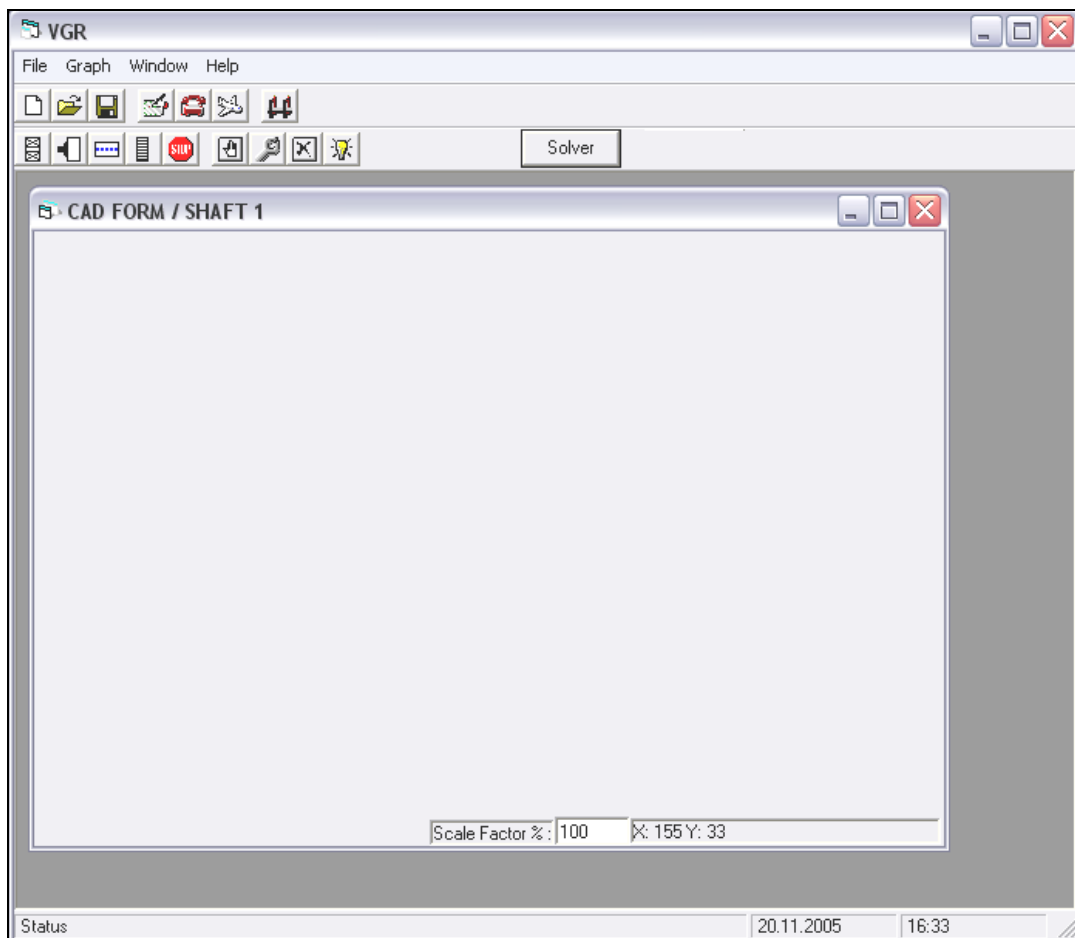


Figure C.1 Main Window of VGR 3.0

C.2 Pre-processor

Connectivity of the system is formed while the user is clicking the basic item buttons. Positions of the items are irrelevant to connectivity. Therefore items must be loaded from left to right, top to bottom. So user must first construct the first shaft from left to right, then click stop button, then start constructing the second shaft and click stop button again when finished. The construction of typical geared rotor system is shown in Figure 4.3.

Loaded items can be dragged anywhere on the screen after clicking the move button. Geometric properties of the items can be defined on screen after stretch button is clicked or first double clicking the item then entering the geometric properties through data windows.

C.2.1 Bearing Element

When the bearing button shown in Figure C.1 is clicked, a new bearing element is loaded on the CAD window. In order to enter bearing stiffness, hysteric damping constants and the radial clearance in millimeters, the user must double click the bearing element. Figure C.2 is displayed immediately after double click.

BEARING DATA

STIFFNESS NLGRD

Kxx (N/m)= 0

Kxy (N/m)= 0

Kyx (N/m)= 0

Kyy (N/m)= 0

DAMPING NLGRD

Cxx (Ns/m)= 0

Cxy (Ns/m)= 0

Cyx (Ns/m)= 0

Cyy (Ns/m)= 0

CLEARANCE NLGRD

Clearance (mm)=

OK

Figure C.2 Bearing Data Window

C.2.2 Weight Element

When the weight button shown in Figure C.1 is clicked, a new weight element (e.g. flywheel) is loaded on the CAD window. As soon as the user double clicks the weight element, Figure 4.4 is displayed on the screen. User can enter the diameter, width and density data through this window.

WEIGHT DATA

NLGRD

Diameter (mm)= 16

Thickness (mm)= 6

Density (kg/m3)= 0

OK

Figure C.3 Weight Data Window

C.2.3 Rotor Element

When the rotor element shown in Figure C.1 is clicked, a new rotor element is loaded on the CAD window. Figure C.4 is displayed when the user double clicks the rotor elements. User can enter outer diameter, inner diameter, length and axial load data through this window.

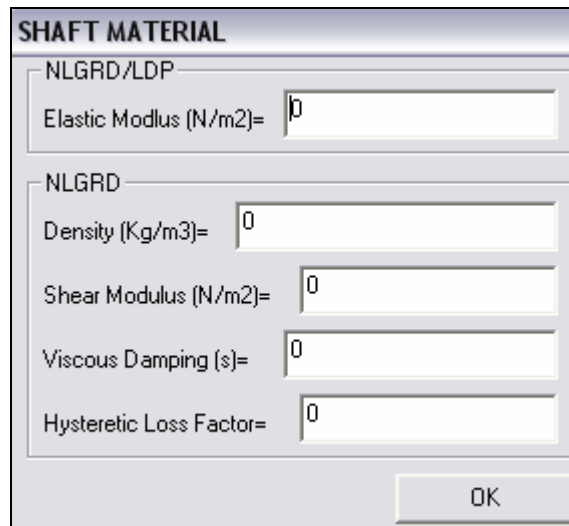
The image shows a software dialog box titled "ROTOR DATA". It is organized into two main sections. The top section, labeled "NLGRD", contains four input fields with the following values: "Length (mm)= 23", "Outer Diameter (mm)= 6", "Inner Diameter (mm)= 0", and "Axial Load (N)= 0". Below these fields is a button labeled "MATERIAL". The bottom section, labeled "LDP", contains two buttons: "MISALIGNMENT" and "SHAFT DIMENSIONS". At the bottom right of the dialog is an "OK" button.

Figure C.4 Rotor Data Window

In order to enter material properties of the rotor material button must be clicked. Figure C.5 is loaded when the *Material Button* is clicked. User can enter the following NLGRD data:

- Density
- Modulus of elasticity (for NLGRD and LDP)
- Shear modulus of elasticity
- Viscous damping coefficient
- Hysteric damping coefficient

through this window.



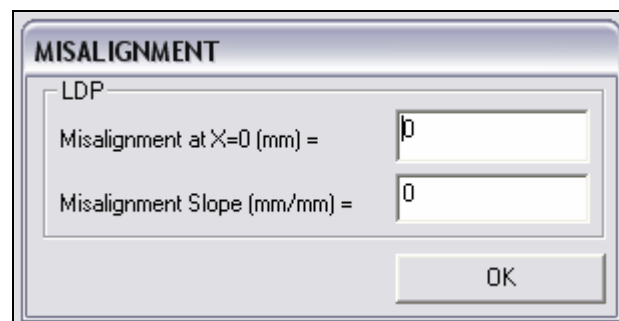
The dialog box is titled "SHAFT MATERIAL". It contains two sections: "NLGRD/LDP" and "NLGRD".

- NLGRD/LDP**: Elastic Modulus (N/m²) = 0
- NLGRD**:
 - Density (Kg/m³) = 0
 - Shear Modulus (N/m²) = 0
 - Viscous Damping (s) = 0
 - Hysteretic Loss Factor = 0

An "OK" button is located at the bottom right of the dialog box.

Figure C.5 Shaft Material Data Window

User can reach misalignment and shaft dimensions window through rotor data window. When the user clicks the misalignment button Figure C.6 is displayed.



The dialog box is titled "MISALIGNMENT". It contains one section: "LDP".

- LDP**:
 - Misalignment at X=0 (mm) = 0
 - Misalignment Slope (mm/mm) = 0

An "OK" button is located at the bottom right of the dialog box.

Figure C.6 Shaft Misalignment Data Window

User can enter the following LDP data through this window:

- Misalignment at X=0
- Misalignment slope

When the user clicks the *Shaft Dimensions* button, Figure C.7 is displayed.

User can enter the following LDP data through this window:

- Outer, inner diameter and length of shaft
 - Before pinion

- After pinion
 - Before gear
 - After gear
 - Gear and pinion hub diameter
- through this window.



Figure C.7 Shaft Dimensions Data Window

LDP can only take single shaft before and after the gear pairs into account. Therefore equivalent shaft dimensions must be entered.

C.2.4 Gear Element

When the *Gear Button* shown in Figure C.1 clicked, a new gear element is loaded on the CAD window. Figure C.8 is displayed when the user double clicks the gear element. User can enter the following NLGRD data:

- Pitch diameter
- Face width
- Density

through this window. Three new windows can be reached through Figure C.8.

Figure C.8 Gear Data Window

When the user clicks *Mesh data* button Figure C.9 is displayed. User can enter number of teeth, viscous damping coefficient, backlash, static load and eccentricity through this window.

When the user clicks *STE* button, Figure C.10 is displayed. User can enter the following NLGRD data through this window:

- Contact ratio
- Amplitude of STE
- Average mesh stiffness
- Name of STE file

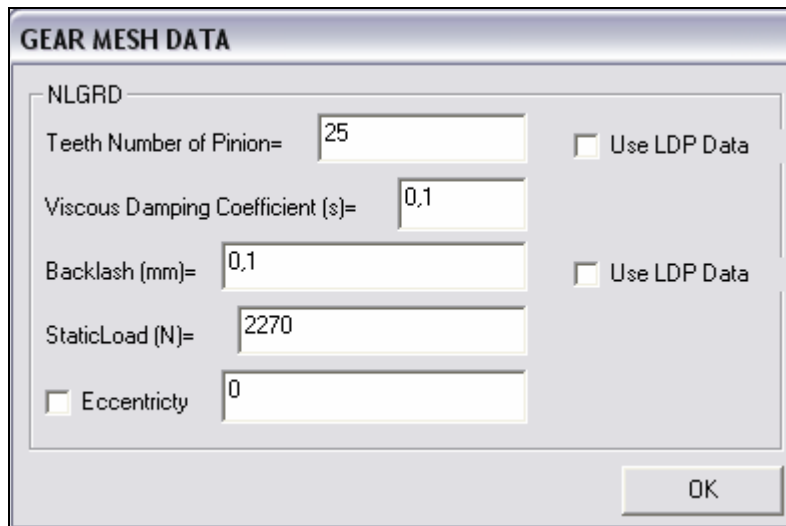


Figure C.9 Gear Mesh Data Window

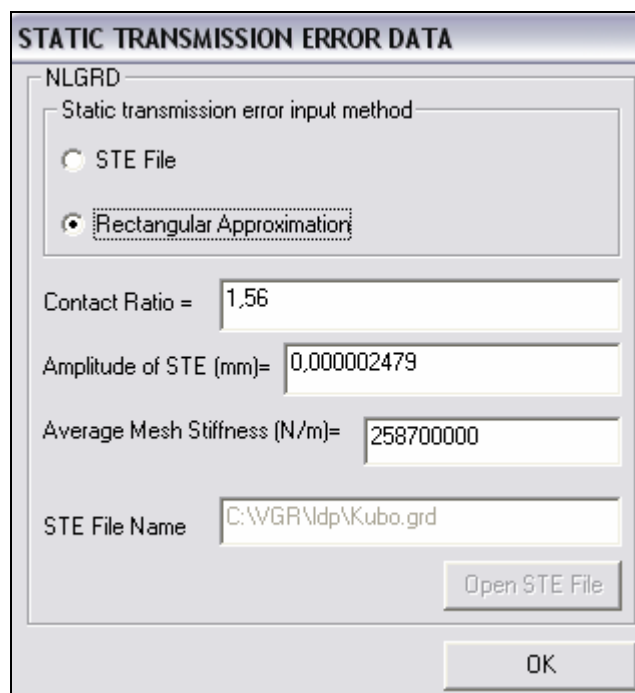


Figure C.10 Static Transmission Error Data Window

User can choose either LDP output file or rectangular wave approximation. User must enter contact ratio, amplitude of STE and average mesh stiffness unless he chooses the STE file option.

By clicking *Data* button user can reach Figure C.11.

The image shows a software window titled "DATA" for the NLGRD processor. It contains several input fields and a section for frequency sweep options. The parameters are as follows:

Parameter	Value
Number of FFT Terms =	5
Starting RPM of Shaft (rpm)=	2000
Upper Limit of RPM (rpm)=	20000
Increment (rpm)=	200
Maximum Number of Iterations =	400
Tolerance in RMS Error =	0,001
Relaxation Factor 1&2 =	0,08 0,13

Frequency sweep options:

- Forward
- Backward

An "OK" button is located at the bottom right of the window.

Figure C.11 Data Window

This window controls the flow of the NLGRD V3.0 processor. User can enter the following parameters shown in Figure C.11:

- Number of FFT Terms: The number of harmonics used in the approximation of STE.
- Starting angular speed (rpm): The simulation starts at this rpm.
- Upper Limit of angular speed (rpm): The simulation ends at this rpm.
- Increment: Speed increment between successive simulations.
- Tolerance : It controls the error limit (Recommended : 0.01)
- Relaxation Factor: The result of NLGRD is modified by a weighted average of the results of the previous and present iterations. (Recommended : Relaxation factor 1=0.001, Relaxation factor 2=0.13)

When the user clicks *Gear (or Pinion) Geometry* button in Figure C.8, Figure C.12 is displayed. User can enter the following LDP data:

- Number of teeth
- Module
- Generating pressure angle
- Helix angle
- Outer diameter
- Root diameter
- Center distance
- Input torque
- Location of the output torque relative to input torque
- Type of gear mesh (External / Internal)

GEAR GEOMETRY

LDP

Teeth Number = Use the same teeth number in NLGRD

Module (mm) = Calculate module using the pitch diameter in NLGRD

Generating Pressure Angle (deg) =

Helix Angle (deg) =

Outside Diameter (mm) =

Root Diameter (mm) =

Center Distance (mm) =

Input Torque (Nm) =

Locate the position of output torque relative to input torque

Same

Opposite

External / Internal Gear

External Gear

Internal Gear

OK

Figure C.12 Gear Geometry Data Window

When the user clicks the *Tooth Data* button, Figure C.13 is displayed. User can enter the following LDP data:

- Starting tooth number
- Face width

- If backlash is chosen
- Amplitude of backlash
- Percentage of backlash attributed to pinion
- If tooth thickness is chosen
- Tooth thickness
- Diameter at which tooth thickness measured

TOOTH DATA

LDP

Gear

Starting Tooth Number = 1

Face Width (mm) = 15 Use NLGRD Data

Face Width Offset (mm) = 0

Supply backlash or tooth thickness

Backlash

Tooth Thickness

Backlash

Amount of Backlash (mm) = 0,1 Use NLGRD Data

Percentage Backlash Attributed to Pinion = 50

Tooth thickness

Tooth Thickness (mm) = 0

Diameter at Which Tooth Thickness is measured (mm) = 0

OK

Figure C.13 Tooth Data Window

When the user clicks the *Tooth Model* button, Figure C.14 is displayed. User must choose the model of the tooth (Flat/Tapered). If the tapered tooth model is chosen, the type of calculation method (manual/automatic) must be decided. If the manual method is chosen, following parameters must be entered:

- Tooth thickness at tip

- Tooth thickness at root
- Beside these, user must enter the following constants:
- Plate bending exaggeration factor
 - Tooth base rotation factor
 - Hertz exaggeration factor

Figure C.14 Tooth Model Data Window

When the user clicks gear material button, Figure C.15 is displayed. User can enter the following LDP data:

- Young's modulus
- Poisson's ratio

When the "use the same material" check box is checked, both gear and pinion has the same material properties.

When the user clicks the lead data button in Figure C.8, Figure C.16 is displayed.

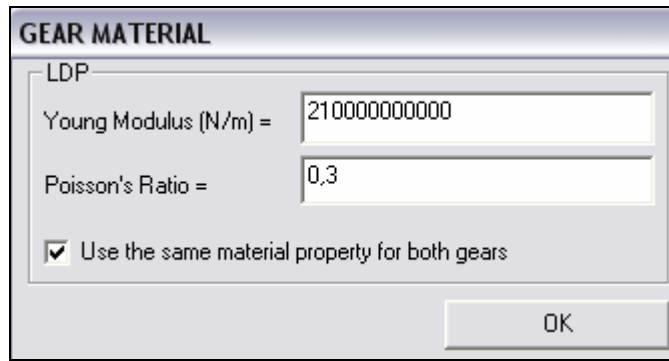


Figure C.15 Gear Material Data Window

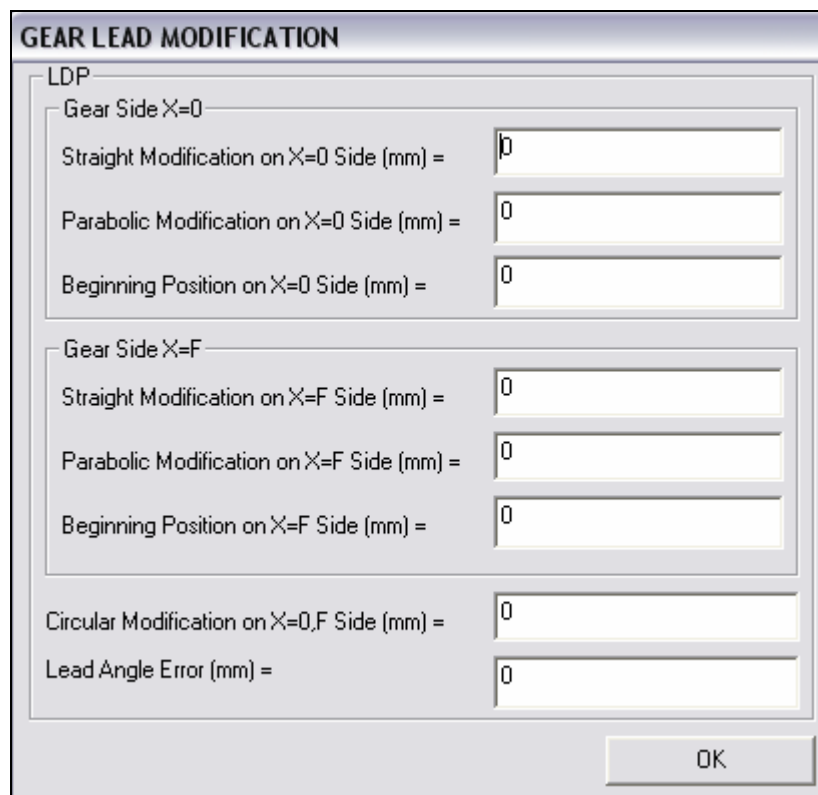


Figure C.16 Gear Lead Modification Window

User can enter the following LDP profile modification data:

- Straight modification on X=0 side
- Parabolic modification on X=0 side
- Beginning position on X=0 side
- Straight modification on X=F side
- Parabolic modification on X=F side
- Beginning position on X=F side

- Circular modification on X=0,F side
- Lead angle error

When the user clicks *Involute Data* button, Figure C.17 is displayed. User can enter following LDP profile modification data:

- Roll angle at start of tip modification
- Parabolic tip modification magnitude
- Straight tip modification magnitude
- Roll angle at start of root modification
- Parabolic root modification magnitude
- Straight root modification magnitude
- Circular modification at tip and root
- Pressure angle error

Figure C.17 Gear Involute Modification Window

When the user clicks the *Program Control* button, Figure C.18 is displayed. This window controls the flow of LDP.

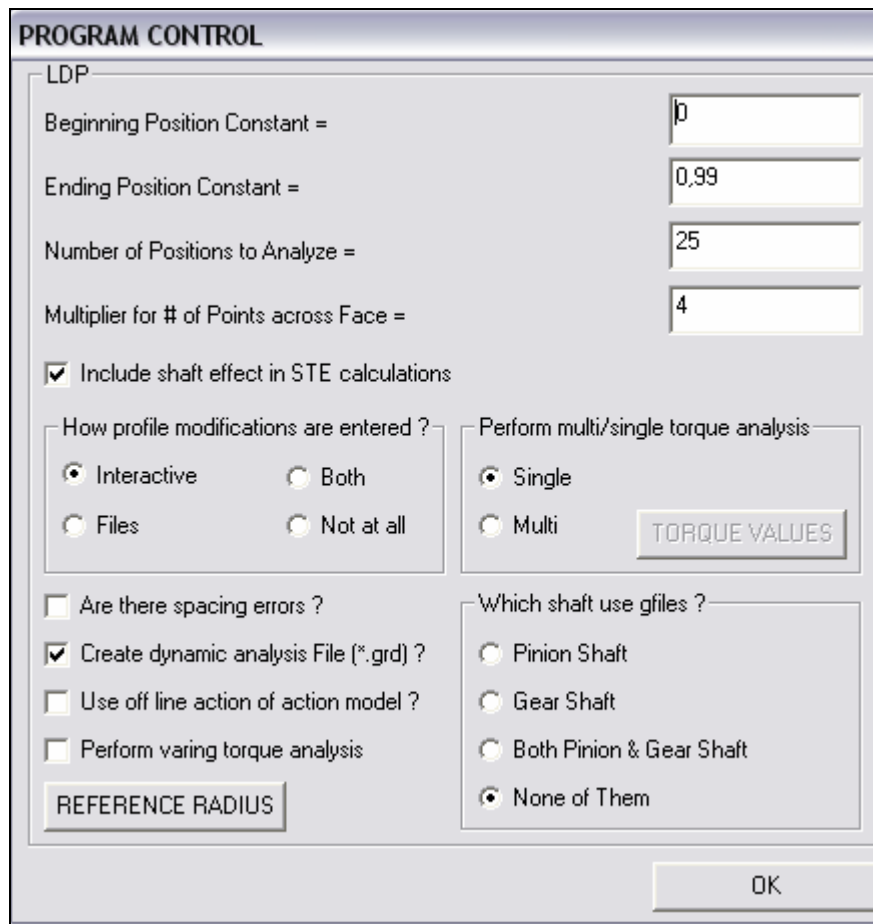


Figure C.18 Program Control Window

User can enter the following LDP data using this window:

- Beginning position constant
- Ending position constant
- Number of positions to analyze
- Multiplier for number of positions across face
- Include shaft effects in transmission error calculation? (Yes/Not)
- How profile modifications are entered?
 - Interactive
 - Files
 - Both
 - Not at all
- Are there spacing errors? (Yes/No)
- Create dynamic analysis file? (Yes/No)

- Use offline action of model? (Yes/No)
- Perform varying torque analysis? (Yes/No)
- Perform multi/single torque analysis?
- Which shaft use gfiles?
 - Pinion shaft
 - Gear shaft
 - Both pinion and gear shaft
 - None of them

When the user clicks title and filenames button, Figure C.19 is displayed.

Figure C.19 Title and Filenames Window

User can enter the filenames necessary for LDP. These are:

- Program identity title

- Output file name
- File name for detailed pinion data (when tooth spacing option is checked)
- File name for detailed gear data (when tooth spacing option is checked)
- File name for torque values (when varying torque analysis is checked)
- File name for pinion shaft (when the pinion shaft use gfiles)
- File name for gear shaft (when gear shaft use gfiles)
- Position constants (number of positions to be printed)
- Do you want detail in output file (Yes/No)

When user finishes constructing the system, *Save* button is pressed in the file menu in Figure C.1. This creates the necessary input files for LDP and NGRD V3.0.

Note that if LDP output is selected to calculate STE, then pine.exe should be run before clicking *Solver* button.

When *Solver* button is clicked, MatLAB 7.0 opens automatically and solves the system equations. Moreover, necessary files are created for post processor.

C.3 Post Processor

After NLGRD version 3.0 solves the system equations, results can be seen through user interface graphically. The post processor window is shown in Figure C.20. User can control the graph window by changing the parameters of control window. X and Y axis variable, X and Y axis scale can be changed. The user can take the advantage of seeing both the results and the model itself at the same time.

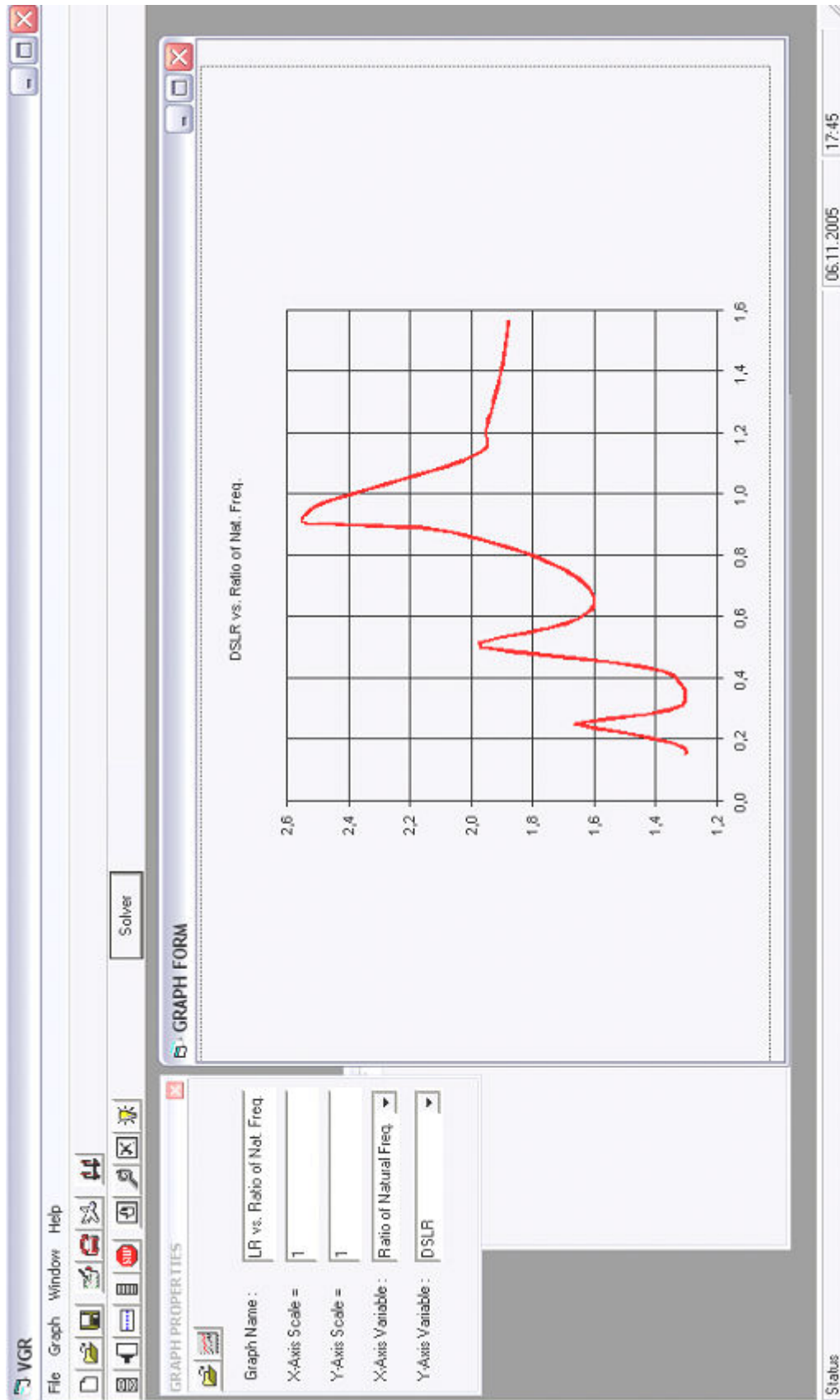


Figure C.20 Post processor window